TISSUE ENGINEERED CONSTRUCTS TO MODEL EARLY AND LATE-STAGE ATHEROSCLEROSIS

A DISSERTATION
SUBMITTED TO THE FACULTY OF SCIENCE
OF THE UNIVERSITY OF ZURICH
IN PARTIAL FULFILLMENT OF THE REQUIREMENTS
FOR THE DEGREE OF
DOCTOR OF PHILOSOPHY

Anna Mallone
January 2018

Abstract

Atherosclerosis is a chronic inflammatory vascular pathology characterized by the formation of fatty streaks, also known as plaques, causing vessel stenosis and impairing the physiological blood flow. Atherosclerotic plaques are cholesterol-induced inflammatory niches accumulating in the vascular sub-endothelial space. Cellular and extracellular composition of human plaques is maneuvered by local inflammation that leads to alterations in the original vascular microenvironment. Up to date, no optimal *in vivo* or *in vitro* model mimicking the human disease pathophysiology does exist. In the present dissertation, I introduce two new tissue engineered human cell-based *in vitro* models for the investigation of atherosclerosis pathomechanisms both in the early and late-stages of disease development. Chapter 1 introduces the key concepts of tissue engineering and atherosclerosis disease onset and progression, and provides an excursus on current models used to mimic different disease stages. Chapter 2 details the design, the fabrication and the computational fluid dynamics investigation of a new fluidic chamber for the simultaneous multiple production of miniaturized tissue engineered vessels. Furthermore, in this chapter, a new *in vitro* human-cell based model mimicking early disease stages is presented. Chapter 3 describes the invention of the first late-stage *in vitro* disease model of atherosclerosis which is based on the production of spheroid, plaque-like cellular aggregates. Finally, Chapter 4 summarizes the models presented in this dissertation and examines advantages and possible use of such models for future research. Collectively these studies deepen our knowledge and understanding of atherosclerosis modeling and disease aetiopathogenesis.

Zusammenfassung

Atherosklerose ist eine chronisch entzündliche Erkrankung der Blutgefäße. Sie ist gekennzeichnet durch die Bildung von Fetteinlagerungen, auch bekannt als Plaques, welche wiederum eine Gefäßstenose und eine Reduzierung des physiologischen Blutflusses verursachen. Atherosklerotische Plaques sind cholesterininduzierte Entzündungsnischen, die sich im subendothelialen Raum der Blutgefäße ansammeln. Die zelluläre und extrazelluläre Zusammensetzung der Plaques wird durch die lokale Entzündung und die daraus resultierenden Veränderungen in der ursprünglichen Gefäßumgebung bestimmt. Bislang existieren keine *in vivo* oder *in vitro* Modelle, die die zugrunde liegende Pathophysiologie optimal nachbilden können. In dieser Dissertation stelle ich zwei neue auf Tissue-Engineering und humanen Zellen basierende *in vitro* Modelle vor, die der Erforschung des Pathomechanismus der Atherosklerose sowohl im Früh- als auch im Endstadium dienen. Kapitel 1 gibt Einblicke in die Grundlagen des Tissue-Engineerings sowie Entstehung und Verlauf der Atherosklerose. Des Weiteren werden aktuelle Modelle zur Simulation der verschiedenen Krankheitsstadien beschrieben. Kapitel 2 behandelt das detaillierte Design, die Herstellung und die computerbasierte Analyse der Strömungsdynamik einer neuartigen „Fluidic Chamber“, die der gleichzeitigen Produktion multipler Miniatur-Blutgefäße dient. Darüber hinaus wird ein neues *in vitro* Modell basierend auf humanen Zellen erläutert, welches das Frühstadium der Krankheit nachbildet. Kapitel 3 umschreibt die Erfindung des ersten *in vitro* Krankheitsmodells, das das Endstadium der Atherosklerose simuliert und auf der Bildung sphärischer, Plaque-ähnlicher Zellaggregate beruht. Kapitel 4 resümiert alle hier präsentierten Modelle und

benennt Vorteile und möglichen Nutzen dieser Modelle für die zukünftige Forschung. Insgesamt vertiefen die hier dargestellten Studien unser Grundverständnis für die Modellierung und für die Ätiopathogenese der Atherosklerose.

Acknowledgements

First and foremost, I want to thank my advisors Prof. Simon P. Hoerstrup and Benedikt Weber. They taught me, both consciously and un-consciously, how good science in the field of tissue engineering and regenerative medicine is done. I appreciate all their contributions of time, ideas, and funding to make my PhD experience productive and stimulating. The enthusiasm they have for their research was contagious and motivational for me, even during tough times in the PhD pursuit. I am also thankful for the excellent example they have provided as successful scientists.

The members of the Hoerstrup group and Nitsch group have contributed immensely to my personal and professional time at the Institute for Regenerative Medicine (IREM) of the University of Zurich. Both groups have been a source of friendships as well as good advice and collaboration. I am especially grateful to Chantal Stenger, master student working with me on the late-stage atherosclerosis model for her enthusiasm, willingness to learn and consistent help. I thank the following people for helpful discussions during the lab meetings in the planning period of my experiments for both disease models: Emanuela Fioretta, Laura Frese, Mareike Göranson, Melanie Generali, Debora Kehl, Agnieszka Ksiazek, Ursula Steckholzer, Steffen Zeisberger, Francesco Pasqualini, Sarah Motta and Valentina Lintas. I am especially grateful for the conversations with current and former PhD students of the Nitsch group. In particular I thank Christoph Gericke for teaching me the t-distributed stochastic neighbor embedding data analysis pipeline, Claudia Späni and Rebecca Derungs for the tips on statistical tests and Sonja Grinschgl, Julian Birnbaum, Sabine Probst and Tunahan Kirabali for their passion and commitment towards research.
Additionally, I thank Sarina Thöni, Maik Krüger, Stefan Kahn, Maria T. Ferretti, Luka Kulic, Uwe Konietzko, Daniel Schuppli, Chad Brokopp, Maximilian Y. Emmert, Christian Tackenberg, Divya Vats, Jiri van Bergen, Sherida de Leeuw, Priyanka Ravikumar, Mrityunjoy Mondal, Clemens Schroeder, Frances Quevenco and Vinod Udayar for their friendship and support.

For this dissertation, I would like to thank my stirring committee: Prof. Grimm, Prof. Von Eckardstein and Prof. Michael Detmar for their time, interest, and helpful comments.

Lastly, I would like to thank my family for all their love and encouragement. For my parents who raised me with love for science and supported me in all my pursuits. For the presence, support and care of my brother Luca. And most of all for my loving son Leonardo Maximilian, and for my supportive, encouraging, and patient boyfriend Christoph whose faithful support during the final stages of this PhD has been so appreciated.

Thank you.

Anna Mallone
University of Zurich
January 2018

Contents

Chapter 3

Chapter 4

Chapter 5

List of Tables

List of Figures

Chapter 1

Adapted from:

Mallone, A., Weber, B. and Hoerstrup, S. P. (2016) *Cardiovascular Regenerative Technologies: Update and Future Outlook*, Transfus Med Hemother. doi: 10.1159/000447749

Mallone, A., Weber, B. and Hoerstrup, S. P. (2017) *Approaches and Recent Advances in Heart Valve Tissue Engineering, in Tissue Engineering for Artificial Organs: Regenerative Medicine, Smart Diagnostics and Personalized Medicine* (ed A. Hasan), Wiley-VCH Verlag GmbH & Co. KGaA, Weinheim, Germany. doi: 10.1002/9783527689934.ch14

Mallone, A., Hoerstrup, S. P. and Weber, B. (2018) *Modeling atherosclerosis*. (Manuscript in preparation)

Introduction

The work for this dissertation is dualistic. First, I have designed and fabricated a fluidic chamber hosting tissue engineered small-caliber vessels. With the aim of modeling the conditions of the early stages of atherosclerosis disease, I setup a specific culturing environment with a focus on key athero-causative factors: (i) shear stress on the mini vessel walls, (ii) concentration of low-density lipoproteins (LDL) in the culture medium and (iii) titer of circulating monocytes. I used the model to investigate time-dependent infiltration and differentiation of monocytes within the tissue engineered vessels and the remodeling of extracellular matrix. For the second part of the dissertation I biofabricated a spheroid model of atherosclerotic plaque. This vascular construct resembles for its cellular and extracellular content the late-stage atherosclerotic lesion. I used the artificial plaque to investigate the role of LDL in cell population remodeling and viability. This chapter introduces the tools and concepts for tissue engineering, gives an introduction to atherosclerosis pathophysiology, and finally overviews the *in vivo* and *in vitro* models available nowadays to study atherosclerotic disease.

1.1 Principles of tissue engineering

Tissue engineering is the science of tissue manufacturing, deeply rooted in the field of biotechnology, cellular biology and biochemistry, and combining them for the purpose of multicellular system manufacturing. The key steps in tissue engineering are (1) cell isolation, expansion, proliferation (ideally cells are isolated from a human tissue), (2)

cell seeding and tissue propagation within a biodegradable support matrix, (3) extracellular matrix deposition with concomitant scaffold degradation. As last step, which justifies the existence of "tissue engineering" is the (4) implantation of the bioengineered construct within the host followed by further tissue remodeling occurring *in vivo*[2-4]. These four key points can be fulfilled with different culturing techniques and using *in vitro* bioreactor systems. The final goal is to promote tissue formation by reproducing physiological mechanical stimuli provided by pulsatile blood flow[5, 6]. The four-step procedure is commonly known as *ex vivo (or in vitro)* tissue engineering strategy. Different tissue engineering approaches have been additionally investigated. A different, promising approach is the *in vivo (or in situ)* strategy which is based on the intuitive concept that the most suitable scaffold for a tissue engineered (TE) construct is the extra cellular matrix (ECM) of the native tissue itself. Following this idea, matrices derived from decellularized tissues[7] as well as biodegradable synthetic scaffold matrices have been studied for direct implantation within the patient. This strategy allows spontaneous transmigration and active recruitment of circulating endogenous cells to achieve an *in vivo* scaffold repopulation [8, 9]. Nowadays, the *in vitro* production tissue engineered constructs through conditioned systems (bioreactors), is the most widespread methodology aiming at stimulating adequate cellular proliferation and ECM deposition via a combination of both biochemical and bio-mechanical stimuli.

In cardiovascular tissue engineering, bio-mechanical stimuli are introduced using pulsating medium flow. Flow pulsatility has been reported to be beneficial for myofibroblasts seeded onto the scaffolds, allowing their alignment in the biomaterial meshes in the early phases of tissue organization[10, 11]. In 2008 Engelmayr and collaborators introduced the flex–stretch–flow bioreactor system for the production of tissue engineered heart valves[12], proving the beneficial effects of these mechanical constrains on *in vitro* tissue formation, and providing evidence then it is possible to obtain artificial constructs with mechanical properties similar to the native tissues.

Design and chemical composition of the scaffold matrices employed for tissue engineering are critical variables for the success of the biological substitute production in both the *ex vivo* and *in vitro* approaches. However, other key players are fundamental in the process of tissue engineering: the cell type used for tissue production (in the *ex*

vivo strategy), the ability of scaffold degradation and the quality of extracellular matrix deposition[13]. Additionally, in case the bioengineered tissue is designed to be used in the clinic, the scaffold material and the culture medium employed for its production have to be proven to be xenogen-free[13, 14]. Today's attempt in developing scaffolds fulfilling the aforementioned strict requirements is proceeding in two directions and is based on the use of more or less complex polymers from different sources: (i) scaffolds from fully synthetical origin or (ii) scaffolds based on biological components. An overview of today's options of biomimetic and biodegradable scaffolds is given in the following paragraphs.

1.1.1 Polymeric scaffolds from synthetic sources

Polymeric scaffolds are up to date the mostly used matrices in the cardiovascular field and in particular for *ex vivo* heart valve tissue engineering and vascular engineering. The reason of their success is their high durability, high reproducibility and low costs as well as their remarkable mechanical strength and predictable physical properties. Their physical properties strictly rely on local scaffold stiffness, the main player in extracellular matrix production and remodeling. In fact, cells are exposed to different local stresses according to the scaffold biomechanical profile. Many studies have investigated various fabrication techniques in order to generate novel structures for TE applications as polymers assembled with porous designs[15], woven, non-woven and electro-spun designs[16]. A huge variety of biodegradable synthetic polymers have been synthesized and proposed as suitable TE matrices, such as polyhydroxyalkanoates (PHA), polyglycolic acid (PGA), polylactic acid (PLA), polyglactin (PLGA), poly (vinyl alcohol), polycaprolactone (PCL) and poly-4-hydroxybutyrate (P4HB)[17], all sutable for tissue engineering, being biodegradable and of high malleability.

1.1.1.1 A focus on aliphatic polyesters: PGA, PLA, PLGA and PCL

Despite materials with lower tendency to calcification like polytetrafluoroethylene (PTFE), polyethyleneterephthalate (PET) and polyurethane (PUR) were initially used for the production of bioengineered vessels[18], they show many disadvantages as they

are non-degradable, rigid and prone to thrombogenesis. For this reason, they appear less suitable for both vascular and valvular graft production when compared to the newest polymers available on the market. Among these new flexible and biodegradable materials, aliphatic polyester composite structures are considered one of the best options for tissue engineering. One of their main features of interest resides in their relative resistance to rapid hydrolytic degradation, a remarkable point since artificial living systems are cultured in aqueous media[19]. PGA, PCL, PLGA and PLA are all synthetic polymers approved for clinical use by Food and Drug Administration (FDA) and belong to the aliphatic polyester family. Their erosive degradation ability resides in the ester bonds of their polymeric backbone. When used for tissue engineering purposes, these compounds undergo macromolecular degradation by random hydrolysis and concomitant enzymatic esterase activity[20]. It is necessary to point out that monomers resulting from the degradative process of aliphatic polyesters are non-toxic and can be easily bioresorbed by cells and reintroduced in normal cellular metabolic pathways (e.g. oxidized to pyruvic acid). Therefore, these compounds can be considered a good choice as starting materials for tissue engineering.

1.1.2 Polymeric scaffolds from biological sources

Biologically derived polymeric scaffolds are either used alone, as plain material, or blended with the synthetic polymers described above (e.g. with PLGA)[21, 22]. This family of bio-scaffolds includes polysaccharides as alginate, chitin/chitosan, hyaluronic acid derivatives and proteins such as collagen, fibrin as well as polyhydroxyalkanoates (PHA) and decellularized extracellular matrices[23-26]. In addition to the range of options described above, pioneer experiments were conducted in order to combine different bio-scaffolds and to create hydrogels of higher complexity[27].

Despite the efforts to introduce these natural polymers in the common TE practice, the synthetic materials are still considered a better choice due to their improved strength and durability. Moreover, a functionality comparison between natural (or decellularized) tissue and natural polymer-based scaffolds still has to be conducted. Furthermore, the scaffolds derived from natural polymers still need to be mechanically

improved. In particular they show pronounced weakness under stress. Such weakness does not allow (for the moment) these biomaterials to be suitable for the culturing conditions used in cardiovascular tissue engineering, where a pulsatile flow is applied.

Although the majority of polymeric scaffolds from biological sources is not suitable for cardiovascular tissue engineering, there are some exceptions. One of them is Polyhydroxyalkanoates (PHA). PHA are polyester isolated from bacteria cultures and can be generated of a desired length (monomer composition) and with a specific degradation time by micro tuning the bacterial production pathways. The PHA family includes poly-3-hydroxybutyrate (PHB), copolymers of 3-hydroxybutyrate and 3-hydroxyvalerate (PHBV), poly-4-hydroxybutyrate (P4HB), copolymers of 3-hydroxybutyrate and 3-hydroxyhexanoate (PHBHHx) and poly-3-hydroxyoctanoate (PHO)[28]. PHO, as well as P4HB, have been largely investigated and utilized for cardiovascular TE [6, 15, 29]. Unfortunately, an unpleasant drawback of these compounds is their slow degradation time which can ultimately impair the tissue growth and the expected histological composition of the final bioengineered construct. For this reason, PHA polymers are generally combined in low concentration with other synthetic polymers to manufacture hybrid scaffolds. The P4HB-coating of PGA meshes, indeed, has been reported to be a successful and promising combination of biophysical characteristics where the high porosity of PGA is combined with the thermoplasticity of P4HB[6, 7].

1.1.2.1 Polysaccharide-based scaffolds

Polysaccharides are the most accessible, cheap, hemocompatible and non-toxic sources of materials for tissue engineering. The monosaccharide units constituting the long polysaccharide chains can be tuned by varying the final monosaccharide composition. Furthermore, interesting physical properties of the monomers are amplified by the polymeric scaffold structure, as different solubility or gelation. Because of their high flexibility polysaccharides have been largely used for a variety of purposes in tissue engineering, e.g. blood vessels, myocardium, heart valves, bone and other tissue engineered constructs but also for encapsulation and delivery of pancreatic islets and ovarian follicles [30]. Among the large polysaccharide family, alginate and chitosan are today's best investigated and used materials for TE[27]. Alginate is a

biodegradable and bioresorbable polysaccharide derived from brown algae. It is composed of repeated glucuronic and mannuronic units that can be easily cross linked in solid gel form at room temperature by simply adding bivalent metallic ions such as Ca^{2+} or Mg^{2+}. Its mechanical and physical behavior is highly influenced by the percentage of different monomers in the final construct and by their chain length. Some disadvantages of alginate have been monitored and reported in literature, i.e. its mechanical weakness and poor cell adhesion on the meshes. However, some of these obstacles, like the low cell adhesiveness have been already overcome[31, 32]. Chitosan is derived from chitin, a biopolymer also found in the exoskeletons of insects. Unfortunately, as for the alginate, its use as scaffold for tissue engineering is limited due to low mechanical properties, therefore, studies on chitosan fibers reinforcement have been recently carried out to increase the polysaccharide strength and stiffness in proportion to the fiber/scaffold mass ratio but reducing the possibilities to use this polymer for cardiovascular tissue engineering[33].

In the long run, scaffolds as similar as possible to the native ECM will be biofabricated. On this regard, hyaluronanic acid (HA) will be largely considered for tissue engineering applications. HA is commonly found in the extracellular matrix of connective tissues, it is a high molecular weight, non-sulfated glycosaminoglycan (GAG) and has been coupled with other biomaterials (e.g. to alginate) to produce 3D-bioprinted hybrid scaffolds for tissue engineering purposes[34]. The idea of using a material which is non-thrombogenic, well structured, retaining space filling physiological properties is remarkable. In addition, mechanic weaknesses have been recently overcome by co-polymerization with other relevant synthetic or natural polymers[35]. Interestingly, the small disaccharides derived from HA degradation, are released in concomitance to tissue formation, were shown to promote extracellular matrix production[36], an advantageous point for the improvement of mechanical features of HA and for a potential use in cardiovascular tissue engineering.

1.1.2.2 Protein-based scaffolds

Protein-based scaffolds can artificially reproduce several features of ECM and also retain the potential to positively influence growth and native organization of cells during tissue formation. Collagen (mainly collagen type I) and fibrin are today's best

options among protein based matrices for TE because of their bioresorbable properties and malleability. Thanks to its fibrillar nature, collagen can be shaped according to structural tissue requirements either into sponges, sheets, gels or fiber-based scaffolds[37-40]. Scaffolds from this polypeptide are characterized by long degradation times and by scarce availability, since human collagen is difficult to obtain from human tissue explants. Fibrin is composed of fibrinogen units and, like collagen, can be derived directly from human tissue samples, with all the advantages of autologous scaffold production[41]. Fibrin is a malleable polymer possibly modified in hydrogels, beads and glue[42]. Degradation of these scaffolds can be diminished or increased by varying the amount of fibrinolysis blocking agents in the culturing medium, such as the serin protease inhibitor aprotinin[24]. The high softness, the tendency to shrinkage and the rapid degradation are still major issues to overcome. Great efforts have been done in this direction, e.g. the use of poly(l-lysine) chemical treatment of the scaffold in order to improve the mechanical properties. However, still more has to be done in view of the use of this interesting biomaterial for bioengineering purposes.

1.1.2.3 Scaffolds derived from decellularized tissues

The excursion on the different scaffolds for *in vitro* engineering of heart valves ends at decellularized tissue-derived matrices. The goal of a good bioresorbable scaffold, besides providing a stable growing substrate for the cells, is to encompass as much as possible the features of the tissue-specific ECM[43]. The use of native tissue-derived templates composed of structured ECM proteins directly organized in their native architecture is inevitably attractive. Additionally, the idea that hemodynamic and biomechanical properties are already similar or identical to those of their native counterpart is even more interesting for tissue engineering applications[3]. When considering tissue-derived ECM scaffolds for TE, one of the main issue is the tissue source. The concerns on using ECM derived from either xenogeneic or allogeneic donors are related to the possible triggering of immune reactions. An additional issue of native ECM is the high risk of disease transmissions due to the use of former living substrates, as Prion diseases and retroviruses. A strategy for safe retrieval and use of tissue-specific ECM in tissue engineering has been recently optimized and is based on

decellularization processes. The use of this technique has been proven to decrease the immunological response without limiting the cellular remodeling capacity and positively impacting the long-term durability of the artificial constructs[7]. Homografts or xenografts are today's most used choices as scaffold matrices. In this regard, Weber et al. investigated the repopulation capacity of decellularized tissue-engineered heart valves in a non-human primate model conducting an 8 weeks follow-up study[7]. They showed for the first time a remarkable and rapid cellular repopulation of the decellularized constructs and high remodeling capacities, proving how such an approach would be feasible for a translation into the clinical practice. The different decellularization protocols described in literature are proven to preserve the resident ECM with its mechanical characteristics[44] and to remove all cells entrapped in the tight, low porosity and branched protein network[45]. The native ECM is characterized by a complex protein structure. In order to preserve matrix integrity and functionality and to maintain the construct biosafety protease inhibitors are use in concomitance with a nucleic acid digestion step[46].

1.1.4 Cells for cardiovascular tissue engineering

Beside the choice of a proper biomaterial, an additional variable has to be considered to ultimate the production a TE construct: the cell type(s) seeded within the scaffolds. Moreover, it has to be considered whether the construct will have a single cell type composition or will be produced in co-culture (e.g. myofibroblasts and endothelial cells). The cell types used for manufacturing a TE tissue should be of easy isolation from the donor via a non-invasive procedure or derived from surgical waste material. Importantly, the cells should be of autologous origin, non-immunogenic and with pronounced plasticity.

Despite the difficulties in finding the cell type encompassing those ideal characteristics, many improvements have been done in research on the best candidates[47], including the attempt to understand the real requirements of scaffold seeding. Recent discoveries proved that circulating blood cells or cells from adjacent tissues can easily migrate and grow within the scaffold *in vivo*[48]. However, considering the case of the scaffold implantation alone, further challenges have to be approached such as the issue of immune response activation by foreign material or by

danger-associated molecular pattern molecules (DAMPs) that are released into extracellular space by necrotic cells in the growing tissue[49]. A wide panel of cell types have been investigated for TE as cells from vascular origin, adipose tissue, umbilical cord, chorionic villi, amniotic fluid or cells directly differentiated from patient's induced pluripotent stem cells (iPSCs). Herein, we focus on the mostly used and most promising sources for cardiovascular bioengineering.

1.1.4.1 Cells from vascular origin

Cells harvested from vascular donor tissues (e.g. from peripheral arteries, saphenous vein), and combined co-cultures of vascular cell populations are so far the preferred approaches for scaffold seeding in experiments with TE vessel[6]. Usually, two main cell lines are isolated from donor tissue: myofibroblasts and endothelial cells (ECs). The first are responsible for the ECM deposition while the second serve in establishing a tightly interconnected and confluent cellular layer in the inner lumen of the TE vessel or in the outer layers of the tissue engineered heart valves. The advantage in choosing these cell types as a seeding option is that they can be directly harvested from the vessel of the recipient patient. However, this implies the use of an invasive procedure. For this reason, big efforts have been done in optimizing the isolation and use of the circulating endothelial progenitor cells (EPCs). EPCs were identified by Asahara et al.[50] in peripheral blood and then proposed as potential cell source for TE. The use of these cells allows a milder and non-invasive isolation procedure, making them a highly attractive alternative to cells derived from tissue explants. Nevertheless, EPCs were employed for *in vitro* production of tissue engineered heart valves and their potential to provide both interstitial and endothelial function was confirmed[51].

1.1.4.2 Cells from the umbilical cord

The human umbilical cord protects and insulates umbilical blood vessels, namely one umbilical vein and two umbilical arteries. These vessels are embedded in mucoid Wharton's jelly, a substance of gelatinous consistency derived from extra-embryonic mesoderm. The latter is today recognized as a great source of mesenchymal progenitor cells (MSC), peculiar adult stem cells retaining the potential of multi lineage differentiation and being of particular interest for tissue engineering applications[52].

The umbilical cord is one of the best cell sources for cardiovascular tissue engineering since cells with different phenotypes that can be ultimately retrieved from it. Not only Wharton's jelly MSCs can be isolated from umbilical cord but also human umbilical vein endothelial cells (HUVECs) and myofibroblasts (HUVMs). Endothelial cells and myofibroblasts can also be isolated from both umbilical arteries and EPCs from the umbilical cord blood[53, 54]. An additional advantage in comparison to the cells from vascular origin derived from adult tissues is the possibility of umbilical cord cryopreservation, providing a life-time, expandable cell source.

1.1.4.3 Stem Cells as promising cell source for tissue engineering

Stem cells are one of today's most attractive options for cardiovascular tissue engineering mainly because of their high growth rate and potential allowing for fate tuning towards different cell types such as endothelial cells, fibroblasts/myofibroblasts and smooth muscle cells[55]. Mesenchymal stem cells, for example, share huge similarity in phenotype compared to heart valve interstitial cells and were proven to stimulate *in vivo* endothelialization and recruitment of autologous host cells by paracrine secretion[56]. Bone marrow and adipose - derived stem cells (BMSCs and ADSCs), among the others, have been widely studied as cell source for TE. They are currently used for the production of tissue engineered heart valves, showing excellent *in vivo* functionality, native like histological profile and ECM organization[57, 58]. However, MSCs have indeed a higher cellular potency compared to BMSCs and ADSCs and can be isolated without severe interventions (from e.g. by puncturing the iliac crest).

One of the most important goals in tissue engineering is the prevention of *in vivo* tissue deterioration and calcification combined with the maintenance of intrinsic growth and regeneration capacity. In accordance with this goal, the best cell candidates for are embryonic stem cells (ESCs). ESCs are pluripotent, undifferentiated and self-renewing cells, able to generate all the adult terminally differentiated cell types, with the exception of extraembryonic tissues[59]. During the embryonal development, at the blastocyst stage, a small number of cells constitutes the inner cell mass (ICM), which then further differentiates into the three germ layers (endoderm, mesoderm and ectoderm) that are considered to be the developmental starting point for the formation

of adult tissues. ESCs are directly derived by the expansion of the ICM *in vitro*. Despite the initial success, the use of ESCs has been associated with with ethical issues and with immunogenic and tumorigenic problems[60]. In the last years another interesting stem cell source has become available thanks to the studies of Takahashi and Yamanaka[61]. They demonstrated the possibility to reprogram terminally differentiated cells, as mouse fibroblasts, to a multipotent status, obtaining induced pluripotent stem cells (iPSCs). The use of iPSCs for tissue engineering could potentially overcome the ethical problems associated with embryonic stem cells due to their non-embryonic origin. However, since they retain a gene expression profile close to the one of ESCs, they are still associated with high risk of tumor formation. The research in this field is now focusing on new transdifferentiation approaches, allowing the direct production of the desired cell type (e.g. endothelial cells) from another (e.g. skin fibroblasts) by adjusting and fine-tuning the biochemical environment and overcoming the harmful iPSC transition step[62].

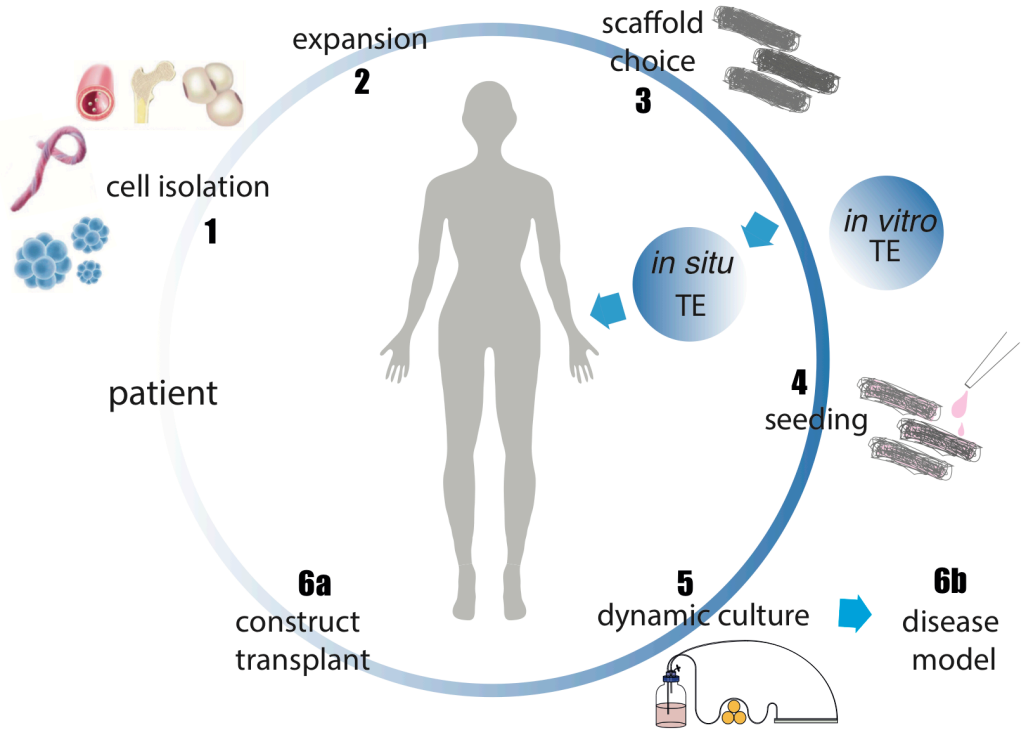

Figure 1. Tissue engineering in short. Cells are isolated from a tissue donor or from the patient himself (1) and expanded via *in vitro* culture to achieve a proper cell number (2). Upon the choice of a proper scaffold (3) the construct is either seeded with a suitable cell type (4) or directly implanted into the patient for *in situ* tissue engineering. When the *in vitro* strategy is chosen, the construct is cultured in a dynamic environment (5) and finally implanted (6a) or used to model the relevant diseases (6b).

1.2 Atherosclerosis - causes and consequences

Atherosclerosis is a life threatening vascular pathology characterized by the accumulation of a fatty plaque in the vascular sub-endothelial space [63]. Atherosclerotic plaque formation is influenced by the synergistic interplay of different risk factors such as sex, age, genetic predisposition, high blood pressure and high levels of LDL [64, 65]. Being a vascular pathology, atherosclerosis can affect different organs of the human body. Stenotic arteries can indeed lead to coronary artery, carotid artery and chronic kidney disease and, in the worst case, to acute ischemic events and stroke[66]. Given this preamble, it is not surprising that in 2010 atherosclerosis caused 1 death out of 4 worldwide [67]. The following paragraphs describe the pathomechanisms of atherosclerosis and focus on todays' approaches, including tissue engineering strategies, for the treatment of heart failure and acute ischemic events caused by the disease.

1.2.1 Development of atherosclerotic plaques

Atherosclerosis is a chronic inflammatory disease but its causative events and phatodynamics are still not clearly understood. Atherosclerotic plaque deposition starts with a small inflammatory lesion in the sub-endothelium witch is triggered by (i) variations shear stress on the vessel lumen[68] and (ii) by local accumulation of LDL and its modified versions (e.g. oxidized, acetylated)[69]. It is not yet understood which of these triggering events comes first or if both events are equally contributing to plaque formation. The process of plaque formation is progressive and reversible [65, 70]: it can be counteracted by a reduction of the modifiable risk factors mentioned above or promoted by their persistence.

The formation of a well-structured plaque microenvironment results from the interplay of cholesterol-rich lipoproteins, endothelial cells, monocytes, macrophages, dendritic cells and fibroblasts in a complex matrix milieu [71]. Plaque formation is initiated by patrolling monocytes, aggregating in the sub-endothelium. Monocytes and other circulating cells from the innate immune system, are recruited by the endothelial cells in the lumen through exposure of adhesion proteins such as intercellular adhesion molecules (ICAMs) and vascular adhesion molecules (VCAMs)[72]. After their

recruitment, monocytes extravasate in the sub-endothelium and are exposed to accumulating low density lipoproteins. Here, differentiation occurs towards either (i) antigen presenting cells (APCs) or (ii) macrophages. The first, beside contributing in LDL clearing, exacerbate inflammation by locally recruiting cells from the adaptive immune response[73]. The second, upregulate the production of scavenger receptors as scavenger receptor class B member 3 (SCARB3 also known as CD36) and scavenger receptor A1 (SRA-1)[74]. The scavenger receptors are responsible for clearing cell debris, LDL and its modified forms. Ultimately, these events result in the formation of the foam cells, a hallmark of the atherosclerotic plaque[75]. The foam cells, not only secrete proinflmmatory chemokines and cytokines promoting further recruitment of inflammatory cells, but also release macrophage retention factors (such as netrin 1 and semaphorin 3E)[76]. These retention factors counteract efferocytosis, namely the clearance of apoptotic or necrotic cells, and prevent the emigration towards the adventitial lymphatics. The result is a growing niche characterized by a necrotic core, foam cells and chronic recruitment of inflammatory cells from both innate and adaptive immune response.

At late developmental plaque stages, the inflammatory niche appears as a well-structured microenvironment[71]. In particular, smooth muscle cells from the tunica media engulf the niche by migrating at its perimeter and differentiating into myofibroblasts[70]. The “fibrous cap” is formed. Myofibroblasts actively contribute to the niche stability though ECM deposition. In particular, myofibroblasts release collagen and glycosaminoglycans, acting as plaque stabilizers[77, 78]. When the necrotic core increases in size, the intra-plaque titer of proteolytic enzymes is incremented. Among these enzymes, matrix metalloproteinases (MMPs) seem to be, in fact, the main responsible for plaque rupture[79].

When a rupture occurs, the exposure of tissue factor in the vascular lumen triggers the coagulation cascade. Here, depending on the arterial branch where the rupture occurred different scenarios are possible: 1) the rupture is healed and re-endothelialized, increasing vessel stenosis by reducing the lumen diameter and incrementing blood flow turbulence at the plaque site[80]. 2) The rupture causes the formation of blood clot that can detach and travel along the vessel and, eventually, interrupt the blood flow and the oxygenation of downstream tissues. If the

atherosclerotic plaque was originally localized in the branches of coronary arteries, scenario number 1 would have led to heart failure, while scenario number 2 to an acute ischemic episode.

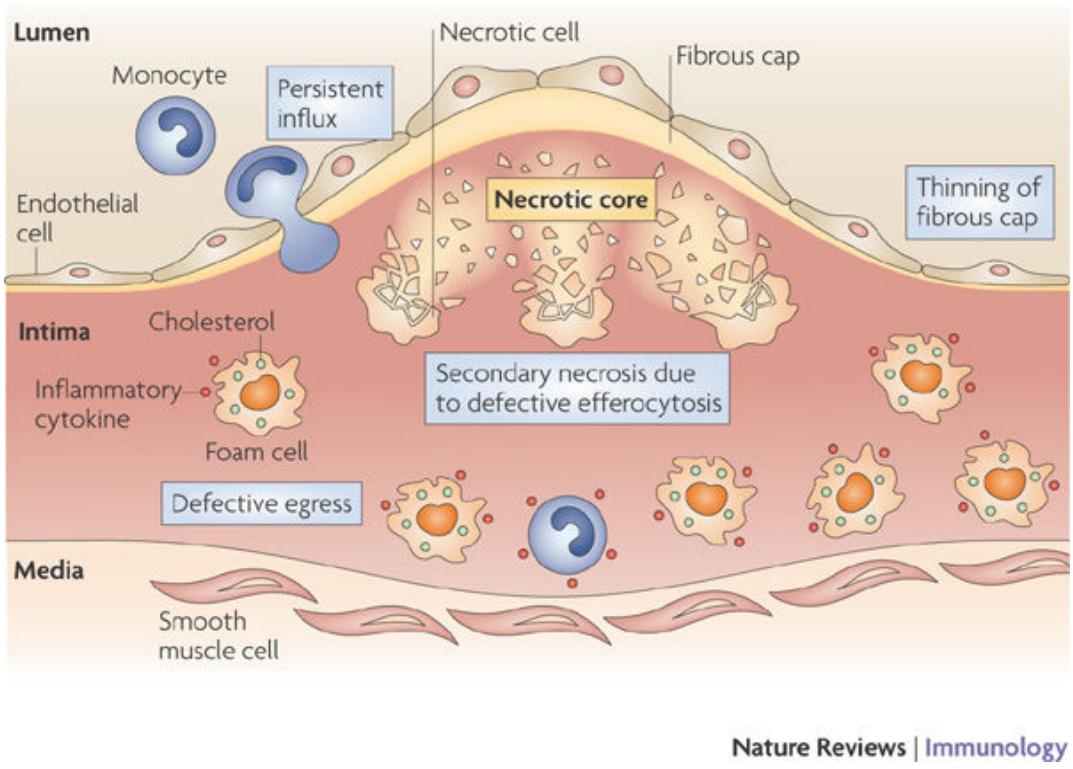

Figure 2. Atherosclerotic plaque development. From Tabas I. *et al.* (2010)[1]. Plaque development is fostered by a persistent recruitment of monocytes in the intima layer. Here, monocyte phagocyte LDL in its native and modified forms, accumulate cholesterol in the cytoplasm and differentiate into lipid-rich cells (foam cells). Foam cells contribute to plaque development by releasing inflammatory cytokines and persisting within the inflammatory niche. Moreover, foam cells fail in phagocyting cell debris and promote the formation of a necrotic core. The release of enzymatic content from dead cells triggers the thinning of the myofibroblast fibrous cap, preamble of plaque rupture.

1.2.2 Cardiovascular disease and atherosclerosis

Cardiovascular disease includes a plethora of disorders affecting the cardiovascular system comprising, among others, heart failure (HF). Frequently, HF is caused by coronary artery atherosclerosis and can lead to acute ischemic episodes (IHD). Due to poor or absent post-ischemic reperfusion of the infarcted myocardial areas, a significant number of cardiomyocytes undergoes apoptosis and is replaced by fibrous scar tissue. The relative unpredictability of acute cardiovascular events, the high mortality rate and the absence of a durable post-ischemic treatment, endorse IHD to one of the most critical clinical hurdle of this century. The long-term survival of patients with heart failure is compromised by a series of complications as the massive proliferation of non-contractile fibrotic tissue in the infarcted areas. Additionally, after acute ischemic episodes, patients endure life-changing treatments ranging from daily medications to surgical interventions as pacemakers, stents, angioplasty or heart transplants.

In this context, regenerative medicine and tissue engineering can be considered as innovative and valid treatment alternative. The identification of progenitor cardiac cells within the adult human heart [81] encouraged the enthusiasm for cell-based regenerative therapies [82-84]. Moreover, the evidence that exogenous cells injected in the myocardium could minimally promote the formation of functional contractile tissue in the scarred areas provided an important contribution in directing the preclinical research towards the investigation of possible new treatments [85]. Despite the recent advances of basic research in the field, the detailed architecture of cardiac repair response upon ischemia is currently not clear. The presence of progenitor cells capable of a local and limited regenerative activity in the adult heart inspired the study and development of both (i) cell-based technologies and (ii) strategies for paracrine stimulation of the resident cardiac progenitor cells. The next paragraphs will introduce and discuss both regenerative approaches.

1.2.2.1 Cell-based Regenerative Technologies: from single-cell to bioengineered microtissues

Over the past decades preclinical and clinical investigations of cell-based technologies for the treatment of the infarcted heart have been carried out. Different cell-candidates were evaluated *in vitro* and are now under investigation for a possible therapeutic use. Examples are autologous *in vitro*-expanded cardiac progenitor cells (CPCs) and autologous adipose or bone marrow derived MSCs [86]. Despite clinical trials based on the intra-myocardial injection of single-cell suspensions have been performed with mesenchymal autologous cells, the interpretation of the results is controversial and roused questions and doubts regarding the power of the technology [87-89]. There is currently a consensus regarding the possible reasons for the single-cell suspension therapy failure; the negative results are addressed to the scarce survival and retention of the cells at the level of the infarcted area [90]. The newest regenerative approaches aim at enhancing survival, grafting and retention abilities of the injected cells using different methodologies. An example is provided by the cutting-edge bioengineered microtissue technology. Microtissues are scaffold-free tissue engineered spheroids generated via hanging drop technique. These microstructures a reproducible with different cell types like CPCs, bone marrow and adipose tissue derived mesenchymal stem cells (Figure 1) [84] and have been tested in a pilot study on infarcted porcine models exhibiting promising results [91]. Other methods currently investigated for increasing cell retention in the infarcted areas include (i) the combination of single cell suspensions with nanoparticles loaded with functional agents [92], (ii) the injection of a compact mixture of cells pre-cultured in hydrogels [93] or (iii) the injection of cell-free hydrogels functionalized with paracrine mediators [94].

1.2.2.2 Paracrine Stimulation of Resident Progenitor Cells

The self-regenerative ability of the adult heart is per-se inefficient in stimulating the functional replacement of necrotic areas and preventing the formation of fibrous tissue after myocardial infarction. Regenerative mechanisms demand tailored triggers that are provided by cell-cell communication. It is known that epicardium and endocardium share a communication network based on vesicular exchange [95]; cells can indeed

exchange information by packing and delivering ribonucleic acids and proteins within micro-vesicles known as exosomes (EVs) [96-98]. A branch of recently developed regenerative technologies adopted this mechanism of cell-cell communication to stimulate and increase the physiological regenerative processes upon injury. The EVs vesicular content varies according to environmental clues (i.e. hypoxic conditions or acute myocardial infarction) and provides growth factors, anti-apoptotic and angiogenic as well as mitogenic signals. In detail, EVs are predominantly enriched in microRNAs (miRNA), small non-coding RNA molecules with the function of post-transcriptional regulators [99]. Cardiomyocyte-specific extracellular factors and miRNAs (e.g. miR-1, -133 and -206) are key regulators of cardiac function and are released in high concentrations upon heart injury, exerting their regulatory role on the surrounding cells [100, 101]. The beneficial and synergic function of specific combinations of miRNAs on CPCs has been proven together with the hypothesis that miRNA families can be selectively secreted into the extracellular environment via exosomes [102, 103]. The recent EV-inspired regenerative technologies focus either on the (i) drug-exerted stimulation of cardiac progenitors [104, 105] or on the (ii) *in situ* miRNA targeted delivery [106]. Different studies contributed to the development of these technologies, like the *in vitro* and *in vivo* investigation of the secretome and extracellular vesicular content of mesenchymal stem cells. These studies led to the discovery of new cardio-protective molecules [107-110]. In this regard, Timmers et al. showed in 2007 the beneficial effects of MSCs-conditioned medium upon injection in a pig model of ischemia/reperfusion, reporting a significant reduction in the ischemic myocardial area after the treatment [109]. More recently, the secretome of human amniotic membrane-derived mesenchymal stromal cells was injected in infarcted rat models, leading to a reduction of the ischemic area and ventricular remodeling [107]. Although these promising studies are still at the preclinical level, have the potential to shorten the distance from clinical trials to a possible therapeutic approach in humans [111].

1.2.2.3 Considerations on future therapeutic directions

It is possible to identify few promising future directions for the treatment of HF and IHD and other cardiovascular diseases caused by atherosclerosis. One of them is (i) the

idea of replacing/combining stem cell-based therapies for the infarcted heart, with an intra-myocardial injection of a cardioprotective cocktail. Other intriguing strategies are (ii) the use of microtissues as a possible alternative to cell therapy performed with single-cell suspensions and (iii) the tissue engineering technology. The first is considered a promising cell-delivery system for enhancing cellular engraftment and survival in the infarcted myocardium. The second aims at revolutionizing the field of cardiac regeneration by promoting the use of decellularized tissues for enhancing *in situ* tissue formation. Finally, (iv) new drugs for effective treatment of atherosclerosis need to be designed to prevent, mitigate or block cardiovascular diseases at their early stages. For this purpose, optimal *in vitro* human cell- based tissue engineered models for atherosclerosis need to be introduced in preclinical investigations, for drug design and screening.

1.3 Modeling atherosclerosis

Since 1856, when R. Virchow described first time the human atherosclerotic plaque, there has been the need to develop disease models to gain a better insight on the pathomechanisms driving plaque formation[112]. However, the first experiment to investigate atherosclerosis development was conducted about 50 years later by the Russian Ignatowski, who used rabbits as *in vivo* model[113]. From then on, different *in vivo* and *in vitro* models of atherosclerosis were proposed and are still employed in today's research. The following paragraphs summarize the large number of atherosclerosis *in vivo* and *in vitro* models that can be found in literature. In particular, models that allowed key discoveries in the field are presented.

1.3.1 *In vivo* models

The cellular mechanisms underlying plaque formation and regression have been investigated *in vivo* in both small and large animals, and predominantly in hypercholesterolemic mice with knock-out of either Apoe or LDL-receptor [114-116] or in non-human primates [117, 118].

Historically, rabbits were the first animal model to be employed for atherosclerosis studies. Due to their peculiar physiology, rabbits fed with a balanced chow are *per se* not prone to manifest the disease. For this reason, at the time where transgenic animals were not available, watanabe hereditary hypercholesterolemic rabbits (WHHL) and New Zeland white rabbit (NZW) were employed[119] . WHHL are characterized by a mutant LDL receptor and were used by Goldstein and Brown for their discoveries concerning the regulation of cholesterol metabolism and for understanding the basis of familial hypercholesterolemia. The New Zeland white rabbit (NZW) are particularly sensitive to high cholesterol diets and are prone to plaque accumulation. More recently different transgenic rabbit models were employed as apolipoprotein E II (apoEII) and apolipoprotein B-100 (apoB-100) [120, 121]. The main advantages in using rabbit model over mice and rats reside in the fact that rabbits: (i) are LDL-animals like humans, meaning low density lipoprotein is the most abundant lipoprotein in circulation; mice and rats are high-density lipoprotein (HDL)-animals instead. (ii) Rabbit develop cerebral and coronary lesions similar to human, whereas

mice do not. Criticisms in using rabbits for atherosclerosis research are linked to two main facts: (i) unlike in human plaques, rabbit plaques are solely constituted by foam cells and (ii) once rabbits are under high-cholesterol chow (more than 1% cholesterol for a long period), their cholesterol concentration is too high in the plasma (exceeding 2000 mg/dl) and it is not comparable even with the levels measured in hypercholesterolemic human patients, and show unusual foamy lesions in the aorta. Despite that, rabbits are still used for the investigation of lipid lowering drugs and for the development of imaging/diagnostic tools[113].

Mice showed to be a great model for investigating the molecular mechanisms of disease pathogenesis. Among dozens of mouse models available to study atherosclerosis, three of them were crucial for elucidating key atheromechanisms such as the role of macrophage colony-stimulating factor (M-CSF), scavenger receptors as CD36 and SRA-1, and acyl–coenzyme A cholesterol acyltransferase (ACAT). The ApoE -/- model is one of them, showing spontaneous disease onset on normal diet but the severity of the disease never reaches plaque rupture[122]. The Ldlr -/- mouse shows disease onset only on western-type diet but the lesions have a quite long development time [123]. Finally, the Ldlr-/- recombination activation gene (RAG)-/- led to the discovery that adaptive immune system is not obligatory required for plaque formation[124]. In addition to the limitations in using mouse models in atherosclerosis studies that were presented in the previous paragraph, mice also show limited tissue availability and generate technical difficulties, due to their small size. Moreover, being HDL-animals, wild type mice are relatively atherosclerosis resistant[125].

Thanks to shared anatomical similarities in the vascular system to human and due to their big size, pigs are considered a very good model to investigate pathological hemodynamics and responses of endothelial layer, and for designing and testing imaging and diagnostic tools[126]. Being so similar to humans, their lesions often do not progress beyond foam cell lesion formation within a reasonable time-frame, therefore, strategies to overcome this obstacle have been developed as: (i) selecting for natural genetic mutations, (ii) introducing other risk factors for atherosclerosis and, most recently, (iii) performing genetic engineering in the Yucatan minipig model[127, 128]. An outstanding example of genetic engineering in pigs was conducted by Davis

et al. in 2014 where the targeted knock-out of the Ldlr gene allowed to obtain hypercholesterolemic pigs[129].

Other large animals employed for the investigation of atherosclerosis pathomechanisms are non-human primates. They are optimal models due to their outstanding resemblance to humans, spanning from close genetical homology to similar omnivorous diet, anatomy, metabolism and aging processes[130]. Studies conducted in Rhesus monkeys allowed to prove that plaque can regress upon drastical changes in diet[131]. Moreover, investigations performed in cynomolgus macaques demonstrated that there are connections linking atherosclerosis gender and social behavior[132]. Other studies compared LDL profiles, density and molecular weight among non-human primates and between human and non-human primates. The first were especially conducted on African green monkey and cynomolgus monkeys and concluded that, despite ApoB-100 was the major apoprotein in both species, as it is in humans, LDL sub-fractions of cynomolgus had lower densities and larger dimensions[133]. This characteristic promotes cynomolgus as one of the best *in vivo* model for human atherosclerosis together with chimpanzee [134]. Beside the significant ethical issue raised when such animals are involved in scientific studies, non-human primates are expensive to maintain and require long experimental periods[130].

In conclusion, the "perfect" animal model should be easy to purchase and maintain, of relatively small size for optimal handling, have a stable genetic background, being able to breed in the lab and develop the disease in reasonable time. In addition, the model should be an LDL-animal and share similarities to human in plaque composition and location. This implies that such animal should have anatomical structures comparable to humans and similar inflammatory response. The above requirements, at the moment, are impossible to find in a single animal. In fact, despite the stunning contribution to the field, major differences in anatomy, lipoprotein profiles and inflammatory mechanisms hampered the translation of results obtained *in vivo* to the human pathophysiology.

1.3.2 *In vitro* models

To overcome the translational gap, human cell-based co-culture *in vitro* models have been established and provided a first glimpse into the mechanisms and initial events of plaque deposition in humans [6, 135-137]. *In vitro* atherosclerosis models can be classified in two main categories: indirect and direct models. The first are characterized by two or multiple cell types without direct cell-cell contact, that can coexist within the same volume, the second are instead characterized by two or multiple cell types are in direct cell-cell contact[138]. Within these categories there are two main subtypes of model systems: (a) static and (b) dynamic culture systems.

Examples of relevant *in vitro* indirect models are conditioned media (CM) cultures, bilayer membranes (BiM) and transwell co-culture models (TW). In CM cultures, different cell types are grown separately and the culture medium of one culture is later transferred onto a different cell substrate to investigate the reactions elicited. In the contest of atherosclerosis research such culturing method was used mainly to investigate the interactions between smooth muscle cells (SMCs) and monocyte/macrophages cultures, to study the process triggering MMPs production in plaque SMCs[139, 140]. BiM cultures allow closer proximity between the co-cultured cells and were principally employed to investigate interactions between cells from triple co-culture, namely SMCs, ECs and monocyte/macrophages[136, 141, 142]. Finally, in TW cultures one cell type is grown on the bottom chamber of the culture plate while the other is grown separately on top of a porous membrane insert. In atherosclerosis research TW systems were used to study cell-cell and cell-substrate interactions and, in particular, a majority of the studies carried out have examined SMCs proliferation, calcification and apoptosis[143-145].

Direct models for atherosclerosis encompass different types of cell-cell interaction happening at the same time as (i) cell-cell adhesion, (ii) cell-ECM contact and (iii) interactions between cell-soluble factors. Examples of such models are and gel-based co-cultures (GC) and tissue engineered (TE) constructs (with or without supporting scaffold material). GC methods create a biomimetic three-dimensional microenvironment in the culture dish, using scaffolds of synthetic and native hydrogels. These models are principally used for drug design and screening and aim at maximizing

the representativeness and the translation of the results obtained. GC-cultures mimic selected *in vivo* characteristics that influence drug distribution in a standardized and reproducible manner[146-148]. TE constructs share the same advantages of GC cultures but, in addition aim at avoiding cell co-cultures carried out in a well environment and rather provide a surrounding culturing system as similar as possible to the native conditions (bioreactor)[138]. TE models are the best available human-cell based atherosclerosis models. Such models were recently used to either investigate early lesion events, as monocyte anchoring at the endothelial surface and extravasating in the sub-endothelium[6] or to investigate cellular phenotypes within the biofabricated late-stage plaque microenvironment[149].

A side category of atherosclerosis *in vitro* models is based on the „on-a-chip" technology. Such models are based on the direct or indirect co-culture of two or more cell types in a Polydimethylsiloxane (PDMS)-based microfluidic chamber [150]. Despite these models ease the culturing process and facilitate imaging and drug testing they lack the complete „set" of vascular features. In fact, they do not retain the classical vascular morphology and ECM composition. The atherosclerosis models that will be discussed in the next chapters are human cell-based direct co-culture, TE models. The following table summarizes the state-of-the-art human cell-based in vitro co-culture direct models for atherosclerosis. Advantages and disadvantages are listed.

Ref.	Cell type	Culture system	Focus	Comments
[151]	Endothelial cells (EC), smooth muscle cells (SMC)	Static Direct	EC regulation of SMC proliferation in co-culture	Advantages: Presence of EC Disadvantages: No 3D culture, No LDL in culture medium, No monocyte/macrophages/dendritic cells
[141, 142]	EC, SMC, monocytes	Static Direct	Monocyte transmigration	Advantages: Presence of EC Disadvantages: No 3D culture, scaffold coated with gelatin (not physiological –like condition)
[139]	SMC, monocytes and lymphocytes (PBMCs)	Static Direct	SMC and monocyte interaction causing MMP secretion	Advantages: - Disadvantages: no ECs, presence of a gel scaffold, no investigation of lymphocytes function (useless for the model).
[152]	EC, SMC, PBMCs	Static Direct	Investigated role of Heme Oxygenase-1 in early atherosclerosis	Advantages: presence of cells from adaptive immune response (lymphocytes) Disadvantages: No 3D culture, no investigation of lymphocytes function (useless for the model).

[153]	EC, PBMCs	Static Direct	Reverse transmigration of phagocytes across endothelium	Advantages: presence of cells from adaptive immune response (lymphocytes) Disadvantages: No SMC, No 3D culture, no investigation of lymphocytes function (useless for the model), presence of a gel scaffold.
[140]	SMC, Thp-1 monocytes	Static Direct or Indirect (transwell)	Investigating MMp-1 production from SMC+ monocytes co-culture	Advantages: - Disadvantages: No EC, No 3D culture, No LDL in culture medium.
[154]	SMC, Thp-1 monocytes, PBMCs	Static Direct or Indirect (transwell)	Calcifying phenotype in SMC	Advantages: - Disadvantages: No EC, No 3D culture, No LDL in culture medium, no investigation of lymphocytes function (useless for the model).
[155]	SMC, monocytes	Static Direct	SMC apoptosis	Advantages: - Disadvantages: No EC, No 3D culture, No LDL in culture medium.
[156]	SMC, PBMCs	Static Direct	SMC proliferation	Advantages: - Disadvantages: No EC, No 3D culture, No LDL in culture medium.
[144]	SMC from different vascular origins, PBMCs	Static Direct or Indirect (transwell)	Influence of TNFa on SMC apoptosis	Advantages: SMC from different vascular origins Disadvantages: No EC, No 3D culture, No LDL in culture medium, no investigation of lymphocytes function (useless for the model).
[157]	SMC, Thp-1 monocytes, PBMCs	Static Direct or Indirect (transwell)	Monocyte differentiation and apoptosis	Advantages: - Disadvantages: No EC, No 3D culture, No LDL in culture medium.
[137]	EC, SMC, Monocytes and macrophages (Mono-Mac 6)	Static Direct	Study early atherosclerosis events	Advantages: presence of Macrophages Disadvantages: presence of a gel scaffold
[158]	EC, SMC, Granulocytes (PMN)	Static Direct	Sub endothelial infiltration and plaque destabilization	Advantages: presence of PMN Disadvantages: No monocytes, No 3D culture
[159]	EC, SMC from different vascular origins	Static Direct	Model healthy and diseased blood vessels based	Advantages: SMC from different vascular origins Disadvantages: No monocytes, No 3D culture, no LDL in culture medium
[160]	SMC, PBMCs, monocyte like cell line U-937	Static Direct	Inflammatory mediators produced by SMC+ monocyte co-culture	Advantages: - Disadvantages: No EC, No 3D culture, no LDL in culture medium
[161]	EC, SMC, PBMCs	Static Direct or Indirect (transwell)	Modulation of SMC behavior by macrophages	Advantages: - Disadvantages: No 3D culture

Table 1. Direct co-culture *in vitro* models of atherosclerosis.

Chapter 2

Adapted from:

Mallone, A., Gericke C., Hosseini V., Vogel V., Hoerstrup, S. P. and Weber, B. (2018) *Human cell-based tissue engineered small-caliber vessels for investigating early atheroma development*, (Manuscript in preparation)

In vitro bioengineering of the early lesion

2.1 Introduction and experimental setup

Atherosclerotic plaque development begins with the formation of a small lesion in the sub-endothelium where cells from the innate immune response engulf LDL in its native and modified state. Among different risk factors it has been shown that high LDL cholesterol levels and high blood monocyte count correlate with the progression of atherosclerotic lesions[162-165]. In this work we modeled, designed and produced a fluidic chamber for the culture of small-caliber tissue engineered vessels to serve as *in vitro* model for early-stage atherosclerosis. In order to biofabricate a construct as similar as possible to the coronary artery environment we first produced a tubular, biodegradable scaffold matrix of 0.5 mm in diameter. Second, we studied the flow within the chamber to investigate the best culturing conditions for the TE constructs. For this purpose, we established a computational fluid dynamics (CFD) model providing information on velocity, pressure and wall shear stress within the fluidic chamber. Third, we set up two different culturing environments to mimic either a (i) high-risk, athero-prone condition (190 mg/dl of LDL and $7x10^5$ monocytes/ml) or (ii) a low-risk condition (40 mg/dl of LDL and $5x10^5$ monocytes/ml)[166, 167]. We sampled the vessel after 3, 4 and 5 weeks of culture. We sorted and investigated the sub-endothelial monocyte-derived populations at each time point using flow cytometry coupled with t-distributed stochastic neighbor embedding data analysis (t-SNE)[168, 169]. In both low and high-risk culturing environments, we found a time-dependent increase of CD36, CD14 and SRA-1 positive monocyte-derived populations. Finally, we assessed the mechanical strength of fibronectin in the TE early lesion disease model

using bacterial fibronectin-binding peptide 5 (Fn-BPA5) which is able to bind to relaxed fibers, representing an indirect indicator of collagen I deposition in the ECM[170].

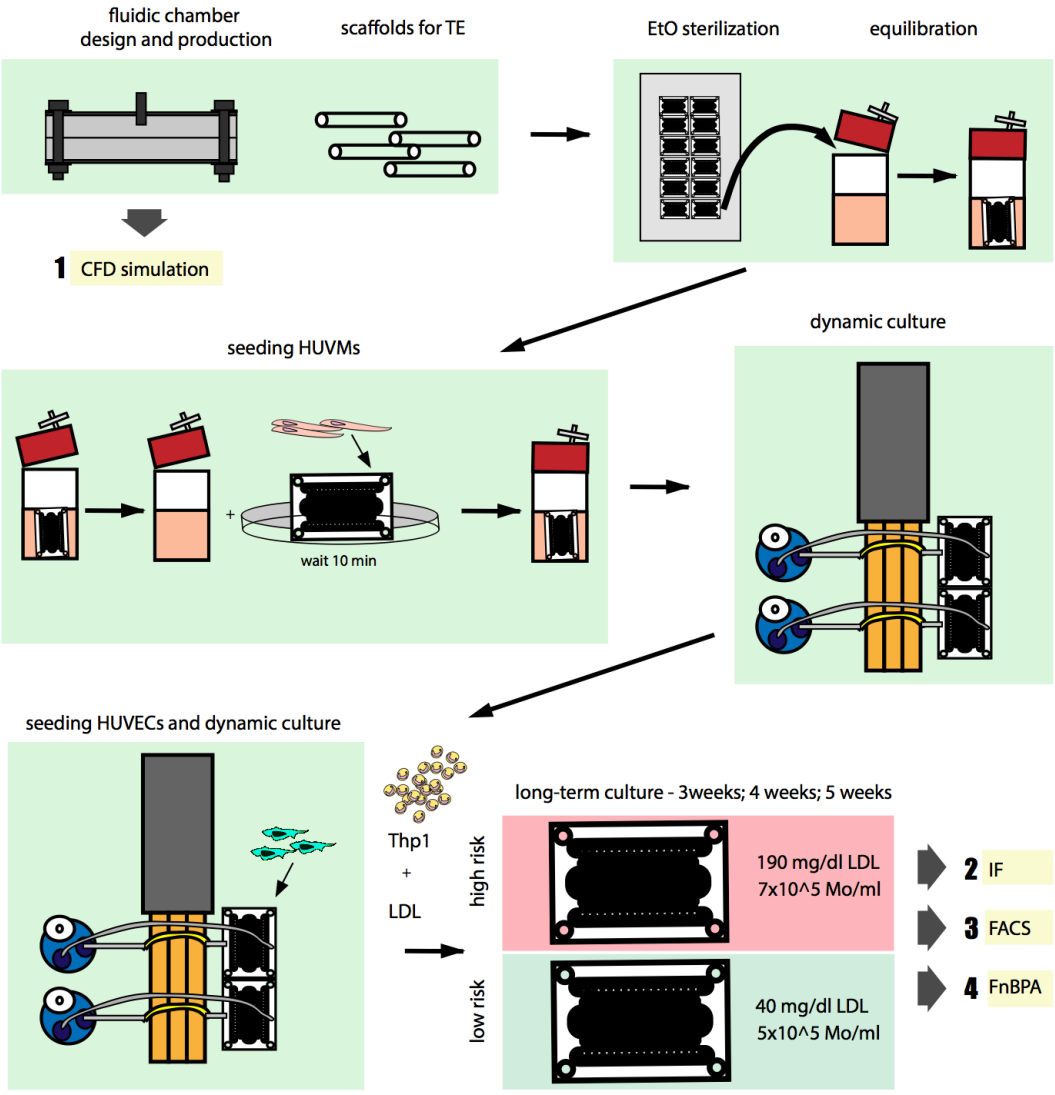

Figure 3. Graphical abstract: human cell-based tissue engineered small-caliber vessels for investigating atheroma development.

2.2 Material and methods

2.2.1 Isolation of endothelial cells and myofibroblasts

Human umbilical vein endothelial cells (HUVECs) and myofibroblasts (HUVM) were isolated from human umbilical cords. The tissues were processed following the guidelines described in the ethical allowance from Kantonale Ethikkommission Zürich (KEK-Stv-21-2006). Umbilical cords were stored at 4°C in Dulbecco's Modified Eagle's Medium (DMEM, Sigma) prepared with 10% Fetal Bovine Serum (FBS, Gibco), 1% GlutaMax (Gibco) and 1% penicillin/streptomycin (Penn/Strep, Gibco) for maximum 2h prior to processing. The umbilical vein was carefully extracted from the umbilical cord and the inner lumen was flashed twice with 1×PBS. The adventitia layer was discarded and the intima layer was gently detached by incubation with a solution of 1mg/ml collagenase/dispase (Roche) for 30 min in 1×PBS. The endothelial cells were collected by flashing 12 ml of M200 medium (Gibco) with low serum growth supplement (Gibco) and distributed in a gelatin coated 6 well plate. The endothelial cells were maintained in supplemented M200 medium for two weeks at 37°C, 5% CO_2 and 95% humidity and the medium was changed every 72h. The isolated endothelial cells were sub-cultured in larger vessels at about 80% confluence. The remaining media layer was minced into small pieces of approximately 2mm length and let adhere for 10min on the bottom of a petri dish. The tunica media fragments were then covered in DMEM medium and maintained at 37°C, 5% CO_2 and 95% humidity. The medium was replaced every 48h. After about 20 days myofibroblasts sprouting from the minced pieces reached about 80% confluence and were ready for sub-culturing.

2.2.2 Cell culture

HUVECs were cultured in supplemented M200 and the medium was replaced every 48h. At about 80% confluence HUVECs were detached using trypsin 0.5% (Sigma) for 2 min and seeded at a density of 5,000 cells/cm^2. HUVECs used for this study were expanded up to passage 2. HUVM were cultured in DMEM medium with 10% FBS

and 1% GlutaMax and the medium was replaced every 48-72h. For sub-culturing, HUVM were detached using trypsin 0.5% for 4 min and seeded at a cell density of 4,000 cells/cm^2. HUVM were expanded up to passage 5 prior to use for the experiments in this study. Human monocytic leukemia cell line (thp-1) isolated from the peripheral blood of a 1-year-old human male with acute monocytic leukemia, were purchased from Sigma. Thp-1 cells were cultured in suspension in xVivo15 medium and the medium was replaced every 2-3 days. Thp-1 cells were seeded at a density of 100,000 cells/ml and sub-cultured at a density of 800,000 cells/ml.

2.2.3 Scaffold preparation

Biodegradable tubular scaffold matrices (length 1.5 cm and inner diameter 0.5 mm) were fabricated using non-woven polyglycolic-acid meshes (PGA, Cellon) coated with a 1.5% solution of poly-4-hydroxybutyrate (P4HB, TEPHA Inc.) in tetrahydrofuran (THF, Sigma). Briefly, 1mm thick PGA foils were cut in rectangular shapes, brushed with the P4HB/THF solution on both sides and rolled onto an aluminum wire with an external diameter of 0.5 mm. The tubular shape was obtained by heat-sewing the rolled rectangular meshes at 80°C. The scaffolds were sterilized in 70% ethanol for 30 min and let dry O.N. in a sterile cell culture hood. Both extremities of the tubular mesh were glued on the fluid with a biocompatible 12.5% polyurethane (Sigma) glue in THF.

2.2.4 Tissue engineering

Scaffolds and fluidic chambers were sterilized with ethylene oxide plasma treatment, washed with sterile 1×PBS for 30 min and equilibrated O.N. in DMEM medium. HUVMs were seeded at a cell density of 6×10^6 cells/cm^2 using a fibrinogen: thrombin 1:1 hydrogel as cell carrier [171] and maintained for 6 days in static culture with DMEM medium. The medium was replaced every 24h. The chamber was then assembled for dynamic culture and maintained in a pulsatile flow generated by the Masterflex®exr peristaltic pump (ColeParmer, USA) with a velocity of 0.02 m/s for additional 6 days. During dynamic culture the DMEM medium was replaced every 48h and additioned with 1mM L-Ascorbic acid 2-phosphate sesquimagnesium (A2P).

HUVECs were seeded in the vessel lumen at a cell density of 1×10^5 cells/cm^2 using a 25G needle. After a short static incubation period of 24h in DMEM:M200 (1:1) medium, vascular constructs were exposed to dynamic culture in DMEM:M200 additioned with 1mM A2P for further 5 days. The tissue engineered mini-vessels were perfused for the 5 following weeks in DMEM: M200: xVivo15 (1:1:1) medium enriched with either (i) 190 mg/dl LDL (Lee Biosolutions) and $7x10^5$ THP-1/ml or (ii) with 40 mg/dl of LDL and $5x10^5$ THP-1/ml. The medium was replaced every 48h.

2.2.5 Design and CFD of the fluidic chamber

The fluidic chamber was designed using the 123D design software (Autodesk) and the resulting stereo lithography interface format (STL) file was used to manufacture the chamber using computer numerical controlled (CNC) milling. The chamber was milled in poly-methyl methacrylate while the external frame in aluminum. Details on the chamber design are described in Figure 5. For the computational fluid analysis (CFD) the chamber geometry was processed using the platform SimScale (https://www.simscale.com). The geometry mesh operation was conducted using the meshing algorithm Hex-dominant automatic, specific for internal flow. The fluid dynamic simulation was conducted on the obtained polyhedral mesh considering the system as incompressible fluid-based steady-state on a laminar turbulence model. The kinematic viscosity of the fluid of 9.3379e-7 m^2/s and a fluid density of 997.33 kg/m^3. The velocity at the flow inlet was set as 0.02 m/s. The solution fields were prost-processed in SimScale and the simulation results are accessible at https://www.simscale.com/projects/bf2af267032049/flow_in_a_chamber/ .

2.2.6 Flow cytometry

The tissue engineered small-caliber vessels were digested with 1mg/ml collagenase/dispase solution in 1×PBS for 15min at 37°C under continuous agitation. DNase1 was added to the cell suspension for at a final concentration of 0.1 mg/ml and

the tissues where incubate for additional 30 min. Cells were gently pipetted through cell strainers with the mesh size of 100 μm and through a 40 μm strainer (Falcon) and incubated for 5min at 4°C with magnetic beads coated with anti CD45 antibodies, according to the provider instructions (MACS Miltenyi Biotec). CD45+ cells were magnetically sorted, stained with Zombie Aqua™ fixable viability kit (BioLegend) for 5min and fixed over night at 4°C in a 1% Paraformaldehyde (PFA, Sigma) solution in 1×PBS. The single cell suspension was stained for 15min at room temperature in Fluorescence-activated cell sorting (FACS) buffer prepared with 5% FBS and 0.01% NaN_3 (Sigma) in 1×PBS with an optimized FACS antibody panel including: CD14-PerCP (#325631, Biolegend), CD16-Alexa 700 (#360717, Biolegend), CD11b-Alexa594 (#101254, Bioloegend), CD11c-PE-Cy5 (#301609, Biolegend), CD36-BV605 (#563518, Becton Dickinson) and SRA-1-PE (#REA460, MACS Miltenyi Biotec). Each antibody was previously titrated to establish the optimal working concentration. Samples were acquired using LSR Fortessa analyzer (Becton Dickinson) and signal compensation was performed using OneComp eBeads (eBioscience).

2.2.7 the vi-SNE workflow

The Flow Cytometry Standard (FCS) files obtained from the FACS analysis were pre-processed using the software Flowjo (FlowJo, LLC). First, the cell populations of interest were gated according to forward and side scatter parameters (FSC and SSC). Second, singlets and Zombie Aqua™ dye negative events were selected, representing the living cell population of interest. Data post-processing was performed using the R platform and the Cytofkit package. Briefly, pre-processed FCS files from each sample were loaded onto Cytofkit, randomly down-sampled to 1,000 events (ceil; n=1,000) and computed using t-Distributed Stochastic Neighbor Embedding (t-SNE) algorithm[172]. Each event recorded was positioned in a specific location of the high-dimensional space. The output was a vi-SNE biaxial plot where distances between events are representatives of cell proximity in high-dimensional rather than two-dimensional space. The proximity between events is based on similarities in surface marker expression levels. Different myeloid subsets were positioned in separate

regions in high-dimensional space according to surface marker similarities. Automatic gating of myeloid subsets was performed through a preliminary clustering step with PhenoGraph algorithm (k=42) and a following metaclustering step with FlowSOM algorithm (k=10). The output of the above-described vi-SNE workflow is a vi-SNE map for each sample analyzed using FACS. Different biological replicates from each sample were combined to obtain a cumulative vi-SNE map.

2.2.8 Immunofluorescence

The tissue engineered vessels were harvested, washed 3 times in 1×PBS and transferred O.N. at 4°C in a 4% PFA solution in 1×PBS. The samples were then washed in 1×PBS, transferred in a 25% sucrose (Sigma) solution for 6h at 4°C and embedded in OCT matrix (CellPath). The vessels were then cryopreserved at -20°C until usage. Slices of 5μm were cut, rehydrated in 1×PBS for 15min and stained with primary antibody vascular endothelial cadherin (#PA5-19612, Invitrogen) for 1h at 37 °C. Secondary antibody (anti-rabbit #A11008, Life Technologies) and phalloidin (#A12381, Life technologies) staining was performed for 1h at 37 °C. Nuclei were counterstained with DAPI (10 μg/ml) and the slides were mounted in Vectaschield® (Vector Laboratories). Images were acquired with the confocal microscope (Leica SP8). Image post-processing, specifically the choice of appropriate pseudo-colors, was performed using ImageJ.

2.2.9 Fn-BPA analysis

For the Fn-BPA staining, cryopreserved slides were rehydrated for 15 min in PBS and incubated for 1h in 10 μg/ml of FnBPA5-Alexa- 488 (ETH, Prof. Vogel's lab) peptide. The stained slides were washed 3 times in 1×PBS and stained with anti-fibronectin (#ab2413, Abcam) for 1h at R.T. followed by 3 washes in 1×PBS 1h at room temperature of secondary antibody staining (#ab6564, abcam). Nuclei were counterstained with DAPI (10 μg/ml) and mounted in Vectaschield®. Samples were imaged with an Olympus FV 1000 confocal microscope (Olympus AG, Switzerland) and Images were analyzed using Fiji-ImageJ. For investigating the Fn fibers in the TE

construct, the pixel area of FnBPA5-Alexa-488 signal intensity and of Fn-Cy intensity was calculated for each fiber. A mean of 10 fibers was imaged per experiment.

2.2.10 Statistical analysis

vi-SNE cluster counts, cluster median fluorescence intensity (MFI) and FnBPA5-Alexa-488 signal intensity vs of Fn-Cy5 intensity were analyzed using multiple comparison analysis. First, Gaussian distribution of the data was confirmed with Shapiro-Wilk normality test. Second, repeated measures (RM) two-way ANOVA with Sidak's multiple comparison test was applied. All statistical analyses were performed with GraphPad Prism Version 7, GraphPad Software, San Diego, CA, USA). Significance was accepted at $p<0.05$. All data are presented as mean ± s.d..

2.3 Results

2.3.1 Selection of the optimal tissue engineered vessel diameter and culturing settings

To bioengineer a culturing microenvironment fulfilling the native coronary arteries physiology we followed a twofold strategy. First, we investigated the optimal diameter that the TE vessel needed to have in order to develop a similar wall shear stress (WSS) to the one of coronary arteries using Masterflex®exr peristaltic pump. Second, we studied the flow turbulence within the fluidic chamber in order to establish a linear flow as starting condition for the computational fluid dynamic simulation. To study the intra-vessel WSS we investigated the flow velocity for each setting of the dynamic system employed (1-10). Therefore, we calculated the wall shear stress according to the formula below derived from the Newton's law.

$$\tau = \gamma \cdot \eta$$

Where τ is the shear stress measured in Pa, γ is the shear rate measured in s^{-1} and η is the dynamic viscosity of the fluid measured in Pa·s. The shear rate of a flow in a pipe is calculated with the formula:

$$\gamma = 8v/d$$

where *v* is the linear fluid velocity measured in m/s and *d* is the inside diameter of the vessel. Finally, the linear fluid velocity v is related to the volumetric flow rate and it is calculated with the following formula.

$$v = Q/A$$

Where Q is the volumetric flow rate measured in m^3/s and A is the area of the cross-sectional vessel area. We calculated the WSS values for each of the possible vessel diameter combined with each available setting of the bioreactor system employed (Table 2, Figure 4). From the WSS evaluation we selected the vessel diameter of 0.5

mm. To choose the best culturing parameters and in order to avoid bioreactor settings in which the flow is unstable and transitioning from linear to turbulent we calculated the Reynold's number for each setting (Table 3). For a flow in a pipe (or vessel) the Reynold's number (Re) is derived from the equation below.

$$Re = \frac{QD_H}{vA}$$

where Q is the volumetric flow rate measured in $m^3 \cdot s$, D_H is the inner diameter of the pipe measured in m, v is the mean velocity of the fluid in m/s and A is the pipe's cross-sectional area in m^2. Considering that the blood flow in the human coronary arteries reaches a velocity of about 5ml/min [173] and that, according to the Reynold's number, the flow resulted linear at that velocity in our system, we selected parameter 3.

	4 mm	2 mm	1 mm	0,5 mm
1	0,00066879	0,00535032	0,04280255	0,34242038
2	0,0066879	0,05350318	0,42802548	3,42420382
3	0,01110191	0,08881529	0,71052229	5,68417834
4	0,01738854	0,13910828	1,11286624	8,90292994
5	0,02407643	0,19261146	1,54089172	12,3271338
6	0,03076433	0,24611465	1,9689172	15,7513376
7	0,03745223	0,29961783	2,39694268	19,1755414
8	0,04414013	0,35312102	2,82496815	22,5997452
9	0,05082803	0,4066242	3,25299363	26,023949
10	0,05751592	0,46012739	3,68101911	29,4481529

Table 2. Wall shear stress for each vessel caliber and peristaltic pump setting.

setting	ml/min	Re (0,5mm)
1	0,3	15,16530179
2	3	151,6530179
3	5	251,7440097
4	8	394,2978465
5	11	545,9508644
6	14	697,6038823
7	17	849,2569002
8	20	1000,909918
9	23	1152,562936
10	26	1304,215954

Table 3. Reynold's number for each setting of the peristaltic pump.

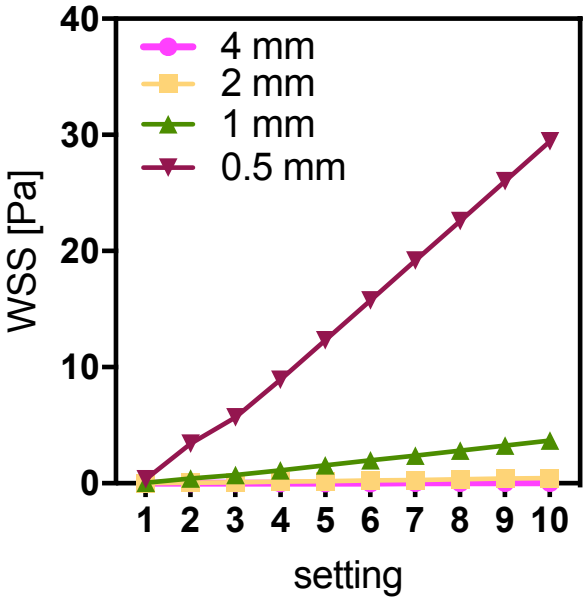

Figure 4. Wall shear stress for each vessel caliber and peristaltic pump setting.

2.3.2 Design and computational fluid dynamic model of the fluidic chamber

We designed a fluidic chamber that could bear the simultaneous co-culture of 16 vessels (Figure 5). We investigated the flow within the empty chamber to verify the presence of equal culturing conditions for each tissue engineered vessel. To do so, we processed the geometry of the inner fluid volume (Figure 5d) with the Hex-dominant

automatic mesh operation and we obtained a mesh of 1'588'550 nodes, 4'400'442 faces subdivided in 1'355'466 hexahedra, 8'861 prisms and 42158 polyhedra. For a successful simulation, we considered the system as linear, steady-state with incompressible fluid and established as a boundary condition the inlet flow velocity at 0.02 m/s. We simulated the first 100s of flow in the chamber and we imaged the simulation environment every 20s (Figure 6). We observed that the flow speed at the steady state is similar in every nozzle, being about 0.024 m/s, and is similar to the inlet flow velocity of 0.02 m/s (Figure 6a). The hypothesis of identical culturing condition can be proven also to pressure and shear stress, considering the identical values at the nozzles of c.a. 1.5 Pa and 2×10^{-4} Pa respectively (Figure 6 b, c).

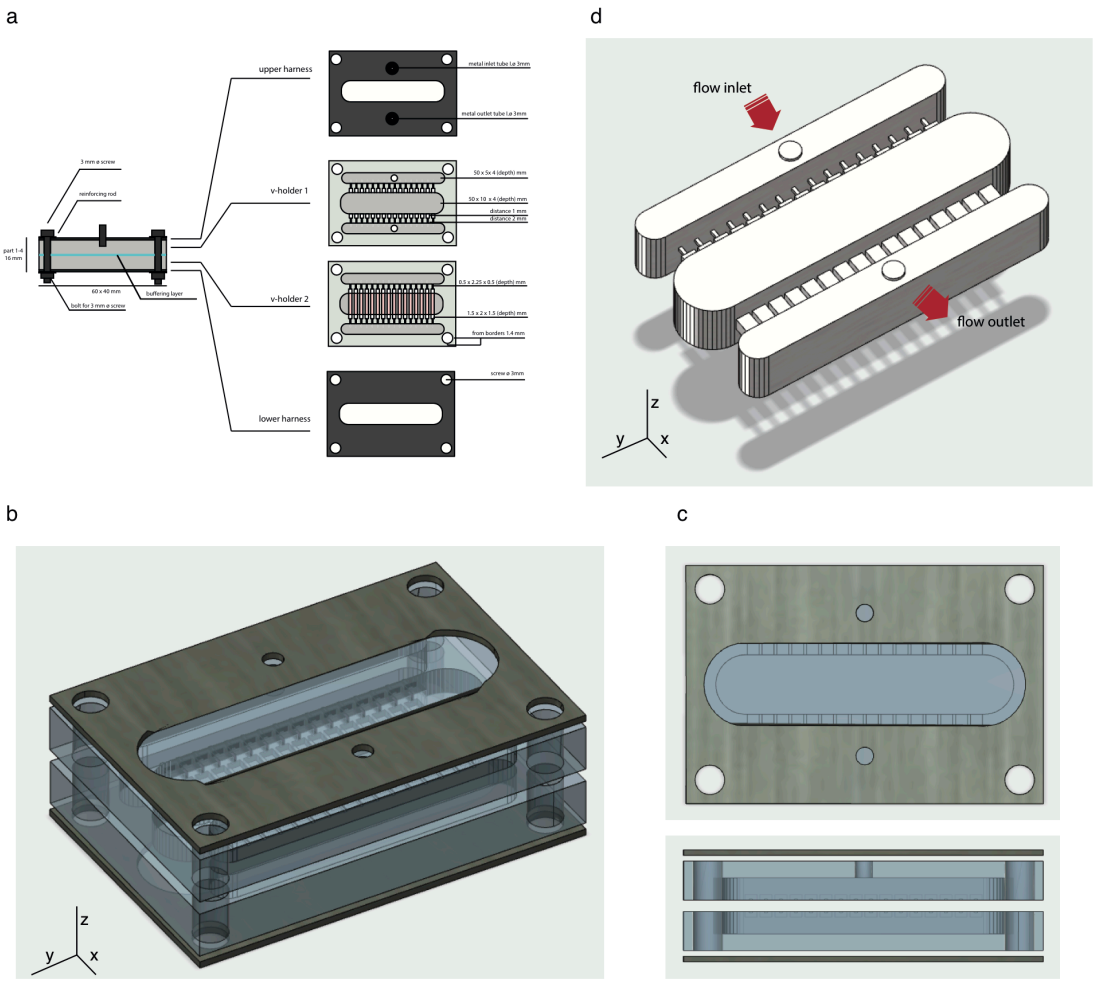

Figure 5. Fluidic chamber design and inner flow model. (**a**) Design of the fluidic chamber for the production of small-caliber TE vessels. (**b, c**) 3D view of the fluidic chamber in its assemblable components. (**d**) Inner flow model representing the volume occupied by the fluid within the chamber.

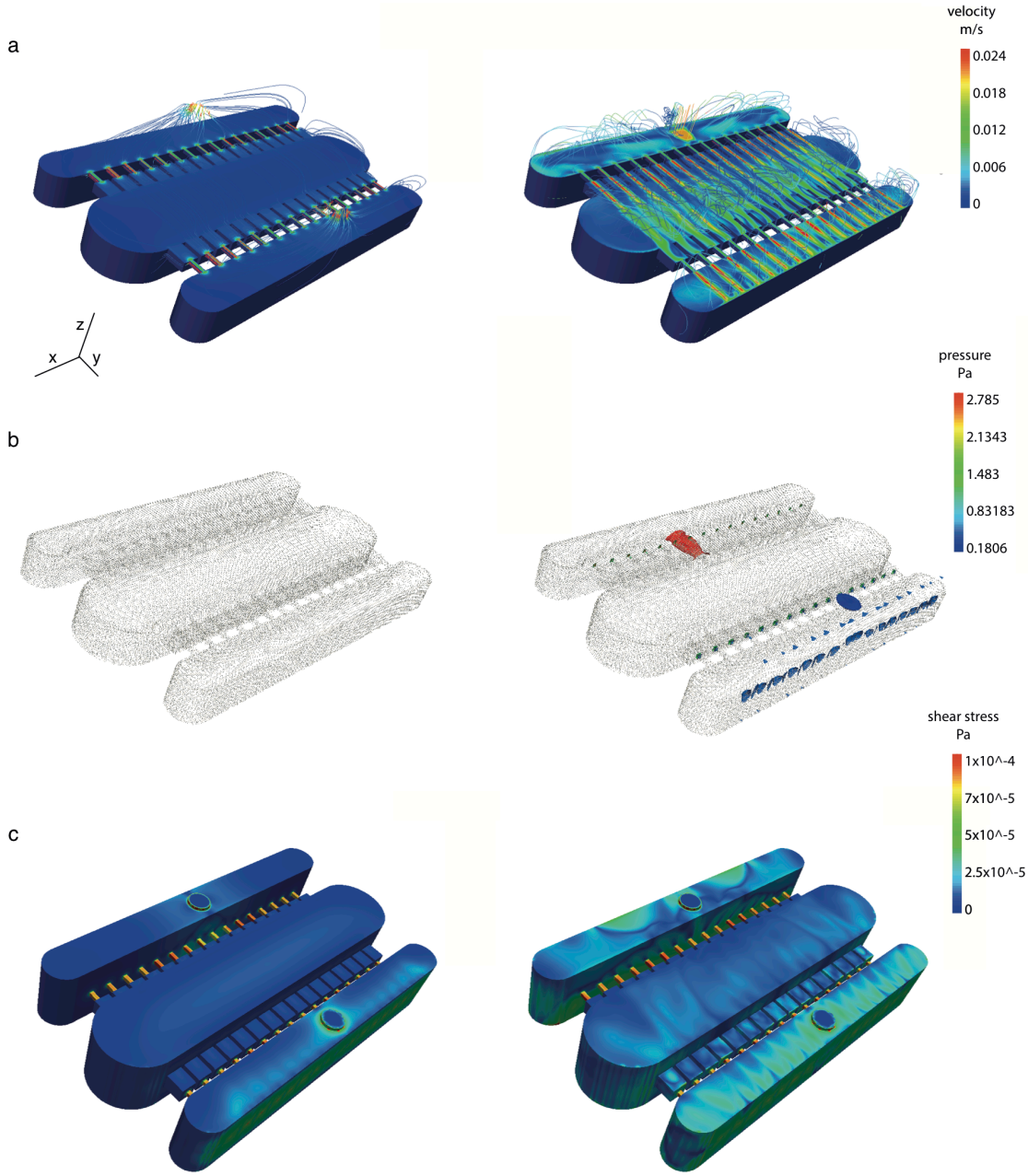

Figure 6. Simulation of the inner flow. The inner flow forces are reported here at the beginning (20s time-point, left side) and at the end (100s time-point, right side) of the fluid dynamic simulation. (**a**) Flow velocity, (**b**) pressure and (**c**) wall shear stress are reported.

2.3.3 Tissue engineered vessels architecture

The tissue engineered vessels produced within the chamber were sampled and inspected at the end of the dynamic culturing process. The vessels show excellent tissue formation (Figure 7a) characterized by high cellular density with extensive myofibroblast growth within the scaffold (Figure 7c, d) and endothelial cells forming a layer facing the inner lumen (Figure 7c). After 5 weeks of culture most of the vessels showed the formation of a thickened area close to the vessel outlet (Figure 7b).

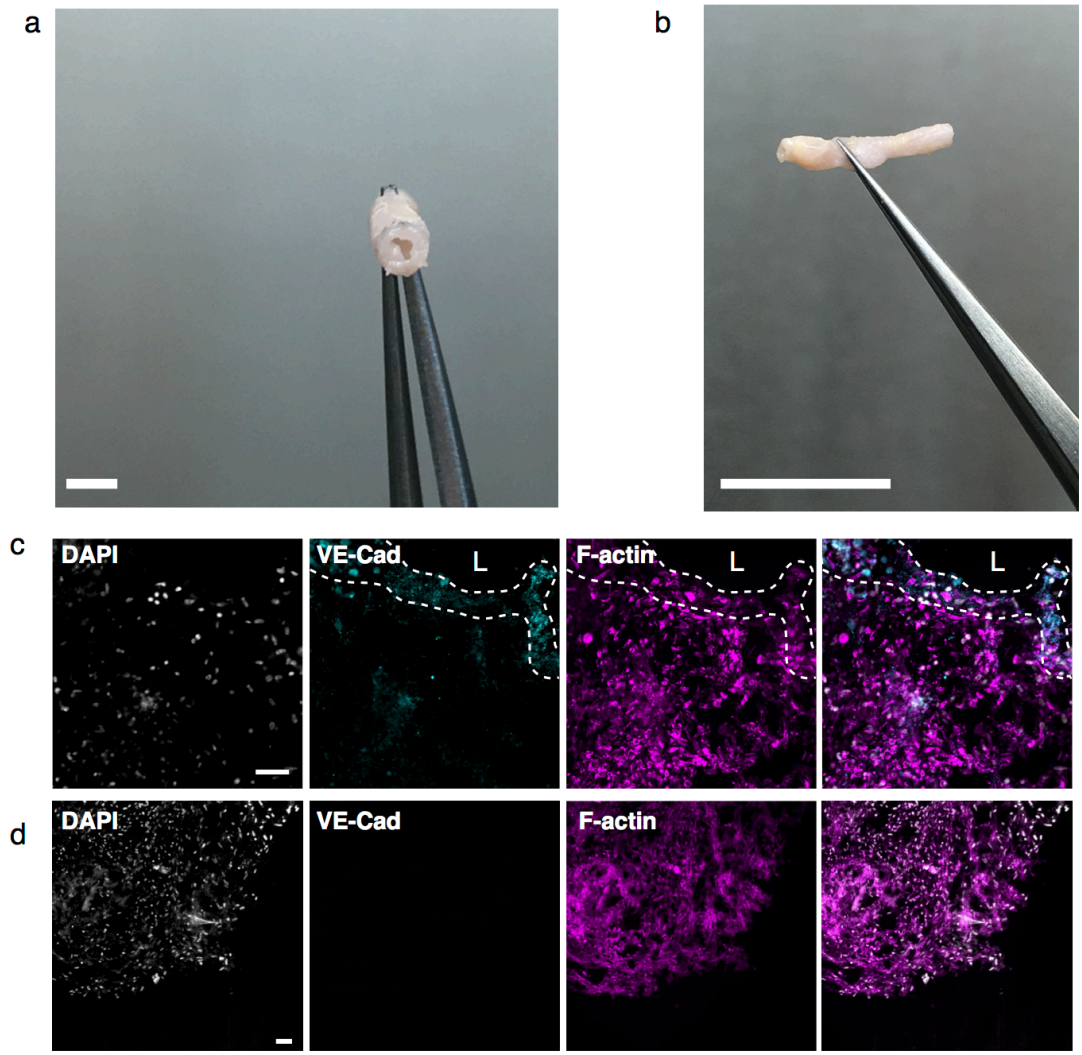

Figure 7. Small-caliber tissue engineered vessels. (**a**) TE vessel biofabricated using the fluidic chamber. Scale bar 1.5mm. (**b**) TE vessel after 5 weeks of culture in high-risk condition. Scale bar 1.5cm, (**c, d**) Vessel architecture with VE-Cadherin (VE-Cad) positive HUVECs and F-actin positive HUVMs. L = lumen. Scale bar 100 µm.

2.3.4 Time-dependent study of THP-1 derived populations within the TE vessels

To verify weather monocytes were extravasating in the TE vessel sub-endothelium and differentiating into phagocytic populations, we investigated the THP-1 derived populations within the vessel at different time points. We found that CD45+ cells not only were present in the vessel, but also they differentiated into scavenger populations characterized by high expression levels of CD36. Importantly, we compared the CD45+ populations within tissue engineered vessels cultured in a high-risk and low-risk environment. In both culturing conditions, we found that two populations, 4 and 7, were the most represented and together covered about 80% of the total number of events recorded (Figure 8). Importantly, population 4 retained a clear phagocytic phenotype, expressing $CD11b^{+}$, $SRA\text{-}1^{+}$, $CD14^{high}$ and $CD36^{high}$. Population 7 shows high expression of CD14 and CD36 but is negative for CD11b (Figure 9). We observed a significant increase of population 4 over-time in vessels cultured in both high-risk ($p=0.006$) and low-risk ($p<0.001$) condition while population 7 displayed no variation (Figure 8c). In cell-free scaffold controls cultured in both conditions we did not find any significant change over-time in population 4 and 7, despite we observed a tendency of population 4 to increase in cell-free scaffold maintained in the high-risk condition and of population 7 in scaffold cultured in low- risk condition (Figure 8c). When we took a deeper look in the median fluorescence intensity (MFI) time-dependent changes we noticed that population 4 showed a significant gain of CD36 from week 3 to 4 ($p<0.001$ both low and high-risk) and from week 4 to 5 ($p<0.001$ only high-risk) (Figure 10a). Moreover, we observed that population 7 had an over-time fluctuation of surface expression levels of CD14 and CD36, displaying their highest MFI at 4weeks (Figure 10b).

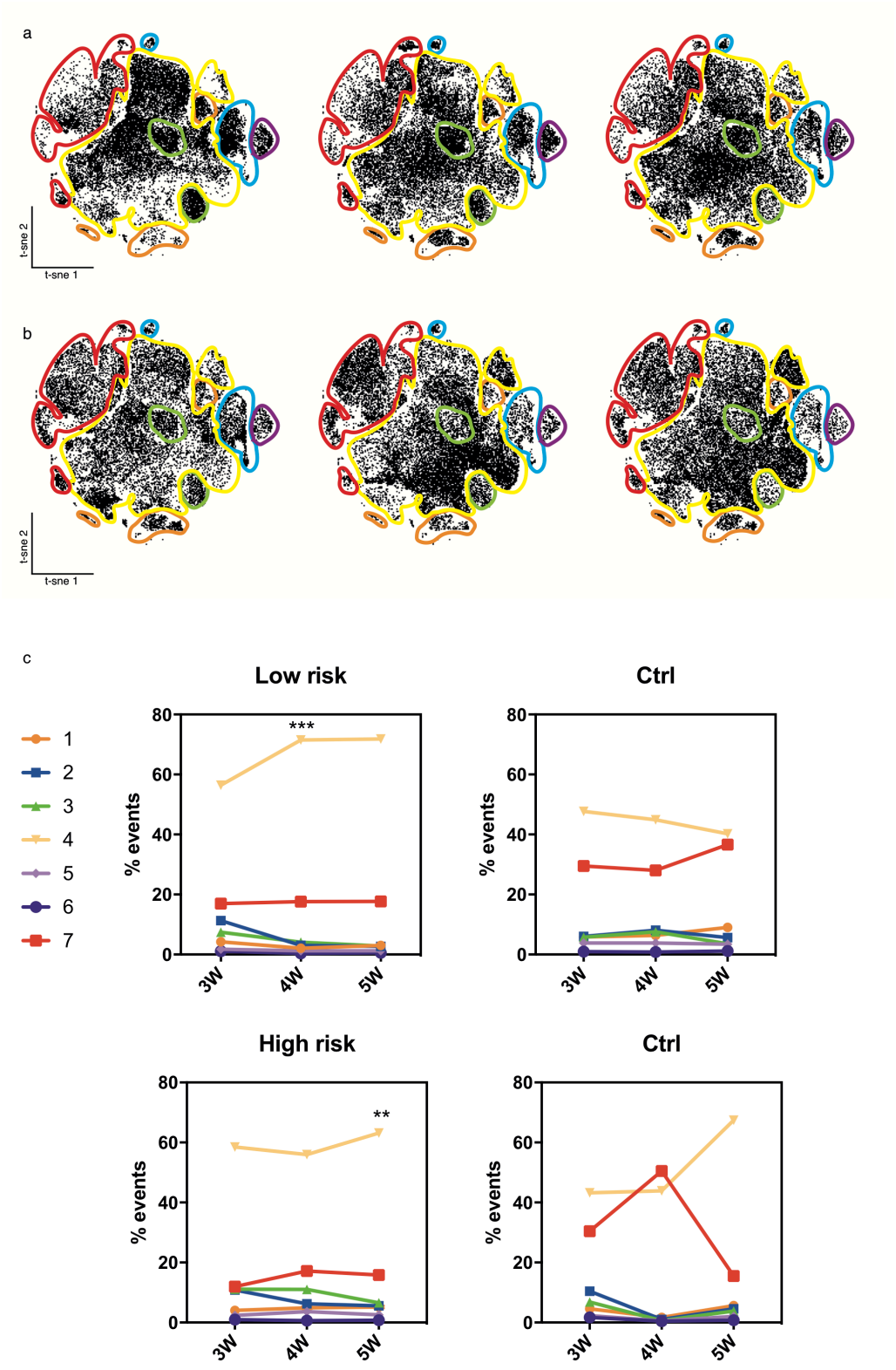

Figure 8. Intra-vessel THP-1 derived cell populations over time. vi-SNE maps showing THP-1 derived populations from vessels cultured in low-risk (a) and high-risk (b) condition. 3 weeks, 4 weeks and 5 weeks culturing time-points are shown to the left, center and right respectively. n=3. A total number of 2000 events is shown in each vi-SNE map presented. (c) Quantification of each THP-1 derived intra-vessel population over the modeling time. ***p=0.006, ***p<0.001*

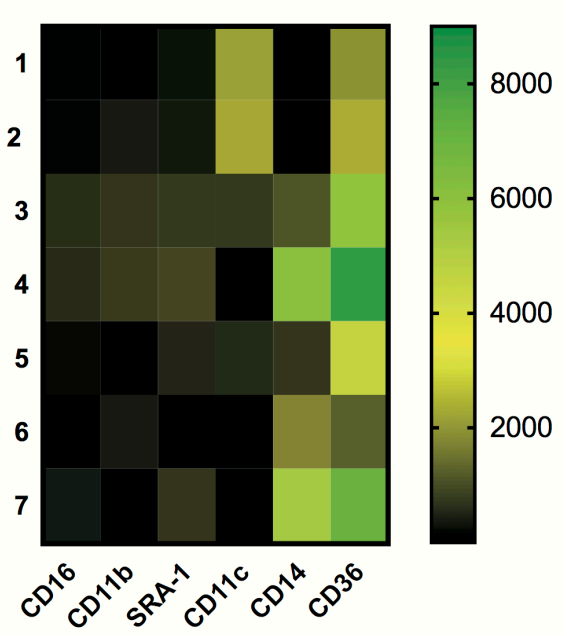

Figure 9. Surface markers expression profile. Median fluorescence intensity for each marker analyzed in each THP-1 derived cell population.

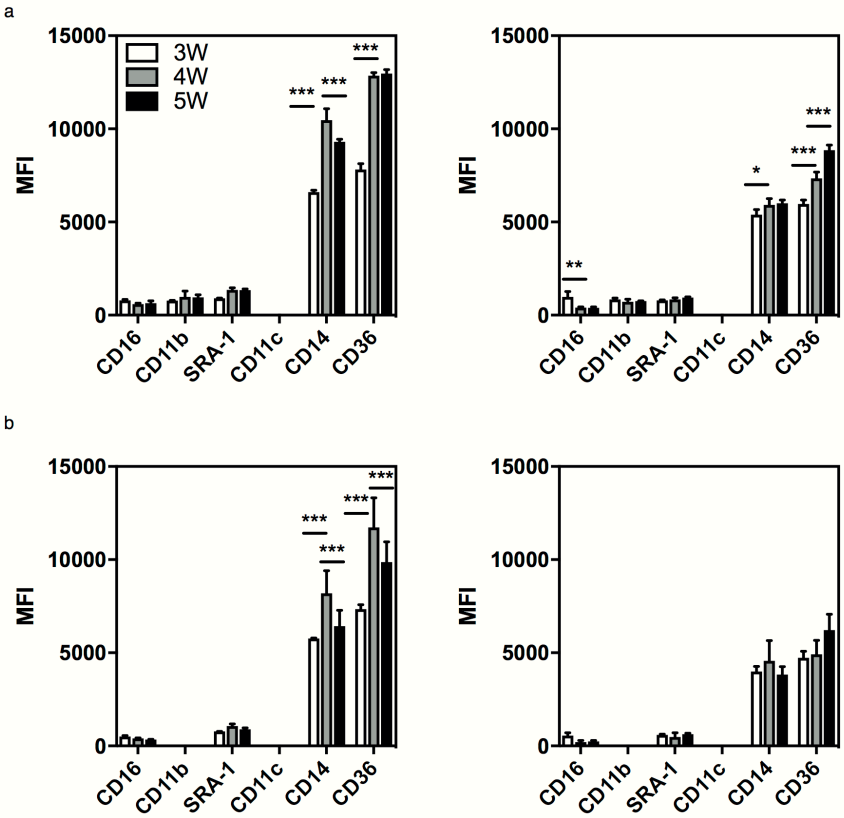

Figure 10. MFI variation over time. Variation of the median fluorescence intensity during the disease modeling time in population 4 (**a**) and 7 (**b**) for both low-risk (left) and high-risk (right) culturing condition. *p=0.05, **p=0.002, ***p<0.001

2.3.5 Investigation of Fn tensional state over-time and condition

To study the tensional state of fibronectin (Fn) in the extracellular matrix of the tissue engineered vessels we performed an investigation based on the use of the Fn-BPA5 peptide. The latter intercalates in the loose fibers of Fn providing information on the fiber state in the tissue. We observed that immature, loose fibronectin fibers stained with Fn-BPA were significantly decreasing over-time in both high and low-risk condition (Figure 11b). Importantly, this process appeared to be faster in vessels cultured in low-risk condition where immature Fn showed a reduction of more than 3 folds in a time gap of 3 weeks ($p<0.001$) (Figure 11b). In vessels cultured in high-risk condition such reduction of immature Fn was only observed after 4 weeks ($p=0.01$) (Figure 11b). From 4 weeks of culture on we reported no significant differences of immature Fn levels between high-risk and low-risk condition (Figure 11a). We showed that the decrease in immature Fn was concomitant with the formation of mature fibers (Figure 11a, b and c). Interestingly, after 5 weeks of culture mature fibers were significantly less in high-risk compared to low-risk condition ($p=0.01$) (Figure 11a). We then compared the results of immature and mature Fn levels from the TE early-lesion vessels to those obtained from late-stage plaques isolated from human carotid explants. We observed that human late-stage plaques were characterized by persistence of immature Fn and low levels of mature fibers at the plaque side meanwhile displaying a reverse pattern in the rest of the vessel (Figure 11e, f). Overall, we observed that till 3 weeks of culture there was no clear prevalence of mature fibers over immature Fn, independently from the culturing condition, while at week 4 and 5 mature Fn significantly prevailed over immature fibers ($p<0.001$) (Figure 11c).

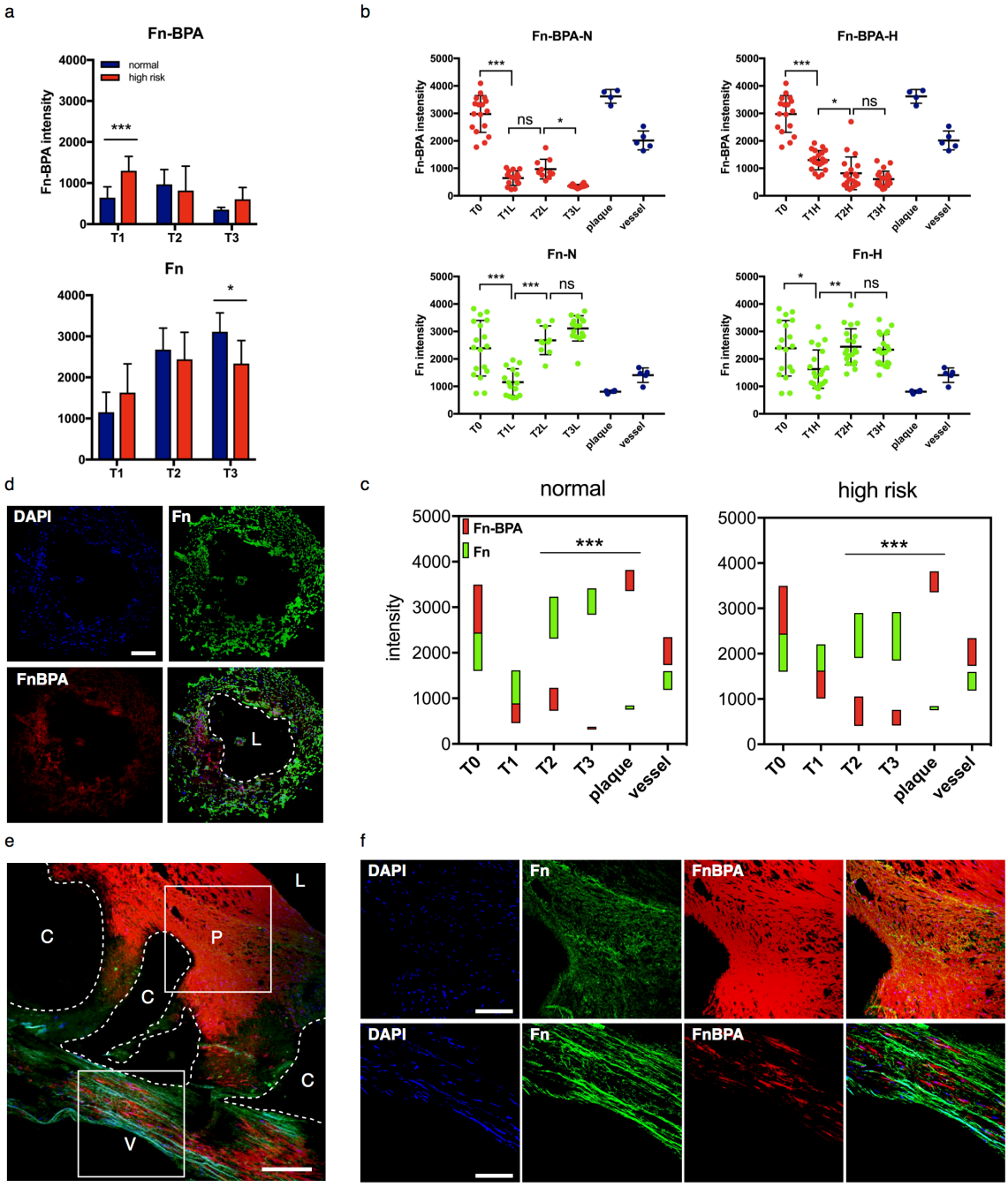

Figure 11. Investigation of fibronectin tensional state over time. Fn-BPA and fibronectin signal intensity are shown and results compared between low-risk and high-risk culturing conditions (**a**, **b** and **c**). cross-section of a tissue engineered vessel at the end of the modeling process. Scale bar 200µm (**d**). Fn-BPA and Fn intensities are compared to the results obtained from human atherosclerotic plaques isolated from carotid explants and from the respective native carotid vessel. Scale bar 200µm (**e**, **f**).

2.4 Discussion

With the fabrication of a fluidic chamber hosting multiple tissue engineered vessels we aimed at developing an upscalable early-stage atherosclerosis disease model. Such model is based on a dynamic triple co-culture supported by PGA, a biodegradable scaffold material. Several *in vitro* models of early-stage atherosclerosis are available but they are mainly based on static 2D co-culture systems[137, 174]. Recently, our lab developed a 3D human cell-based system to mimic early disease stages [6]. Despite the success in modeling early events as endothelial activation, monocyte recruitment and sub-endothelial extravasation, this model showed several weaknesses. In detail, the 3D model (i) investigated early atherosclerosis events spanning only 24h after vessel tissue engineering, (ii) did not employ monocyte cell titer and LDL concentration in the culture medium comparable to pathophysiological/physiological environment, (iii) did not allow simultaneous co-culture of multiple tissue engineered constructs and (iv) did not investigate flow velocity, WSS and fluid pressure in order to fine-tune and optimize the culturing conditions.

To improve such promising 3D disease model, we started by investigating the vessel dimension to employ for the early-lesion model. First, we studied the WSS that could be achieved with our dynamic flow propeller (settings from 1 to 10) at different putative vessel diameters. Diameters spanning from 4mm, average proximal diameter of the right coronary artery, to 0.5mm were investigated[175]. Second, we selected the vessel diameter that alone could allow us to possibly set up different WSS scenarios. We chose to biofabricate vessels of 0.5 mm in diameter, which is also close the average diameter of the human coronary arterial tree, calculated as cross-sectional area of the vasculature from proximal to distal (0.93+/-0.26 mm)[176]. Such diameter coupled with our peristaltic pup settings allows to model from low (0.57±0.23 Pa) to medium (0.18±0.47 Pa) WSS environments [177] by fine tuning flow velocity. To select the best culturing flow environment, we investigated the status of the medium flow at each setting, considering the chosen vessel diameter. To do so, we calculated the Reynold's number (*Re*) for each setting. *Re* is a fluid dynamics dimensionless quantity allowing the prediction of flow patterns in different fluid flow situations. In detail, for $Re \leq 1000$ the flow is considered laminar while for higher Re values the flow becomes either

transitional ($1000 \leq Re \leq 2000$) or turbulent ($Re \geq 2000$). We showed that the flow remains linear for setting 1 to 8 (flow velocity 0.3-20 ml/min) and becomes transitional at setting 9 (flow velocity of 23 ml/min) and 10 (26 flow velocity of ml/min).

In order to simultaneously culture multiple tissue engineered vessels, we designed and fabricated an easy-to-assemble fluidic chamber. We hypothesized that each vessel was subjected to equal force load. To test this hypothesis, we performed a computational fluid dynamic simulation using the chamber geometry. We considered the simulation environment as steady-state with incompressible fluid and as boundary condition we set a flow velocity at the chamber inlet of 0.02 m/s (corresponding to setting number 3, 5ml/min). We confirmed our hypothesis and we identified the velocity, pressure and WSS at the TE vessel inlet as 0.024 m/s, 1.5 Pa and 2×10^{-4} Pa respectively. A velocity of c.a. 0.02 m/s is comparable to the average blood flow velocity in human coronary arteries[178] . A low WSS as the one simulated at the inlet of the tissue engineered vessel is associated with plaque formation and progression [177, 179].

Once the dynamic culture system was set up we proceeded with the bioengineering experiments. The TE vessels obtained after 3-weeks of tissue engineering protocol showed extensive tissue formation and the deposition of an endothelial cell layer in the vessel lumen. The tissue engineered constructs were kept in dynamic culture for further 5 weeks. In these additional 5weeks the constructs were cultured in two different conditions modeling either and athero-prone (high-risk) or a normal (low-risk) condition [166, 167]. Interestingly, after these additional 5 weeks of culturing (early atheroslcerosis modeling period) we observed the accumulation of a cellular plaque close to each vessel flow outlet, independently from the culturing condition. Further CFD simulations considering a fully loaded fluidic chamber and detailed immunofluorescence-based investigations are needed to elucidate the dynamics triggering the formation of such cellular structures.

To investigate the effects exerted from the different culturing conditions on the TE vessels we conducted a twofold study. First, we inquired the THP-1 derived populations accumulating over time in the vascular sub-endothelium using flow cytometry. Second, we studied possible changes in the structure of ECM protein fibronectin (from immature to mature) triggered by the culturing conditions. From the

FACS analysis we identified 7 putative THP-1 derived cell populations, probably encompassing various stages of THP-1 functional differentiation[180]. We reported the presence of two cell populations that appeared to be the most abundant, population 4 and 7, both with high CD36 expression levels. We hypothesize that population 7 represents the circulating THP-1, being negative for CD16, CD11b and CD11c but positive for CD14 and CD36 [181-183] while population 4 are THP-1 derived macrophages with high surface levels of CD36 and being positive for CD11b and SRA-1 [183, 184]. Both populations show high expression levels of CD14, that is described to be CD14 was described as monocyte/ macrophage differentiation antigen that is generally lost or reduced during monocyte to macrophage differentiation [185]. Recently CD14 role has been discovered to be involved in phagocytic clearance of apoptotic cells[186, 187]. This justifies the high levels of CD14 measured on the surface of putative THP-1 derived macrophages. Interestingly but not surprisingly, we noticed an increase of population 4 (putative macrophage population) over-time within the TE vessel in both conditions. Despite population 7 did not show any variation in number over time in both culturing environment, we reported fluctuations in surface expression of CD14 and CD36 in low-risk condition, but not in high-risk. This might be linked to the fact that the high LDL concentration prevented flexible exposure of different surface proteins, driving the differentiation of population 7 (putative monocytes) directly towards macrophage fate and excluding possible other differentiation paths as previously shown [188, 189]. From the flow cytometry data we concluded that, in such early stages of plaque formation, no LDL-driven change in surface antigen expression is noticeable in THP-1-derived populations recruited in the sub-endothelium. As formerly known and previously mentioned, high circulating LDL levels are not the sole risk factor to initiate and drive plaque development. Such condition might be of relevance for the differentiation of monocyte population during later stages of disease development and incentivize plaque progression rather than regression[189]. Further experiments are needed to elucidate at which stage of plaque development high circulating LDL concentrations can influence population remodeling in the tunica intima.

Finally, we investigated the tensional state of fibronectin over time aiming at identifying possible condition-dependent change in fibronectin maturation. Fibronectin

is one of the most abundant ECM proteins [190, 191] serving as docking site for several other ECM components. In particular, it has been demonstrated that relaxed, immature Fn fibers serve as nucleation site for collagen and are generally localized in collagen I rich areas[170, 192].We supported these findings by showing for the first time that relaxed Fn is present in high concentration in human late-stage atherosclerotic plaques, well known to show an ECM rich collagen I [193]. We measured the levels of relaxed fibronectin at the end of the bioengineering process (T0) and we found Fn-BPA (binding to relaxed Fn) intensity was significantly higher compared to native human carotids, indicating a still immature ECM composition in the bioengineered constructs. Furthermore, we observed that the levels of Fn-BPA in vessels cultured in high-risk conditions where higher and decreasing slower compared to low-risk condition. This might indicate that high LDL concentrations and high monocyte titer negatively influence the maturation of ECM matrix and provide the basis for the formation of an ECM rich in collagen I. Longer culture periods in high-risk environment could reveal weather this hypothesis is correct.

In conclusion, despite this model represents the most advanced early-stage atherosclerosis disease model, there are still some hurdles to overcome. Among them there is (i) the need of performing computational fluid dynamic simulations considering the fully loaded chamber (chamber + vessels) in order to deepen the understanding of the flow in the TE vessel during the biofabrication and disease modeling processes. Additionally, (ii) changes in fluid viscosity due to variation in LDL concentration have to be considered to optimize the simulation results.

Chapter 3

Adapted from:

Mallone, A., Stenger C., Von Eckardstein A., Hoerstrup S.P. and Weber B. (2018) *Biofabricating atherosclerotic plaques: In vitro engineering of a three-dimensional human fibroatheroma model*. Biometerials. doi: 10.1016/j.biomaterials.2017.09.034.

In vitro bioengineering of the late lesion

3.1 Introduction

Among different plaque stages, the thin-cap fibroatheroma is the one most prone to rupture and to potentially cause thrombus formation and vessel obstruction [194]. The fibroatheroma is characterized by the presence of a necrotic core, macrophage-derived foam cells and dendritic cells all being enriched with cholesterol and embedded in a collagenous matrix surrounded by a thin layer of fibrotic cells [70, 71]. In the present study, we introduce a bioengineered *in vitro* model of fibroatheroma that we call pseudo plaque (ps-plaque). The ps-plaque architecture is characterized by a spheroid core of monocytes, macrophages and dendritic cells embedded in a collagenous and lipid-rich matrix, surrounded by a thin layer of myofibroblasts. In order to investigate a possible source for model up-scaling we biofabricated ps-plaques using either blood-derived myeloid cells or cells from the thp-1 cell line. We explored the similarities in surface antigen expression patterns of myeloid populations from ps-plaques and human carotid plaques isolated from patients undergoing carotid endarterectomy. Additionally, we compared the expression levels of key pro-inflammatory and remodeling gene-targets in both plaque types. We found similarities in population distribution and gene expression profiles between ps-plaques and human samples. Finally, we used the ps-plaque to investigate the role of LDL in plaque population remodeling and cell viability. With this work, we introduce a new technology for investigating atherosclerosis pathomechanisms, aiming at providing a novel human cell-based platform for drug design and high-throughput screening.

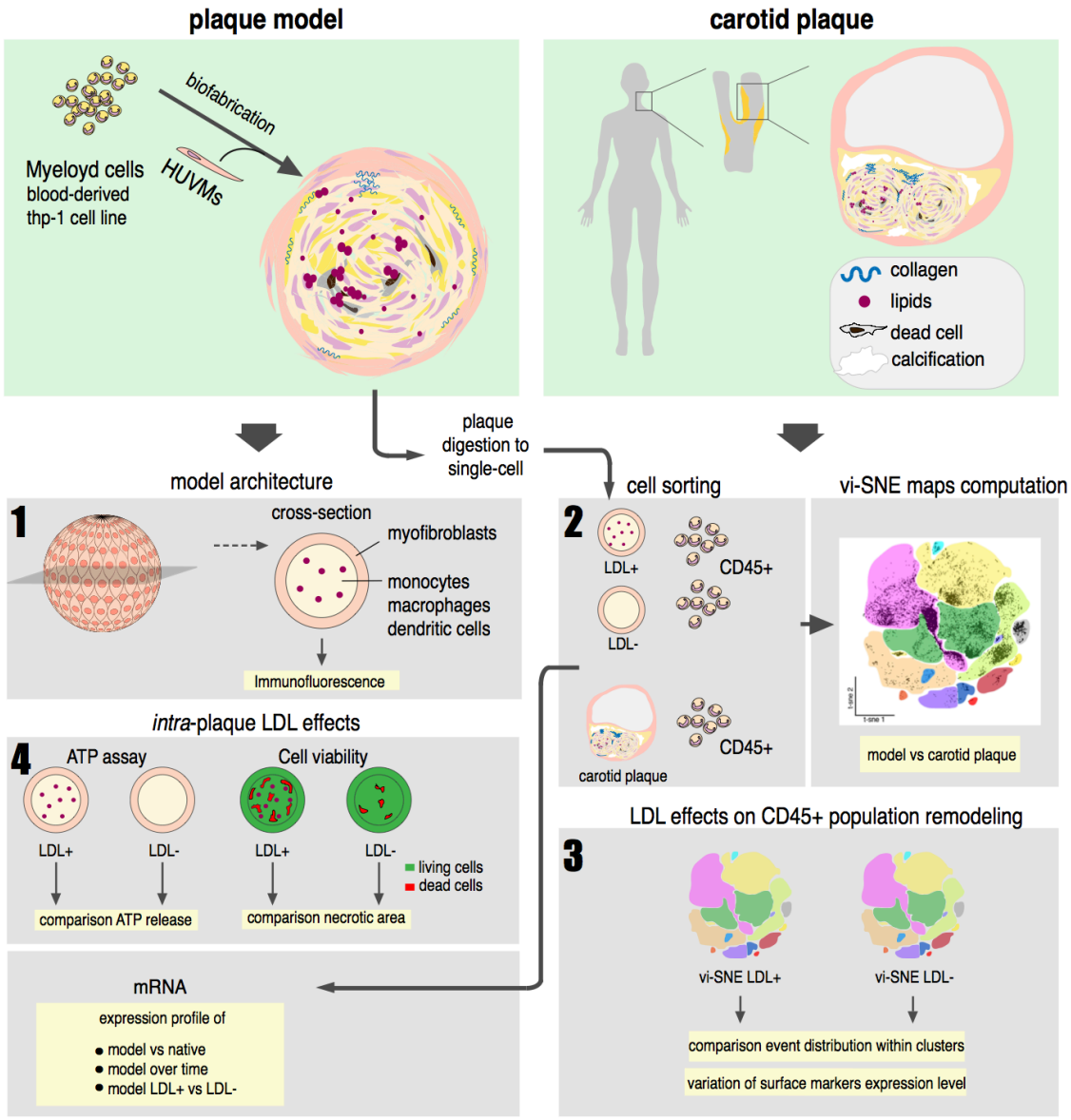

Figure 12. Graphical abstract: *In vitro* engineering of a three-dimensional human fibroatheroma model.

3.2 Material and methods

3.2.1 Isolation of myeloid cells from blood

Myeloid cells were isolated from human blood using a double gradient centrifugation. The blood was provided by the Zurich blood bank (Blutspende Zürich – Nr.6676) and maintained at room temperature in slow rocking motion until processing. First, 20ml of blood from each donor were diluted 1:2 with 1× Phosphate Buffer Saline (PBS, Sigma) at room temperature and layered onto a Ficoll solution (1.077 g/ml, Sigma). Samples were then centrifuged at 400g for 30min without break. Second, a 46% iso-osmotic Percoll gradient was performed to separate the lymphocytes from the peripheral blood mononuclear cells (PBMCs) as previously described [195]. Briefly, the buffy coat was re-suspended in 20ml of xVivo15 chemically defined medium (Lonza) without red phenol and carefully layered on top of a Percoll solution prepared with 50% Roswell Park Memorial Institute (RPMI) medium with red phenol (Sigma), 46% Percoll (GE Healthcare) and 4% 1×PBS (Sigma). The second gradient was centrifuged at 550g for 30min without break and the white cell ring at the interphase was collected for further processing.

3.2.2 Myofibroblasts isolation

Human umbilical vein myofibroblasts (HUVM) were isolated from human umbilical cords. The tissues were processed in accordance to the ethical permit released by the Kantonale Ethikkommission Zürich (KEK-Stv-21-2006). Briefly, umbilical cords were stored after labor at 4°C in Dulbecco's Modified Eagle's Medium (DMEM, Sigma) prepared with 10% Fetal Bovine Serum (FBS, Gibco), 1% GlutaMax (Gibco) and 1% penicillin/streptomycin (Penn/Strep, Gibco) for maximum 2h prior to processing. The umbilical vein was carefully extracted from the umbilical cord and the inner lumen was flashed twice with 1×PBS. The adventitia layer was peeled off with the help of forceps and scalpel. The intima layer was removed by incubating the inner lumen for 30min in a 1mg/ml collagenase/dispase (Roche) solution in 1×PBS. The remaining endothelial cells were washed out from the lumen with 1×PBS. The remaining media layer was

minced into small pieces of approximately 2mm length and let adhere for 10min on the bottom of a petri dish. The tunica media fragments were then covered in DMEM medium and maintained at 37°C, 5% CO_2 and 95% humidity. The medium was replaced every 48h. After about 20 days myofibroblasts sprouting from the minced pieces reached about 80% confluence and were ready for sub-culturing.

3.2.3 Cell culture

HUVM were cultured in DMEM medium with 10% FBS and 1% GlutaMax and the medium was replaced every 48-72h. For sub-culturing, HUVM were detached using trypsin 0.5% (Sigma) for 4 min and seeded at a cell density of 4,000 cells/cm^2. HUVM were expanded up to passage 5 prior to use for the experiments in this study. Human monocytic leukemia cell line (thp-1) isolated from the peripheral blood of a 1-year-old human male with acute monocytic leukemia, were purchased from Sigma. Thp-1 cells were cultured in suspension in xVivo15 medium and the medium was replaced every 2-3 days. Thp-1 cells were seeded at a density of 100,000 cells/ml and sub-cultured at a density of 800,000 cells/ml.

3.2.4 *In vivo* models

The pseudo-plaque production pipeline encompasses three steps: differentiation, priming and hanging-drop. First, fresh blood-derived myeloid cells or thp-1 cells were seeded onto petri dishes for 72h and differentiated in chemically defined xVivo15 medium with 10% FBS in order to achieve a macrophage/dendritic cell phenotype. To induce thp-1 differentiation 10ng/ml of phorbol 12-myristate 13-acetate (PMA, Sigma) were added to the culture medium. Second, a priming step was performed to obtain heterogeneous macrophage/dendritic cell populations with both pro-inflammatory and remodeling phenotypes. For this purpose, the differentiated cells were rinsed in 1×PBS and treated for 1h in xVivo15 medium with 10% FBS and 10ng/ml lipopolysaccharide (LPS, Sigma). Finally, the primed cells were transferred in hanging-drop culture. Briefly, adhesive myeloid-derived cells were mechanically detached by 20min incubation in 5mM Ethylenediaminetetraacetic acid (EDTA, Life Technologies) in

1×PBS at 4°C and gentle scraping. Cells were re-suspended at a cell density of 2.4 x 10^6 cells/ml in presence of LDL 50μg/ml (LEE Biosolutions) in xVivo15 medium with 10% FBS. Droplets of 10μl were pipetted on the lead of a 10cm diameter petri dish and kept in hanging-drop culture for 48h. To the core of myeloid-derived cells assembled during the 48h incubation, an external layer of HUVM was added. HUVM were prepared at a cell density of 4 x 10^5 cells/ml in DMEM medium, with or without 50μg/ml LDL. 10μl of the cell suspension were carefully added to each pre-existing drop and cultured in hanging-drop for further 48h.

3.2.5 2D co-culture

Primed myeloid cells from blood or thp-1 origin were seeded in 24 well plates maintaining the same cell ratio used for the ps-plaque biofabrication (myeloid cells: myofibroblasts 6:1). In detail, about 300'000 primed myeloid cells were seeded with or without 50μg/ml LDL in each well in order to achieve a confluent cell layer. Cells were kept in xVivo15 medium with 10% FCS and in 2D culture for 48h. 50'000 fibroblasts/well in DMEM medium (with or without 50μg/ml LDL) were then added on top of the myeloid cell layer and incubated for 48h to obtain a stratified 2D co-culture system.

3.2.6 Flow cytometry

Biopsies of carotid branches were obtained from patients undergoing carotid endarterectomy and shunting, secondary to vascular stenosis (Ethik Kommission der Universität Witten/Herdecke – Nr.79/2012). Carotid plaques and biofabricated ps-plaques were digested with 1mg/ml collagenase/dispase solution in 1×PBS for 15min at 37°C. Cells were gently pipetted through a cell strainer with the mesh size of 40μm (Falcon) and incubated for 5min at 4°C with magnetic beads coated with anti CD45 antibodies, according to the provider instructions (MACS Miltenyi Biotec). CD45+ cells were magnetically sorted and stained with Zombie Aqua™ fixable viability kit (BioLegend) for 5min and fixed over night at 4°C in a 1% Paraformaldehyde (PFA, Sigma) solution in 1×PBS. The single cell suspension was stained for 15min at room

temperature in Fluorescence-activated cell sorting (FACS) buffer prepared with 5% FBS and 0.01% NaN_3 (Sigma) in 1×PBS with an optimized FACS antibody panel including: CD14-PerCP (#325631, Biolegend), CD16-Alexa 700 (#360717, Biolegend), CD11b-Alexa594 (#101254, Bioloegend), CD11c-PE-Cy5 (#301609, Biolegend), CD36-BV605 (#563518, Becton Dickinson) and SRA-1-PE (#REA460, MACS Miltenyi Biotec). Each antibody was previously titrated to establish the optimal working concentration. Samples were acquired using LSR Fortessa analyzer (Becton Dickinson) and signal compensation was performed using OneComp eBeads (eBioscience). The FACS data were analyzed using the vi-SNE workflow as described in the previous chapter.

3.2.8 Immunofluorescence

Myofibroblasts were fixed for 20min in 4% PFA in 1×PBS and maintained in 1×PBS at 4°C until further processing and not more than 7 days. Cells were stained with the primary antibodies anti-alpha smooth muscle actin (αSMA, #ab7817, Abcam) and anti-smooth muscle myosin heavy chain (SMMHC, #ab53219, Abcam) overnight at 4°C and with secondary antibodies (anti-mouse #715-605-151, Jackson Immuno Research; anti-rabbit #A11008, Life Technologies) and phalloidin (#A12381, Life technologies) for 1h at 37 °C. Nuclei were counterstained with DAPI and the slides were mounted in Vectaschield® (Vector Laboratories). The ps-plaques were carefully washed in 1×PBS and fixed in PFA as described above. Plaques were dehydrated overnight in a solution of 25% sucrose (Sigma) in 1×PBS, embedded in OCT matrix (CellPath) and stored at -20°C. Slices of 5μm were cut, rehydrated in 1×PBS for 15min and stained with primary antibodies: anti-Collagen type III (#ab7778, Abcam), anti-αSMA and anti-CD45-PeCy5 (#304009, BioLegend) overnight at 4°C. Secondary antibody staining was performed (anti-mouse, 715-545-151, Jackson Immuno Research; anti-rabbit #A11008, Life Technologies) for 1h at 37°C. For the Filippin sections were quenched for 10min with 1.5mg/ml glycine (Sigma) in 1×PBS prior to addition of 250μg/ml Filippin III dye (Sigma) at room temperature for 2h. Sections were washed 3 times in 1×PBS and nuclei were counterstained with propidium iodide 1mg/ml (BioLegend) for 5min. Slides were mounted in Vectaschield®. Images were acquired in grey scale with

the confocal microscope (Leica SP8). Image post-processing, specifically the choice of appropriate pseudo-colors, was performed using ImageJ.

3.2.9 TEM and SEM

For scanning electron microscopy (SEM) and transmission electron microscopy (TEM), ps-plaques were fixed with a 2.5% glutaraldehyde solution in 0.1M sodium cacodylate (NaCaCo) and maintained O.N. at 4°C. For TEM samples were then washed 2 times in 0.1M NaCaCo and further fixed for 1h in osmiumtetroxide. After 3 washes in 0.1M NaCaCo, a staining of s1h with 1% uranyl acetate in water was performed. Samples were further washed for 3 times in 0.1M NaCaCo, dehydrated with a EtOH gradient, embedded in Epon resin O.N. at 60°C and analyzed at the TEM (FEI Tecnai G2 Spirit). For SEM, the fixed ps-plaques were rinsed 3 times in PBS and incubated in osmiumtetroxide: PBS in 1:2 ratio for 30 minutes. Samples were dehydrated by 30 min incubation with 70% EtOH followed by 30 min incubation in EtOH 100%. Finally, the samples were kept 1h in Hexamethyldisilazane and let dry overnight. Samples then stained in platinum blue 4nM at R.T. for 30 min and analyzed at the SEM (JEOL JSM-6010 tungsten cathode scanning electron microscope).

3.2.10 RT-qPCR

Total RNA was extracted using the GenElute Mammalian Total RNA Kit (Sigma), following the manufacturer's instructions. Reverse transcription was performed for each sample in a 20μl reaction mixture containing 1μg of RNA, 1×PCR buffer, 5mM $MgCl_2$, 10mM of each dNTP, 0.625μM oligo $d(T)_{16}$, 1.875μM random hexamers, 20U RNase inhibitor and 50U MuLV reverse transcriptase (all from Life Technologies). The conditions for the reverse transcription were the following: 25°C for 10min, 42°C for 1h, followed by 99°C for 5min. The resulting cDNA was amplified in duplicate by quantitative real-time PCR in 10μl reaction mixture with 200nM of each specific primer (Supplementary Table 2) and 1×Fast Syber Green qPCR MasterMix (Applied Biosystems). For the amplification reaction, StudioQuant 7 was used (Applied Biosystem). The amplification program was set as follows: 95°C for 5min, followed

by 40 cycles at 95°C for 10 s, 60°C for 15 s, 72°C for 20 s. GAPDH and 18S served as housekeeping genes and their amplification data were averaged and used for sample normalization. The software Excel (Microsoft) was used for the comparative quantification analysis.

3.2.11 Ps-plaque viability assay

Cell viability within the plaque was measured using CellTiter-Glo® 3D Cell Viability Assay (Promega). Briefly, the biofabricated plaques were washed in 1×PBS and dispensed in an opaque-walled 96 well plate (Costar). Each ps-plaque (1 plaque/well) was dispensed in 15μl of 1×PBS. Equal volume of CellTiter-Glo® 3D Reagent was added to each well for a final volume of 30μl. Luminescence was measured after a 30min of incubation at room temperature with SPECTRAmax® Gemini-XS (Bucher biotech) and ATP levels were reported in relative luminescence units (RLU).

3.2.12 Quantification of ps-plaque area and necrotic area

For the measure of the plaque necrotic area, every plaque was stained for 40min in a solution of calcein (5μM) and eth-1 (15μM) from the LIVE/DEAD™ Viability/Cytotoxicity Kit, for mammalian cells (Life Technologies). Ps-plaques were imaged using an inverted microscope (Leica, DM IL LED) and post-processed in ImageJ. Briefly, images underwent color 2D Parallel iterative deconvolution using the Wiener Filter Preconditioned Landweber (WPL) method (Max number of iteration=5; Max number of threads^2=4). The results of the point of spread function obtained from the deconvolution were normalized and the green and red channels were thresholded with the MaxEntropy setting. The ps-plaque necrotic area was measured as necrotic area over alive area and indicated as percentage. Plaque dimension was measured using the bright field images of the plaque circular cross section. First, the image was converted to 8-bit format and tresholded with the MaxEntropy method. Second, the area of the particles was analyzed from objects with a dimension larger than 1,000px in order to exclude debris or single cells not belonging to the bioengineered plaque. Plaque area was reported in mm^2.

3.2.13 Statistical analysis

vi-SNE cluster counts and PCR comparative quantitations were analyzed using multiple comparison analysis. First, Gaussian distribution of the data was confirmed with Shapiro-Wilk normality test. Second, repeated measures (RM) two-way ANOVA with Tukey's multiple comparison test was applied. Luminescence and necrotic area were analyzed with paired t-test. All statistical analyses were performed with GraphPad Prism Version 7, GraphPad Software, San Diego, CA, USA). Significance was accepted at $p<0.05$. All data are presented as mean ± s.d..

Gene of interest	FW primer	RV primer
CXCL10	5' GCA AGC CAA TTT TGT CCA CG 3'	5' ACA TTT CCT TGC TAA CTG CTT TCA G 3'
CCR7	5' GAA AGT CCA GAA ACT GTT CCC ACC TGC 3'	5' CCC CTC TGA AGA ACC GAA CCA CTC CTT 3'
CCL17	5' CCA GGG ATG CCA TCG TTT TTG TAA CTG TGC 3'	5' CCT CAC TGT GGC TCT TCT TCG TCC CTG GAA 3'
CCL26	5' GCC TGA TTT GCA GCA TCA TGA TGG 3'	5' CGG ATG ACA ATT CAG CTG AGT CAC 3'
DC-SIGN	5' TCG AGG ATA CAA GAG CTT AGC A 3'	5' AAG GAG CCC AGC CAA GAG 3'
IL10	5' CTG TGA AAA CAA GAG CAA GGC 3'	5' GAA GCT TCT GTT GGC TCC C 3'
IL23	5' GCA GAT TCC AAG CCT CAG TC 3'	5' TTC AAC ATA TGC AGG TCC CA 3'
PTGS1	5' CGC CAG TGA ATC CCT GTT GTT 3'	5' AAG GTG GCA TTG ACA AAC TCC 3'
ALOX5	5' CGC CGA CTT TGA GAA AAT CT 3'	5' GGC TGC ACT CTA CCA TCT CC 3'
SRB1	5' TCC TCA CTT CCT CAA CGC TG 3'	5' TCC CAG TTT GTC CAA TGC C 3'
GAPDH	5' GTC AGT GGT GGA CCT GAC CT 3'	5' ACC TGG TGC TCA GTG TAG CC 3'
18S	5' CCC GGG GAG GTA GTG ACG AAA AAT 3'	5' GCC CGC TCC CAA GAT CCA ACT AC 3'

Table 4. Primer table.

3.3 Results

3.3.1 Differentiation-priming strategy promotes population redistribution in cells from myeloid origin

We established a two-step bioengineering method for the assembly of the ps-plaque (Figure 13a, 14 and 15). Myeloid cells isolated from freshly drawn blood and thp-1 cells were differentiated towards macrophage/dendritic phenotype and primed with LPS to obtain a mixed population of pro-inflammatory and remodeling cell populations. The success of the differentiation-priming strategy was verified using a fluorescence-activated cell sorting (FACS) and the results were computed using dimensionality reduction and clustering algorithms, PhenoGraph and FlowSOM respectively [168]. With this technique, we identified 15 cell populations in the multidimensional space that we classified according to the differential expression levels of key surface markers (Figure 13c, 16, 17 and Table 5). In samples isolated from the blood we identified 4 over-represented populations: classical monocytes (Mo_{cl}), macrophages ($M\phi_1$), pre-classical dendritic cells (pre-cDC) and an unknown myeloid progenitor population (Prog) (Fig. 1c; Supplementary Fig. 2). We monitored each population at the end of the differentiation-priming process and we observed a significant decrease in the unknown myeloid progenitors ($p=0.005$) coupled with a significant increase in pre-cDC ($p=0.05$) (Figure 13c). Additionally, we observed a priming-induced increase in CD11c surface levels within the pre-cDC population and in the myeloid progenitors (Figure 18 and 19). In cell samples from untreated thp-1 we observed an initial population distribution similar to the one found in blood samples. When we applied the priming process to thp-1 monocytes, we observed a significant reduction in the myeloid progenitors count ($p<0.001$). The latter was concomitant with a decrease in pre-cDC count ($p<0.001$) and the appearance of plasmacytoid dendritic cells (PDC) (Figure 20, 21 and 22). Furthermore, we observed that the priming process triggered the proliferation of classical monocytes ($p<0.001$) (Figure 20). We then analyzed the expression levels of pro-inflammatory and remodeling gene targets. In blood-derived cells we observed induction of *CXCL10* ($p<0.001$), *CCL17* ($p<0.05$), *DC-SIGN* ($p<0.001$) *and SRB1* ($p<0.001$) upon treatment, indicating the overall

stronger induction of remodeling over pro-inflammatory genes (Figure 13b). When we analyzed the changes in thp-1 cells gene expression levels upon differentiation-priming we observed induction of *CXCL10* (p=0.03), *PTGS1* (p=0.05) and *IL10* (p=0.01), indicating pro-inflammatory gene up-regulation over remodeling genes (Figure 23).

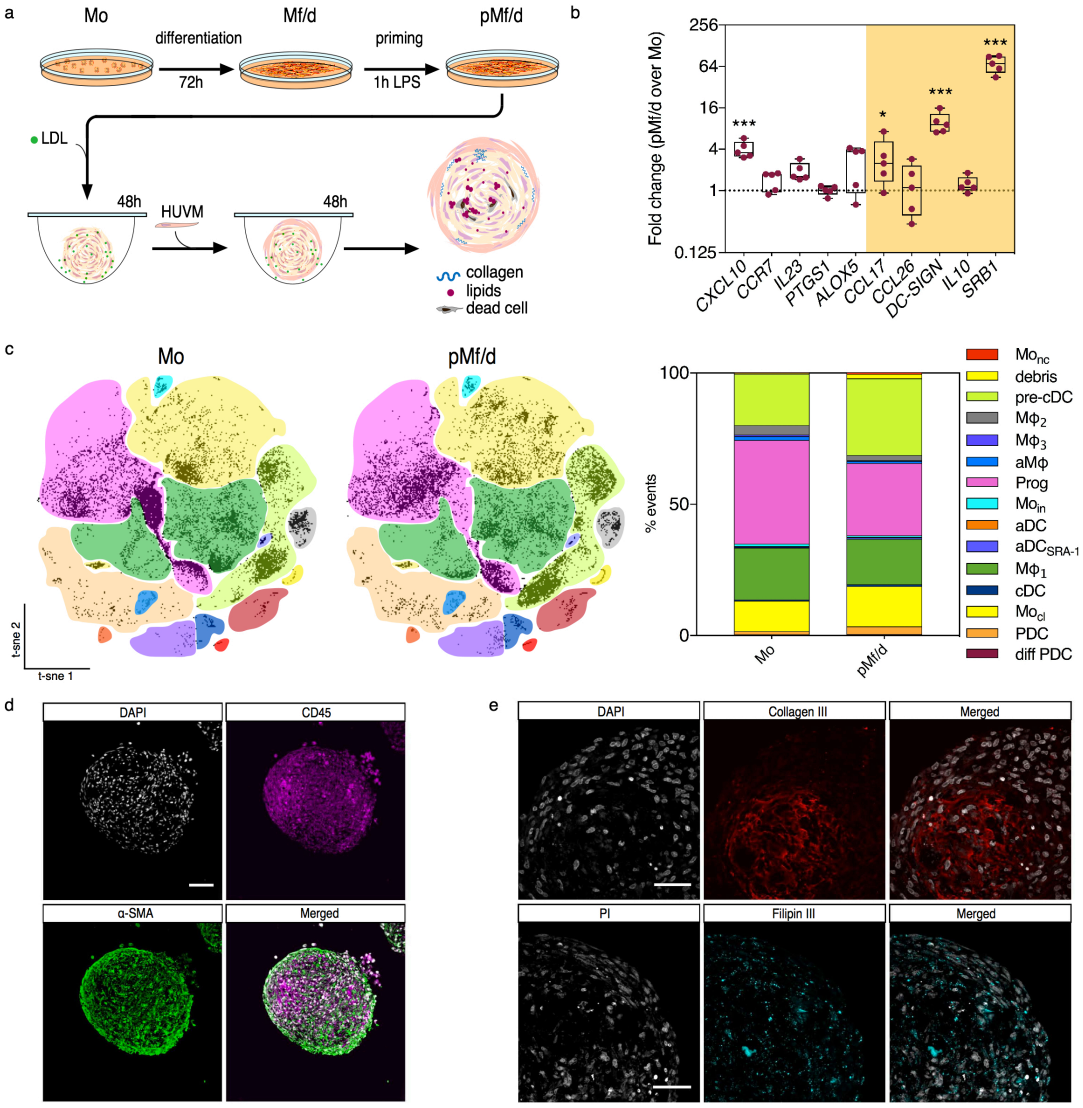

Figure 13. Biofabricated human atherosclerotic plaque. (**a**) Schematic view of the ps-plaque assembly with blood-derived cells. (**b**) Expression profile of pro-inflammatory (left-white panel) and remodeling genes (right-orange panel) over the differentiation-priming process. Data are reported in fold change over gene expression levels at the beginning of the differentiation-priming process. n=5; error bars indicate standard deviation; *p=0.05, ***p<0.001. (**c**) vi-SNE maps indicating the cell populations at the beginning (Mo) and at the end (pMf/d) of the differentiation-priming process. n=7; 2,000 events per sample are reported; 14,000 events are shown in each vi-SNE map. The stacked-bar chart indicates the percentage of events recorded in each population and summarizes the vi-SNE results. (**d**) Representative cross-section captured at the great circle of the spheroid showing inner architecture of the ps-plaque: HUVM (αSMA+, green) and myeloid cells (CD45+, magenta). Scale bar 100μm. (**e**) Collagen III and lipid accumulation in the ps-plaque. Scale bar 50μm.

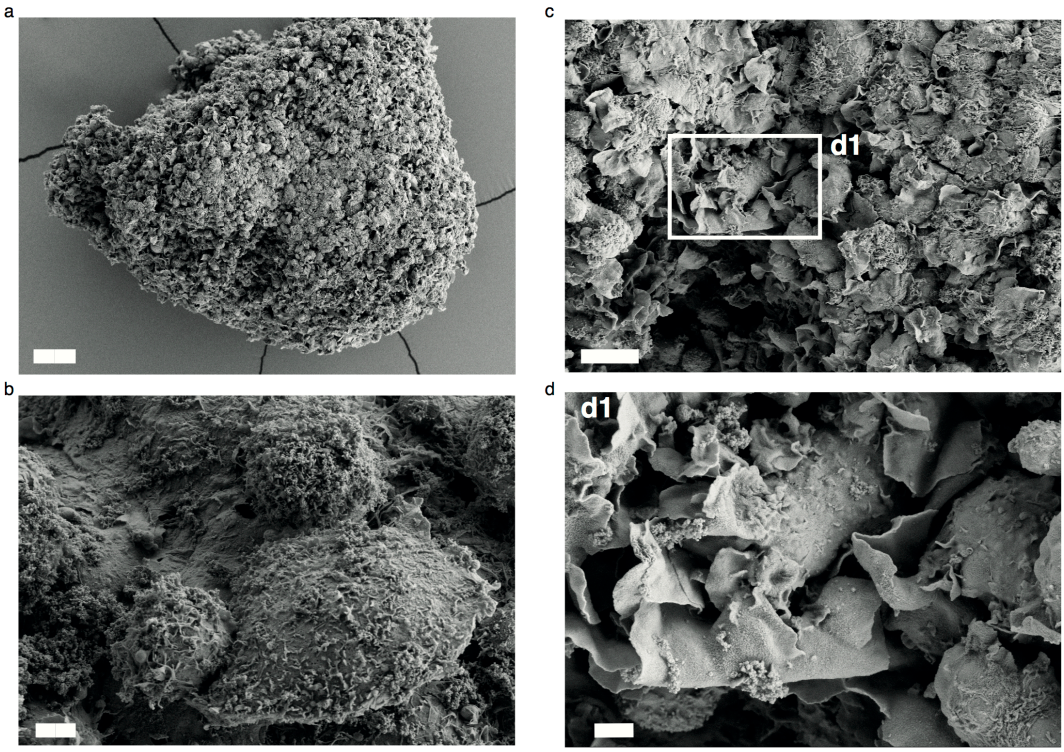

Figure 14. Scanning electron microscopy of the ps-plaque. (**a**) SEM image of a ps-plaque. Scale bar 40μm. (**b**) Detail of the ps-plaque external surface. Scale bar 4μm. (**c**) Inner architecture of ps-plaque. Scale bar 4μm. With a detail (**d**, d1) showing macrophage/dendritic cells surfaces in contact with LDL cholesterol. Scale bar 10 μm.

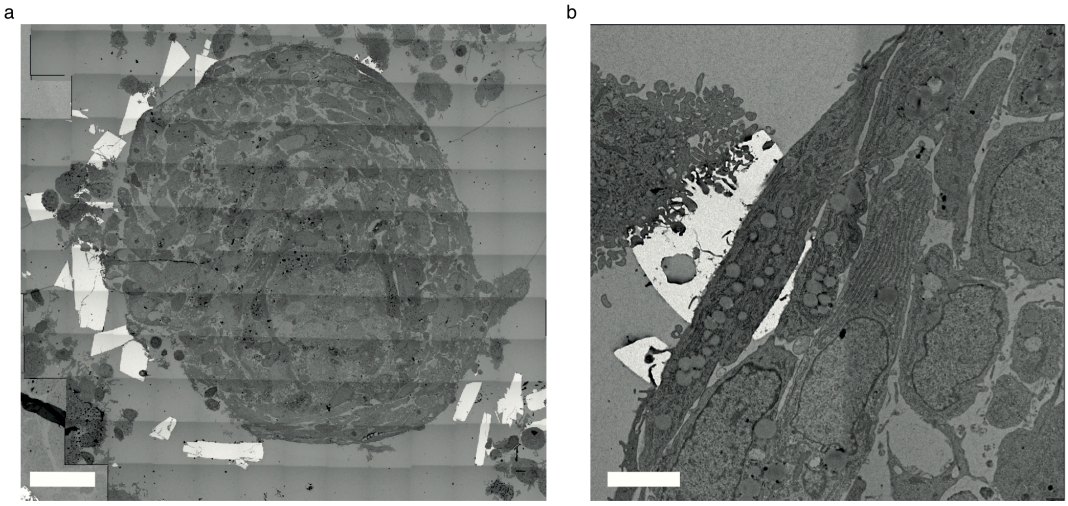

Figure 15. Transmission electron microscopy of the ps-plaque. (**a**) TEM image of a ps-plaque showing accumulation of cholesterol crystals at the external surface. Scale bar 40μm. (**b**) Detail of the ps-plaque external surface. Apoptotic myofibroblast in contact with a cholesterol crystal. Scale bar 4μm.

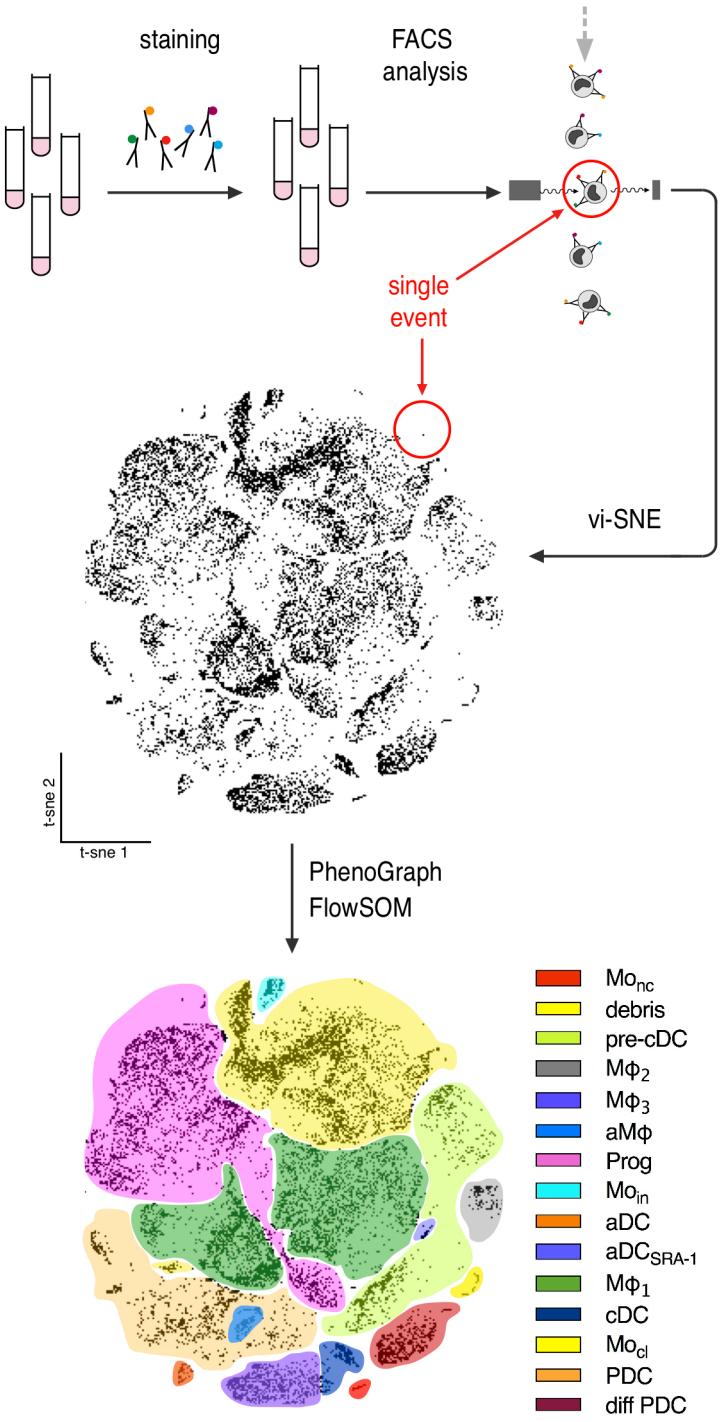

Figure 16. Identification of different myeloid subsets using the vi-SNE workflow. Samples are stained and acquired at the FACS analyzer. The resulting FCS files are processed to generate vi-SNE maps. Each cell recorded (single event) is positioned in a specific area of the high-dimensional space, here represented with commonly used FACS biaxial plots. Different myeloid subsets are positioned in separate regions of the high-dimensional space according to surface marker similarities. Distances between cells are representatives of cell proximity in high-dimensional rather than two-dimensional space. These myeloid subsets are automatically gated with using PhenoGraph and FlowSOM algorithms and identified in the vi-SNE map with different colors.

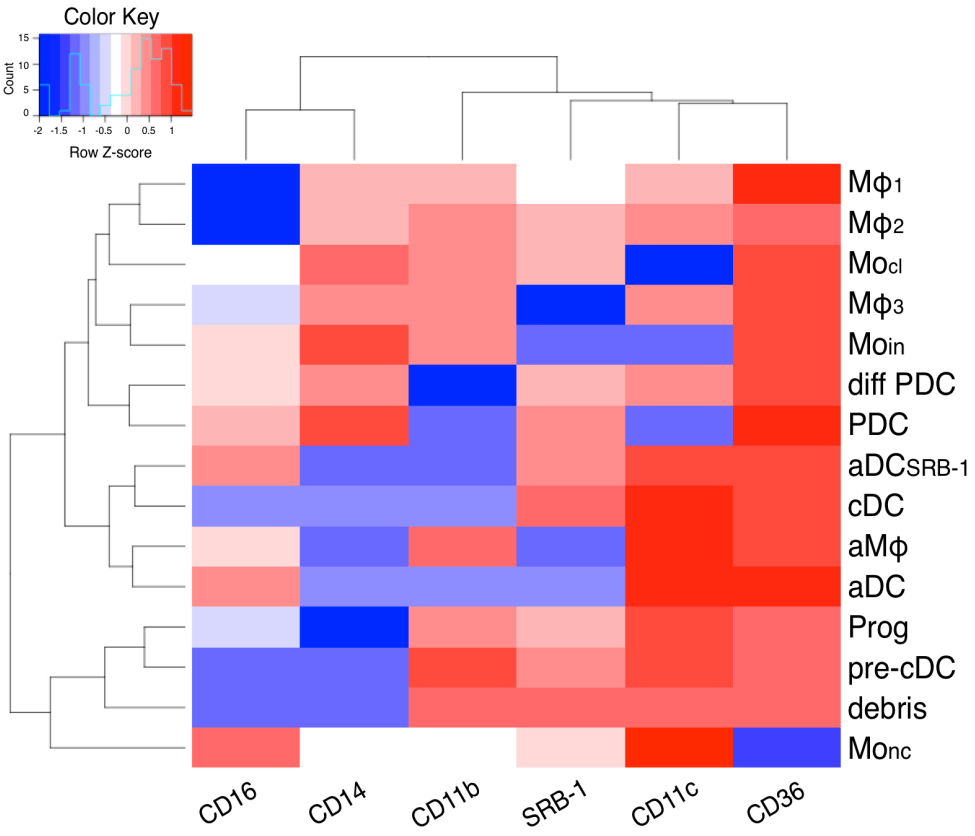

Figure 17. Surface expression levels of key markers in different myeloid subsets. 15 cell populations were identified using the vi-SNE workflow. Each myeloid population retains a specific surface marker expression pattern indicated by the heat-map. The present heat-map represents the median fluorescence intensity of each marker in each myeloid subset and was computed using total of 112,000 events; n=7; 2,000 randomly selected events for each sample analyzed (samples analyzed for both b and t plaques: Mo, pMf/d, T2, T2L).

Plaque components		Abbreviation	% b-plaque	% total	% t-plaque	% total	% nat. plaque	% total
Monocytes	Classical	Mocl	24.92	26.31	34.64	35.14	0.20	0.23
	Intermediate	Moin	0.97		0.44		0.03	
	Non classical	Monc	0.42		0.06		0.00	
Macrophages	Derived from Mocl	Mϕ1	26.66	29.59	38.06	39.18	0.04	0.23
	Derived from Mocl	Mϕ2	1.38		0.11		0.00	
	Derived from Moin	Mϕ3	0.27		0.21		0.05	
	Activated	aMϕ	1.28		0.8		0.14	
Dendritic cells	Plasmacytoid	PDC	5.37	43.83	4.37	24.86	86.68	99.54
	Differentiated PDC	diff PDC	3.85		2.76		4.21	
	Pre-classical	pre-cDC	5.12		0.31		0.06	
	Classical	cDC	1.6		0.42		1.01	
	Activated	aDC	0.93		0.40		2.27	
	Avctivated SRA-1^{high}	aDCSRA-1	6.58		4.18		5.15	
	Progenitors	Prog	20.38		12.42		0.16	
		debris	0.27	0.27	0.82	0.82	0.00	0.00

Table 5. Myeloid populations in ps-plaques and native carotid plaques.

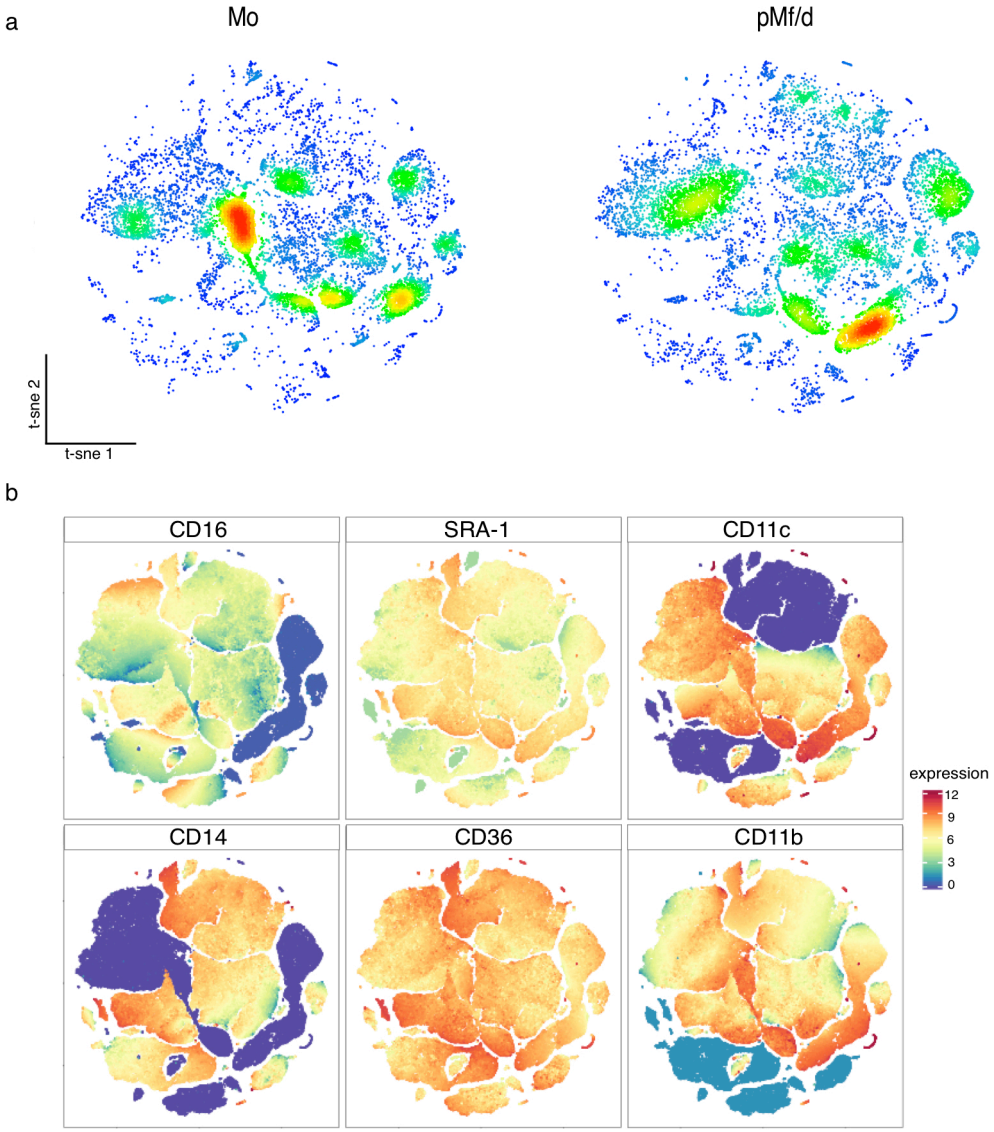

Figure 18. Density plots from blood-derived cells before and after differentiation-priming process. (**a**) Density distribution of recorded events before (Mo) and after (pMf/d) the differentiation-priming process. Areas of high event density are depicted in red and areas with low event density in blue. n=7; 2,000 randomly selected events for each sample analyzed are shown (Mo and pMf/d). Therefore, in each vi-SNE maps 14,000 events are plotted. (**b**) Expression level plots. Each vi-SNE map shows 112,000 events; n=7; 2,000 randomly selected events for each sample analyzed (samples analyzed for both b and t plaques: Mo, pMf/d, T2, T2L).

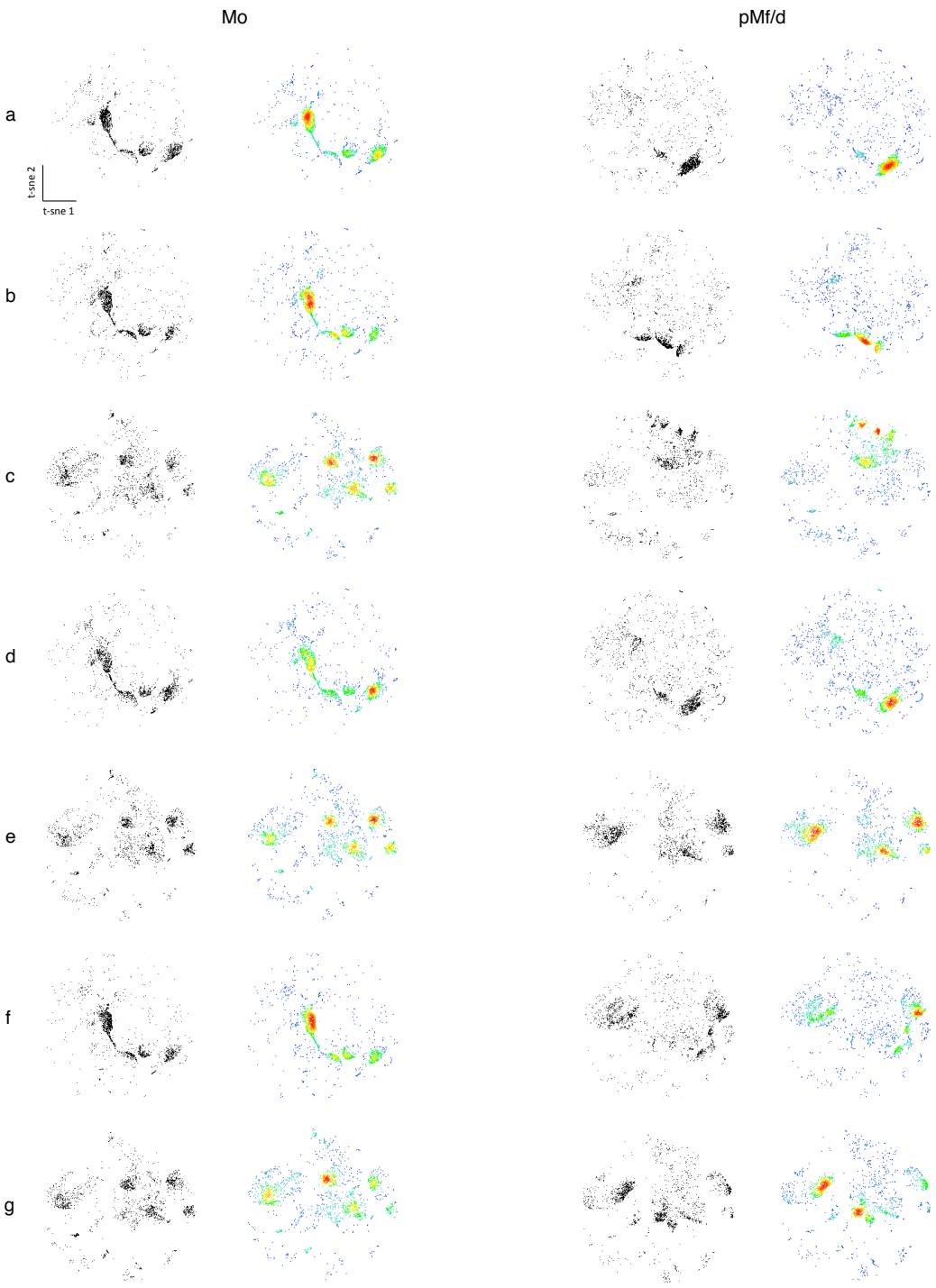

Figure 19. vi-SNE maps from blood derived myeloid cells before and after priming procedure. Vi-SNE maps from each biological replicate (a-g) used to assemble the cumulative vi-SNE maps and cumulative density maps depicted in Figure 18 and Figure 13a.

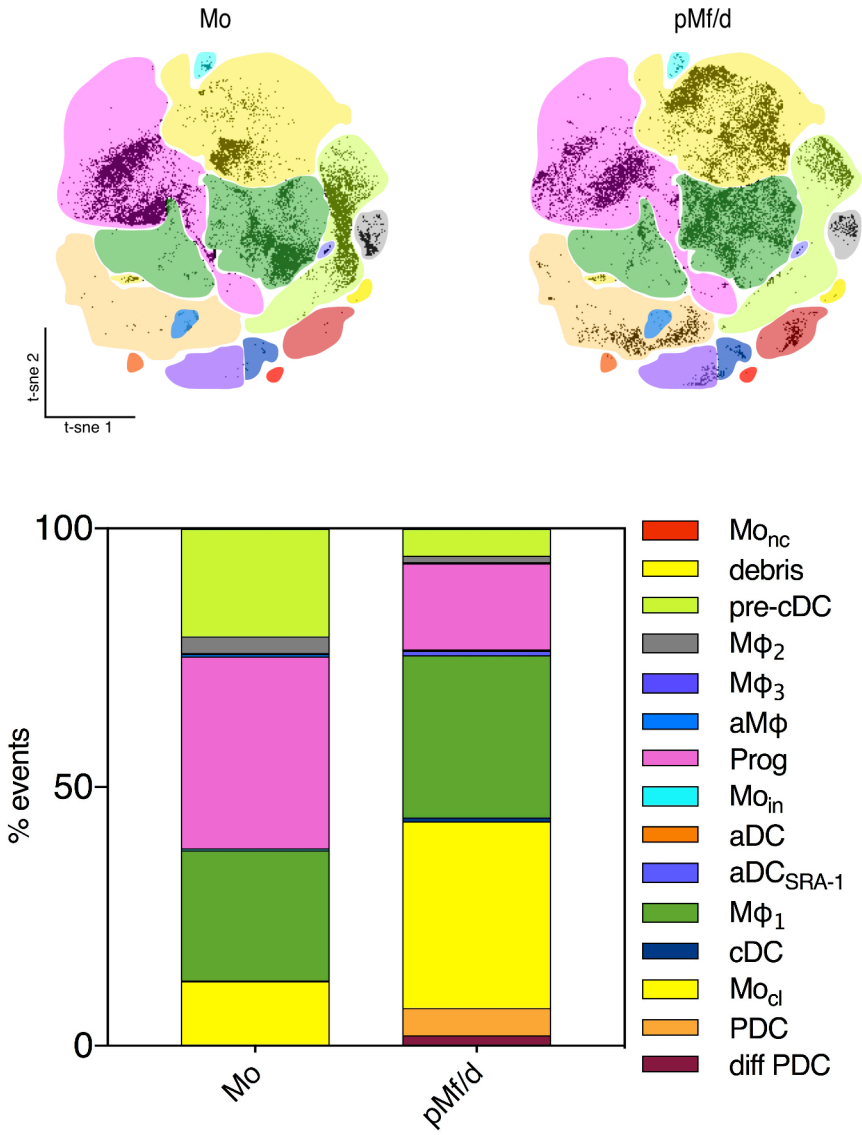

Figure 20. Differentiation-priming effects on thp-1 cells. vi-SNE maps indicate different myeloid populations identified within thp-1 cells at the beginning (Mo) and at the end (pMf/d) of the differentiation-priming process. The part-of-whole graph shows the % of events and summarizes the vi-SNE results. n=7; 2,000 events per sample are reported. A total of 14,000 events are shown in each vi-SNE map.

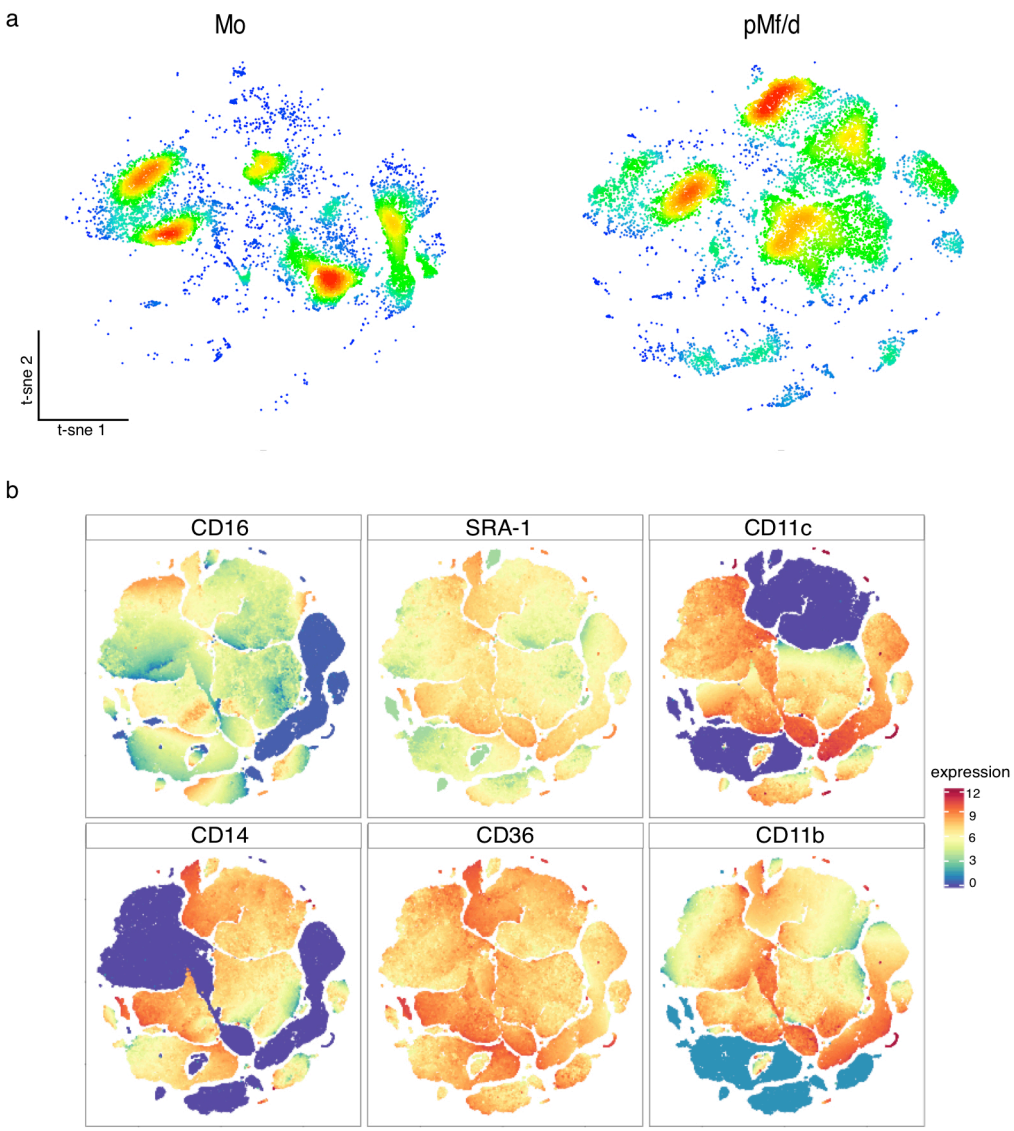

Figure 21. Density plots from thp-1 cells before and after differentiation-priming process. (**a**) Density distribution of recorded events before (Mo) and after (pMf/d) the differentiation-priming process. Areas of high event density are depicted in red and areas with low event density in blue. In each vi-SNE maps 14,000 events are plotted. n=7; 2,000 randomly selected events for each sample analyzed are shown (Mo and pMf/d). (**b**) Marker expression level plots.

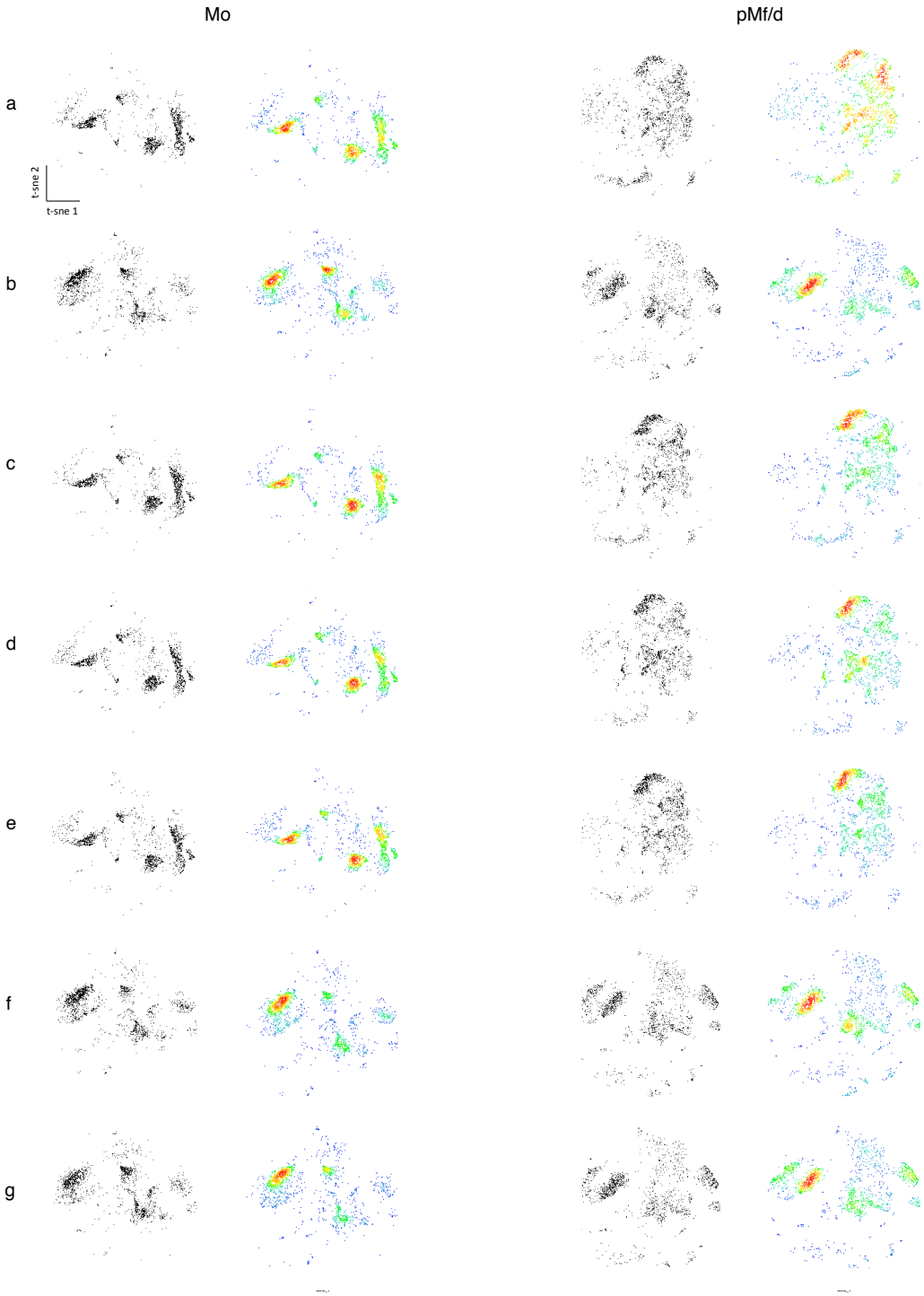

Figure 22. vi-SNE maps from thp-1derived myeloid cells before and after priming procedure. Vi-SNE maps from each biological replicate (a-g) used to assemble the cumulative vi-SNE maps and cumulative density maps depicted in Figure 20 and 21.

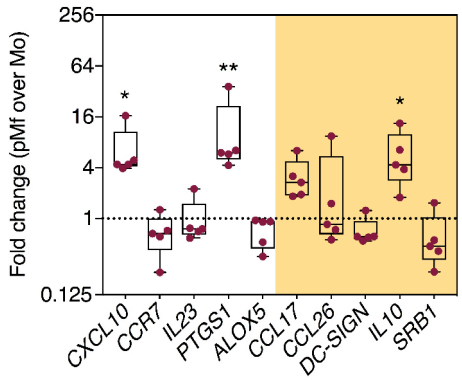

Figure 23. Changes in gene expression profile of thp-1 cells upon differentiation–priming. The expression profile of pro-inflammatory (left – white panel) and remodeling (right – orange panel) genes is reported in fold change over Mo expression levels (where fold change= 1). Data (n=5) were normalized on the averaged GAPDH and 18S expression levels.

3.3.2 Defining the gravity-guided biofabrication of human atherosclerotic plaques

Human primed myeloid cells and myofibroblasts (HUVM) were combined to establish a hanging-drop 3D co-culture system (Figure 13a, Figure 24). The newly established system resulted in α-SMA+ HUVM cells surrounding pre-existing myeloid CD45+ cell aggregates and forming a thin fibrotic layer around the bioengineered spheroid (Figure 13d). The generation of such stratified structure and compact HUVM layer was not observed in 2D co-culture systems when using the same cell-to-cell ratio (Figure 25). Additionally, we observed the assembly of collagen clumps within the ps-plaque and intra-plaque accumulation of lipid aggregates (Figure 13e). We did not detect any extracellular collagen deposition in 2D co-culture systems. Collagen was rather retained in the intracellular space (Figure 25).

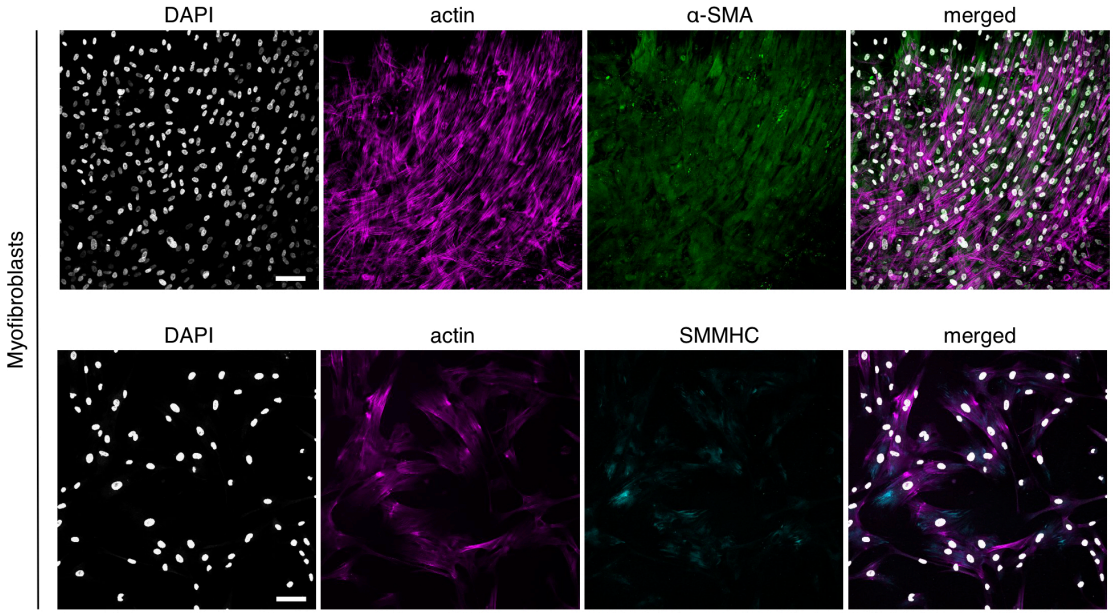

Figure 24. ***Myofibroblasts characterization.*** Myofibroblasts isolated from human umbilical vein express α- smooth muscle actin (α-SMA) and smooth muscle myosin heavy chain (SMMHC); scale bar 100μm.

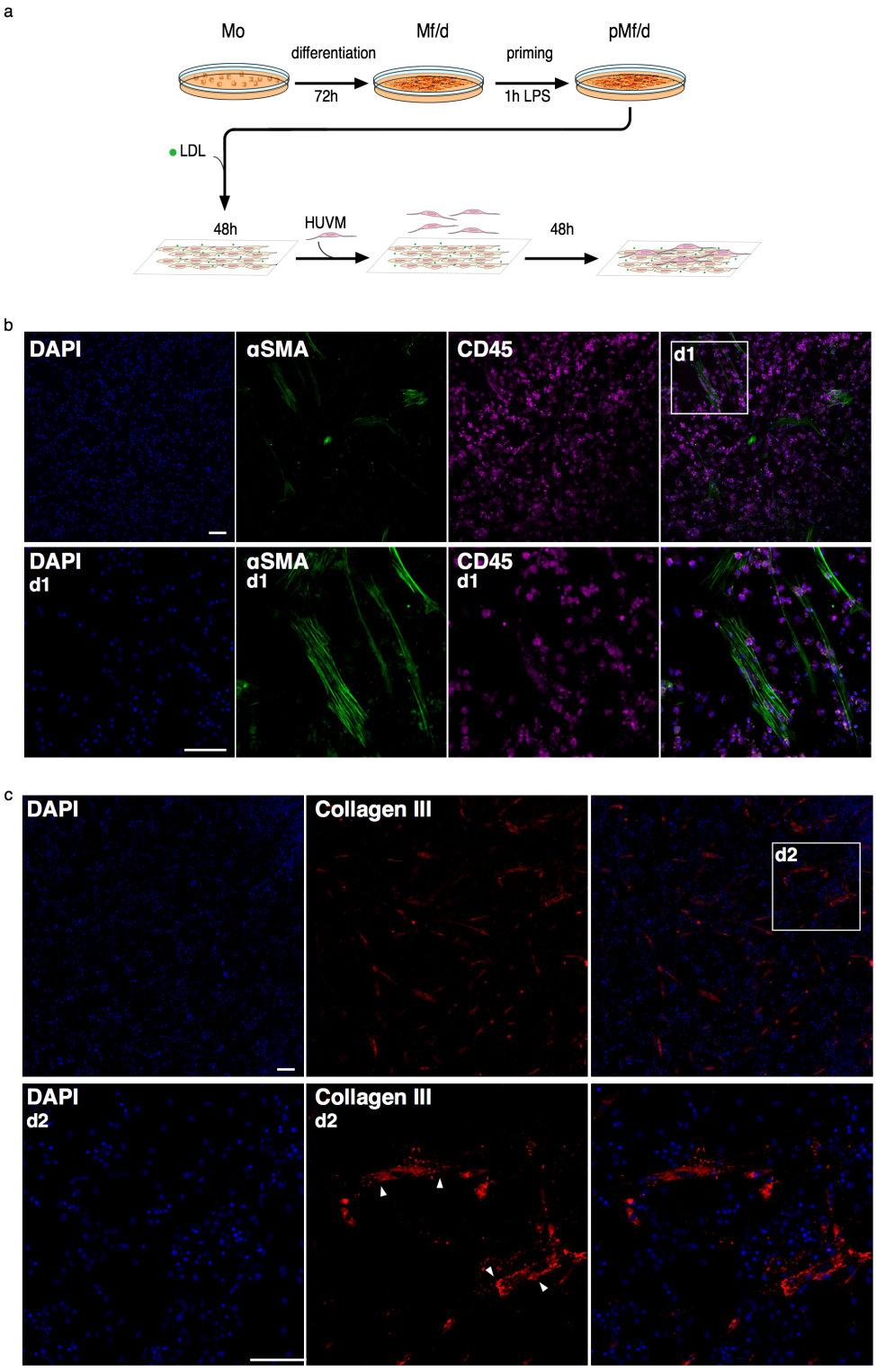

Figure 25. 2D microenvironmental co-culture. (a) 2D co-culture, experiment description. (**b**) The panel indicates the architecture of the 2D microenviroment where myofibroblasts appear insufficient in forming a confluent layer on top of myeloid cells. Detail d1 shows myofibroblasts (aSMA+) leaning on top of adhesive myeloid cells (CD45 +). (**c**) Collagen deposition in 2D microenvironmental co-cultures. Detail d2 shows intracellular retention rather than extracellular release of collagen III. Scale bars 100 μm.

3.3.3 vi-SNE analysis reveals plasmacytoid and activated dendritic cells as main myeloid components in human fibroatheroma

To corroborate the ps-plaque model we conducted a comparison study between bioengineered and human atherosclerotic plaques isolated from patients that underwent carotid endarterectomy. We observed large similarities in population distribution within b-plaques and t-plaques. In detail, we found that the main cell populations are classical monocytes, macrophages, activated dendritic cells and plasmacytoid dendritic cells (Figure 26a, b; Figure 27). When we analyzed CD45+ cells from carotid plaques, we identified PDC and aDC populations as main myeloid plaque components (Figure 26a, b; Figure 28). We further investigated the event density distribution within the PDC populations in human carotid plaques. We identified 3 major areas of the vi-SNE map corresponding to peculiar PDC phenotypes that we classified as α, β and γ (Figure 28). PDC type-α represents a relatively small cluster with phagocytic and lipoprotein clearance predisposition due to high surface levels of scavenger receptors CD36, SRA-1 and CD14. PDC type-β is a larger cell cluster characterized by $CD16^{high}$, indicating a possible involvement in pro-inflammatory reactions. PDC type-γ appears to be exclusively specialized in lipid and lipoprotein uptake, provided the predominant surface expression levels of CD36 (Figure 28). Interestingly, in both bioengineered plaque models (b- and t-plaques) we identify PDC Type-β (Figure 27). Finally, we analyzed the gene expression profile of the CD45+ populations in ps-plaques and carotid plaques. We reported a significant down-regulation of pro-inflammatory and remodeling gene targets in carotid plaques compared to bioengineered plaques (Figure 26c).

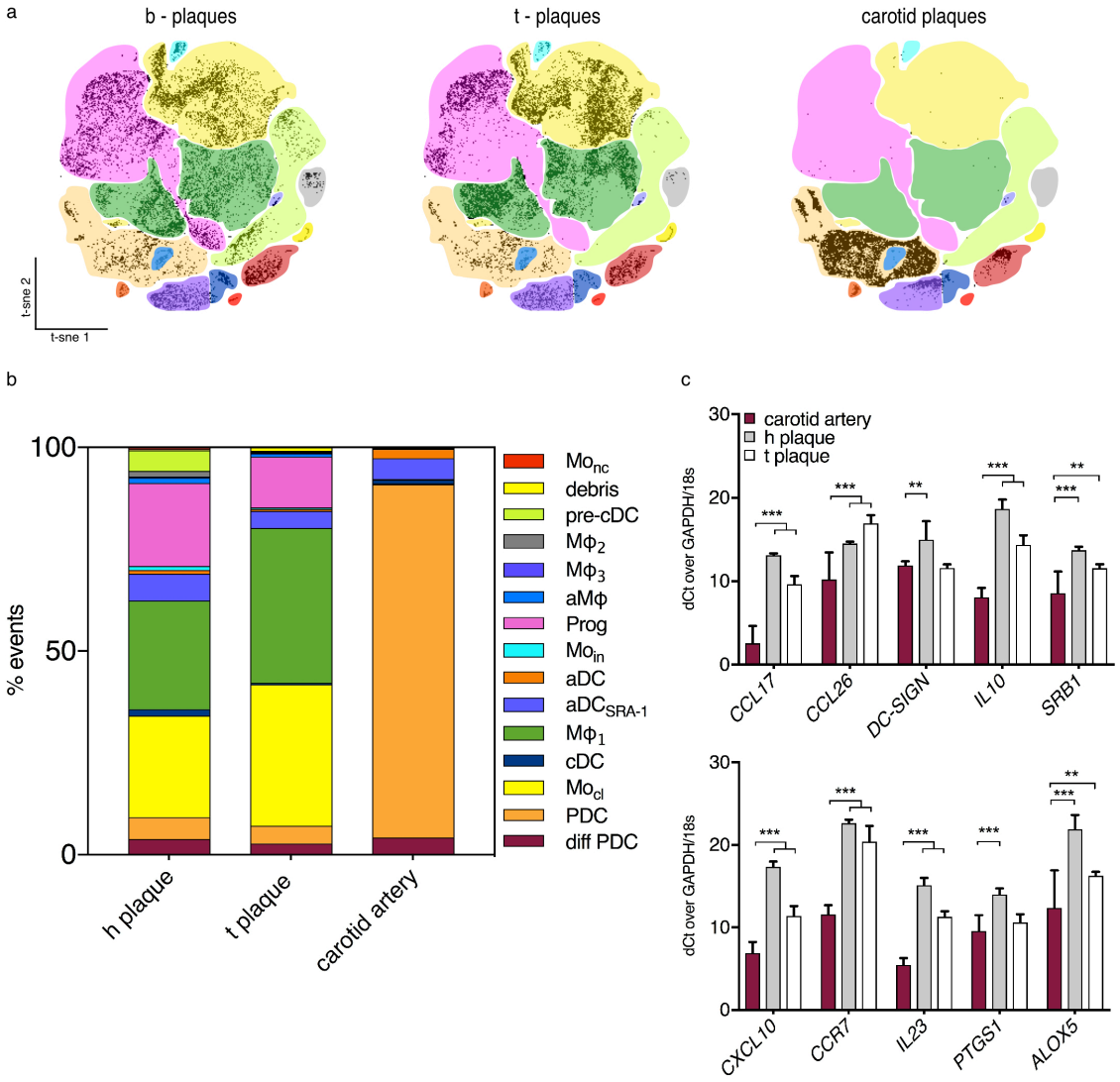

Figure 26. Comparison between biofabricated plaques and human carotid plaques. (**a**) vi-SNE maps from CD45+ populations isolated from blood-derived plaques (b-plaques), thp1 plaques (t-plaques) and carotid plaques. n=7; 2,000 events per sample are reported. A total of 14,000 events are shown in each vi-SNE map. (**b**) The stacked-bar chart summarizes the percentage of events for each population. (**c**) Gene expression profile of CD45+ populations isolated from ps-plaques and plaques from carotid arteries. Expression levels of remodeling genes (upper panel) and pro-inflammatory genes (lower panel). n=5, error bars indicate standard deviation. **p=0.002, ***p<0.001.

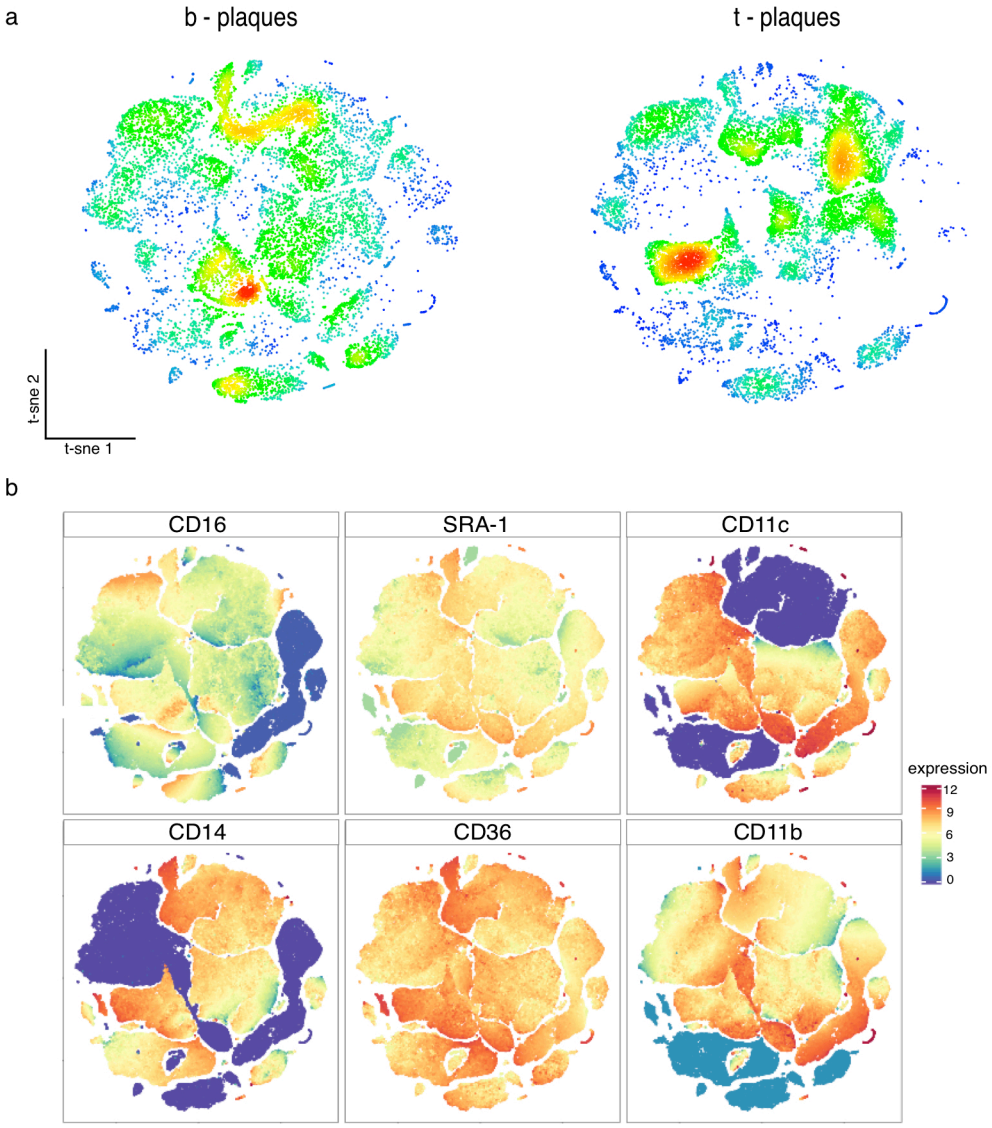

Figure 27. vi-SNE comparison between bioengineered b-plaques and t-plaques. (**a**) vi-SNE density plots. Areas of high event density are depicted in red and areas with low event density in blue. n=7; 2,000 events per sample were randomly down-sampled from each sample. A total of 14,000 events is shown in each vi-SNE map. (**b**) Marker expression level plots.

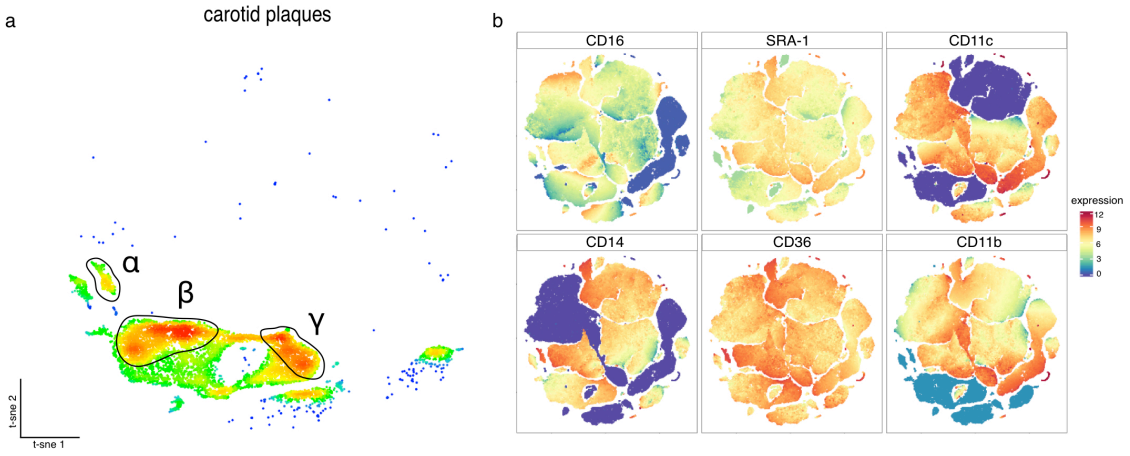

Figure 28. Density plots from myeloid populations isolated from native carotid plaques. (**a**) vi-SNE maps indicate the event density recorded in each myeloid population. Areas of high event density are depicted in red and areas with low event density in blue. PDC sub-populations are indicated in the vi-SNE map: type-α, type-β and type-γ. n=5. 2,000 events per samples are plotted for a total of 10,000 events. (**b**) Marker expression level plots.

3.3.4 Low-density lipoprotein promotes the differentiation of a precursor myeloid population in biofabricated plaques

We investigated the effects of LDL on the differentiation of myeloid (CD45+) subpopulations isolated from b- and t-plaques. To do so, we biofabricated ps-plaques using either the established protocol based on LDL-enriched medium or using LDL-free medium. We applied the vi-SNE workflow to compare the respective cell populations. In b-plaques we observed a reduced count of precursors in LDL-enriched versus LDL-free controls ($p<0.001$, Figure 29a, Figure 30) suggesting differentiation triggered by LDL. The difference in precursor counts can also be appreciated in the respective density plots (Figure 29b, Figure 30). Additionally, we compared vi-SNE density plots from ps-plaques biofabricated in LDL-rich and LDL-free medium. To investigate variations in LDL triggered surface antigen expression within each population we overlapped the density plots with the marker expression level plot. We observed an LDL dependent density shift in aDC towards vi-SNE areas with $CD11c^{high}$, $CD16^{high}$ and $CD36^{high}$ expression levels (Figure 29b, c). In t-plaques, we observed an LDL dependent density shift of $M\phi_1$ towards $CD36^{high}$ and $CD11c^{high}$

areas of the vi-SNE map and of Mo_{cl} towards a $CD36^{high}$ vi-SNE area (Figure 31, 32 and 33).

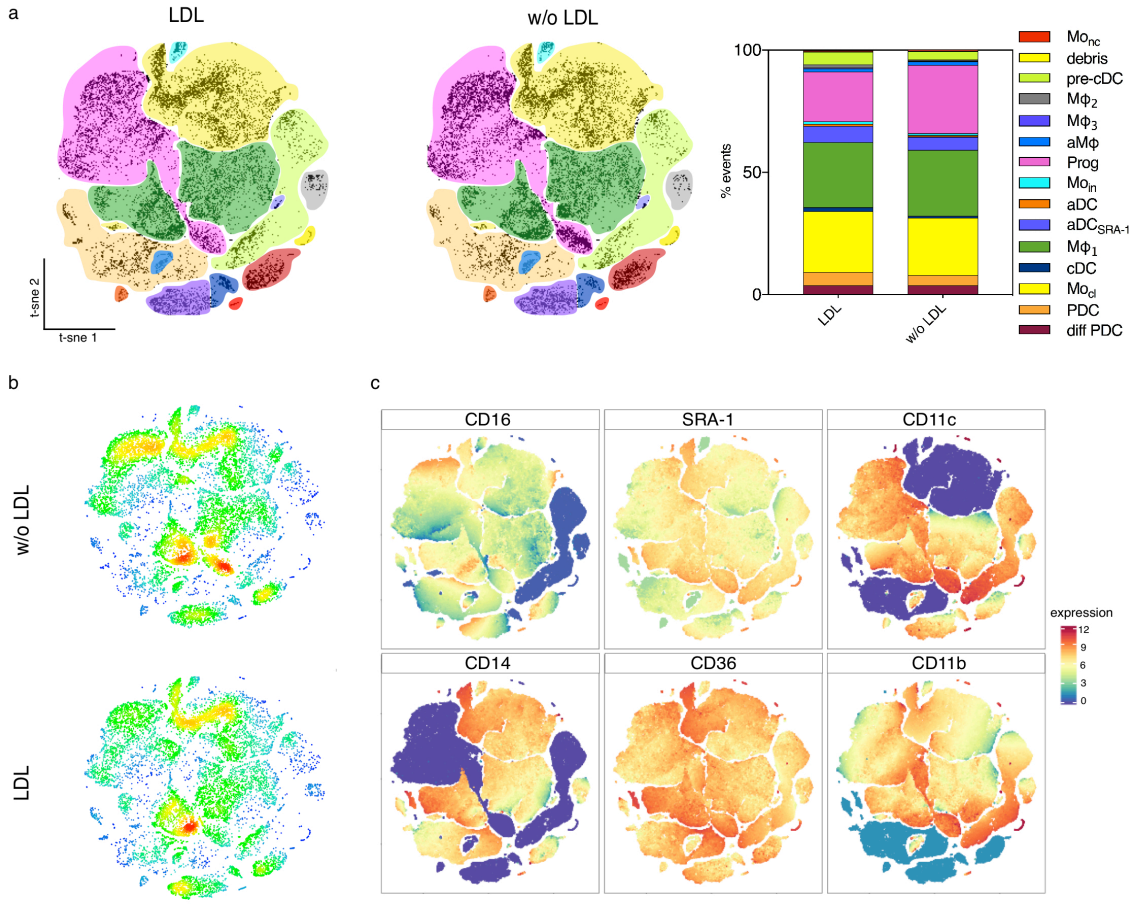

Figure 29. LDL effects on myeloid cells isolated from b-plaques. (**a**) vi-SNE maps indicating myeloid populations identified within b-plaques biofabricated either using LDL-enriched (LDL) or LDL-free (w/o LDL) medium. The stacked-bar chart summarizes the results from the vi-SNE maps and reports the percentage of events recorded in each population. (**b**) Event density distribution vi-SNE maps show high-density (red) and low-density of events (blue) areas. (**c**) Marker expression level vi-SNE plots. n=7; 2,000 events per sample are reported; 14,000 events are displayed in the vi-SNE maps in **a** and **b**. vi-SNE maps in **c** are generated using 2,000 events from all samples.

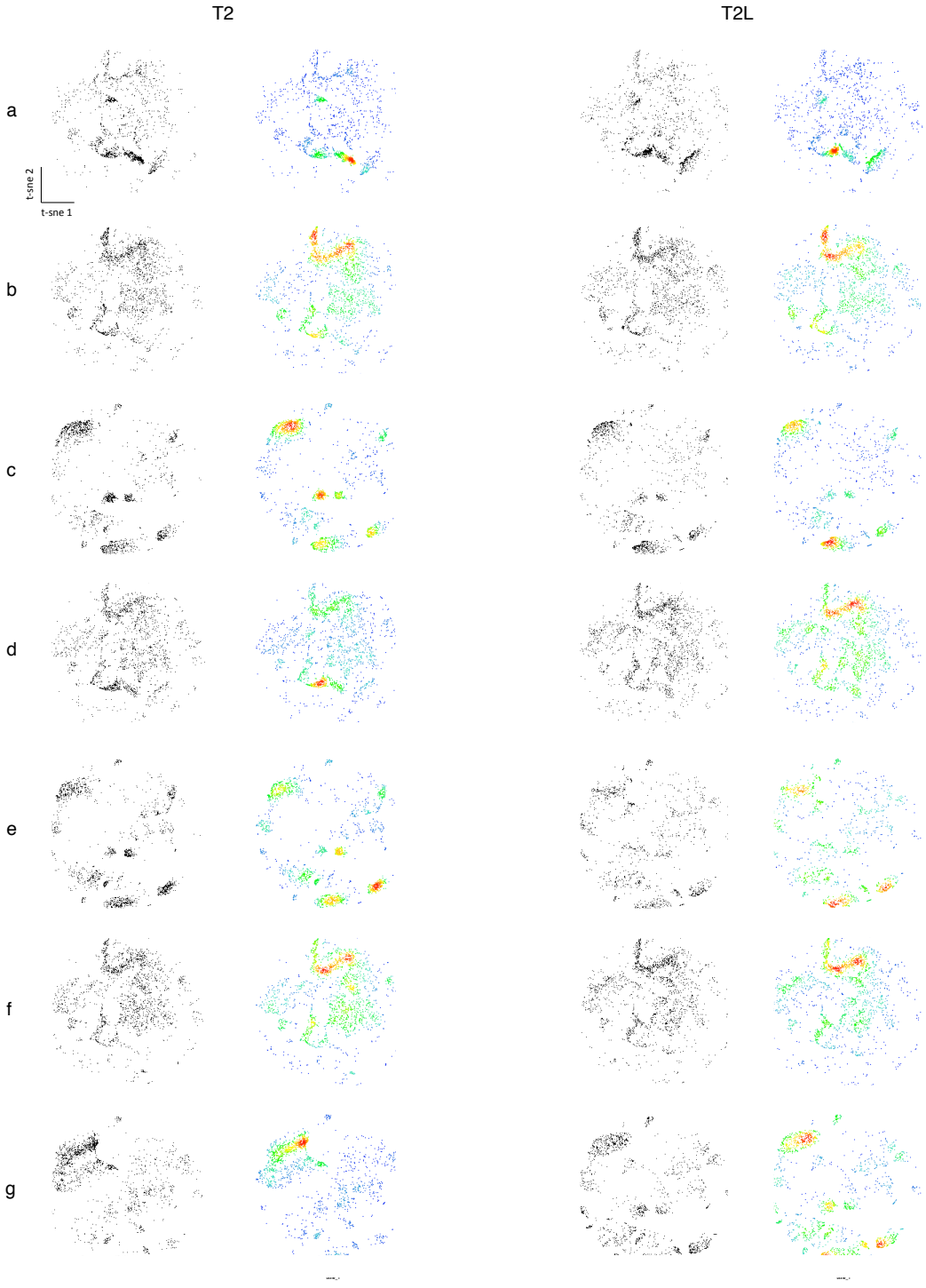

Figure 30. Density plots from CD45+ populations isolated from b-plaques cultured in LDL-enriched (T2L) or LDL free (T2) medium. Vi-SNE maps from each biological replicate (a-g) used to assemble the cumulative vi-SNE maps and cumulative density maps depicted in Figure 29.

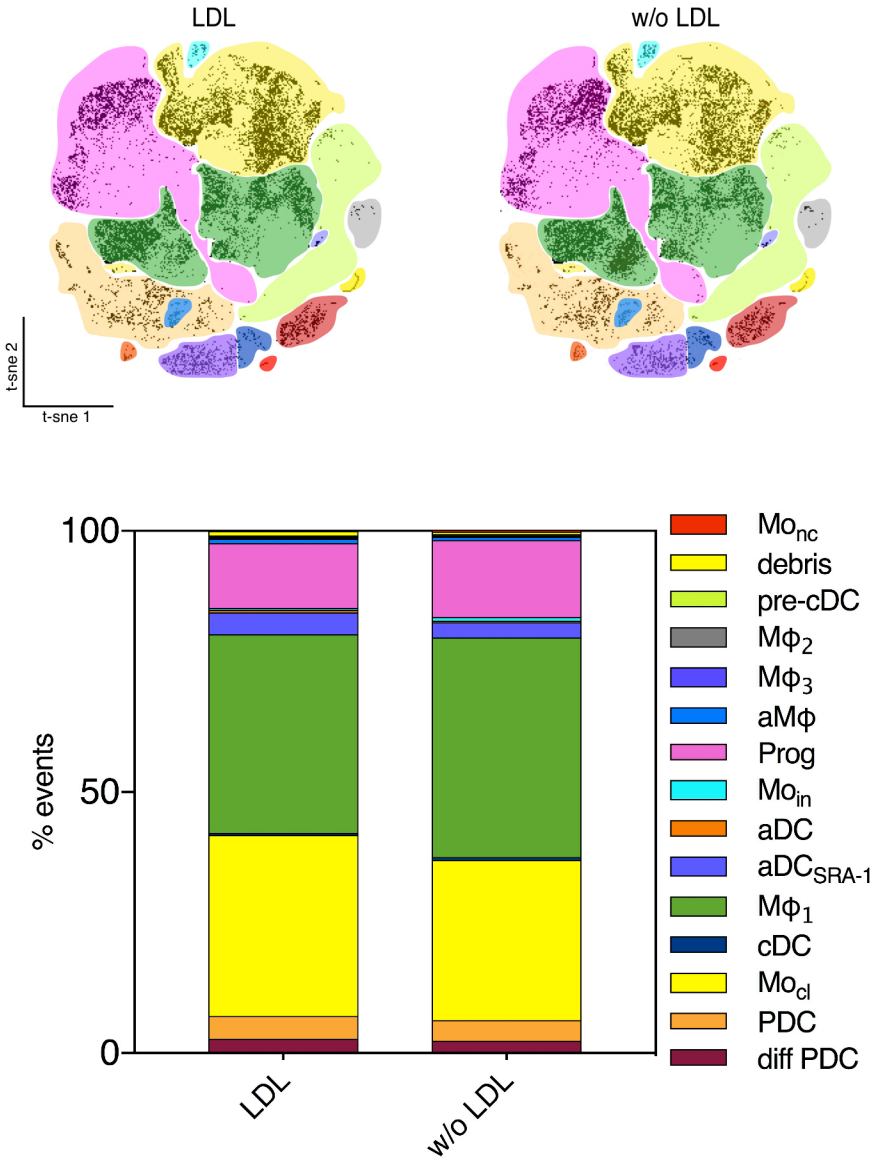

Figure 31. LDL effects on t-plaque myeloid populations. vi-SNE maps indicating different myeloid populations identified in LDL-rich (LDL) or LDL-free (w/o LDL) t-plaques. The part-of-whole graph summarizes the results depicted in the vi-SNE maps. n=7; 2,000 events per sample are reported for a total of 14,000 events in each vi-SNE map.

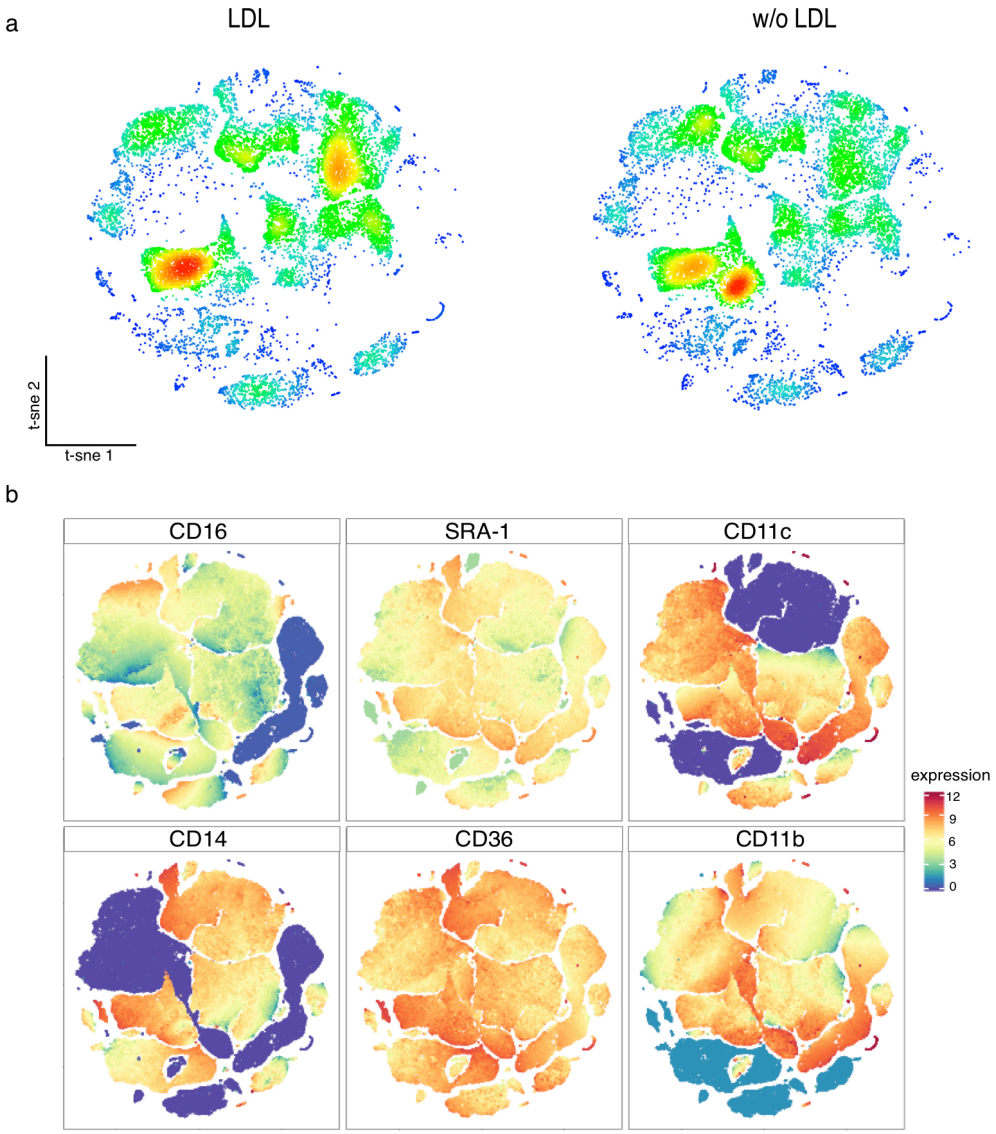

Figure 32. LDL effects on myeloid populations isolated from t-plaques. (**a**) Event density maps of myeloid populations from LDL-rich (LDL) or LDL-free (w/o LDL) t-plaques. High-density (red) and low-density (blue) areas are shown. n=7; 2,000 events per sample are reported. 14,000 events are displayed in each vi-SNE map. (**b**) Marker expression level plots.

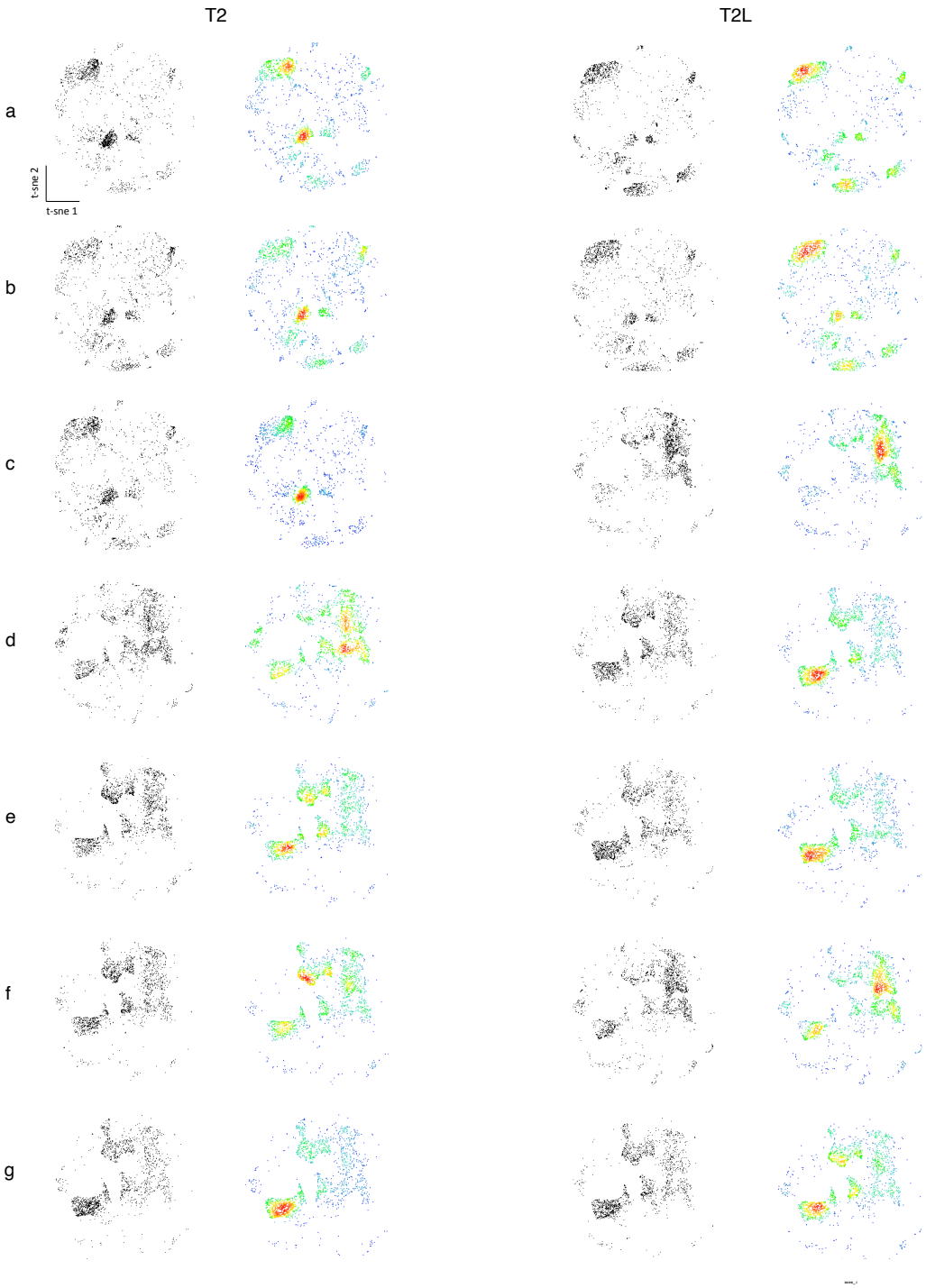

Figure 33. Density plots from CD45+ populations isolated from t-plaques cultured in LDL-enriched (T2L) or LDL free (T2) medium. Vi-SNE maps from each biological replicate (a-g) used to assemble the cumulative vi-SNE maps and cumulative density maps depicted in Figure 31 and 32.

3.3.5 The hanging-drop environment allows the establishment of a pro-inflammatory niche

To uncover possible transcriptional effects exerted by LDL on key target genes, we investigated the expression profiles of the myeloid component during two steps of the ps-plaque biofabrication: (i) after 48h in hanging-drop (T1) and (ii) at the end of the hanging-drop process (T2). We compared T1 and T2 from ps-plaques produced in LDL-free or LDL-enriched environment. Surprisingly, despite the induction of dendritic cell-specific intercellular adhesion molecule *DC-SIGN* ($p<0.001$ versus $p=0.003$, Figure 34a) we did not find any significant LDL-dependent transcriptional change in b-plaques and t-plaques over time (Figure 34a; Figure 35). On the other hand, we found that the hanging-drop process had, per se, a major influence on the gene expression levels by directly or indirectly promoting the establishment of a pro-inflammatory environment. In detail, in b-plaques we observed a significant down-regulation of *CCL26* ($p<0.001$) and up-regulation of key pro-inflammatory genes *CXCL10*, *CCR7* and *IL23* ($p<0.001$) during the transition from T1 to T2 and independently from the presence of LDL (Figure 34a). We observed an indirect pro-inflammatory effect in t-plaques, exerted through the down-regulation of the anti-inflammatory cytokines *CCL26, IL10* and *CCL17* ($p<0.001$, Figure 35). We validated these observations performing a control experiment in which we investigated the gene expression profile of CD45+ cells using a 2D co-culture approach (Figure 36). As for the hanging drop approach, we performed the transcriptomic analysis over time (T1 and T2) in LDL-free and LDL-enriched medium, using both blood-derived and thp-1 cells (Figure 36). When we investigated the transcripts profile of blood-derived cells co-cultured in 2D we did not observe any time-dependent pro-inflammatory effect apart from the down-regulation of CD26 ($p=0.006$ in LDL-rich condition; $p<0.001$ in LDL-free condition). When we repeated the experiment using thp-1 co-cultured in 2D, not only we did not find any time-dependent pro-inflammatory effect but also, we reported a significant time-dependent anti-inflammatory effect achieved with the down-regulation of two pro-inflammatory markers: PTGS1 and ALOX5 (both $p<0.001$, Figure 36).

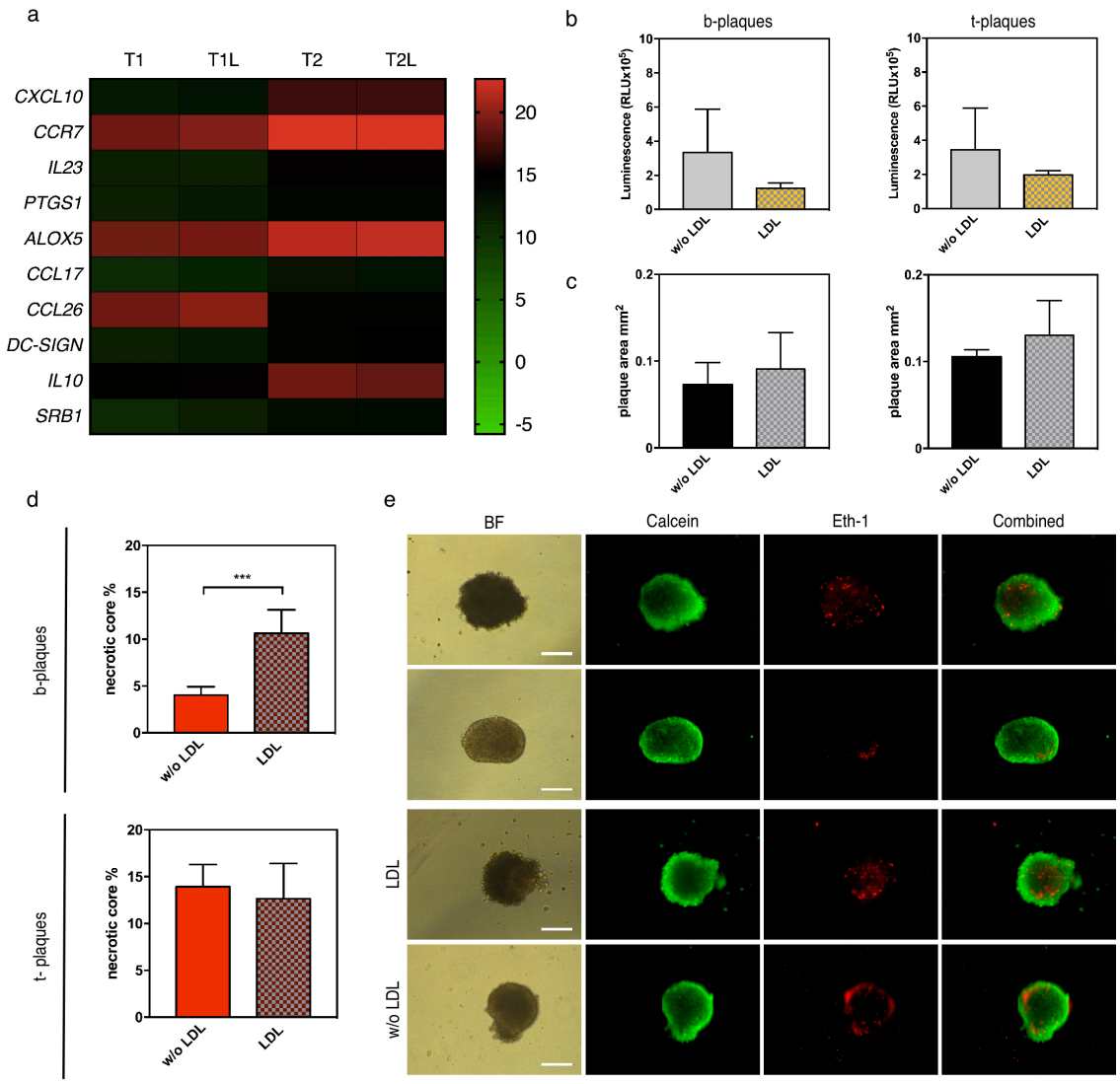

Figure 34. Transcript analysis of pro- and anti-inflammatory gene targets in b-plaques and LDL effects on cell viability and plaque dimension. (**a**) Heat-map indicating the expression levels of target genes of interest at T1 and T2 of b-plaque formation in LDL presence (T1L, T2L) or absence (T1, T2). Expression levels are reported in ΔCt over the mean of the housekeeping genes GAPDH and 18S; n=5. (**b**) ATP levels, indicated in relative luminescence units (RLU), were measured and compared in b- and t-plaques; n=5. (**c**) Plaque circular cross-section area (mm^2) as indicator of plaque dimension; n=5. (**d**-**e**) The ps-plaque necrotic area was measured at the circular cross-section at the great circle of the spheroid, and indicated as percentage over alive cells. Living cells (green) are stained with calcein while dead cells (red) with Eth-1; n=5, *** $p<0.001$, scale bar 100μm.

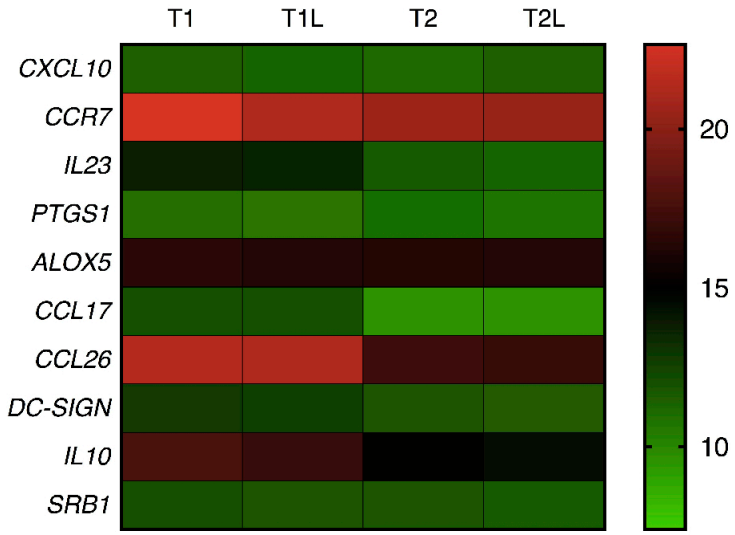

Figure 35. Variation in gene expression profiles during t-plaque formation Heat-map indicating the expression levels of target genes of interest at T1 and T2 of t-plaque formation. Ps-plaques were biofabricated either in LDL-rich (T1L, T2L) or LDL-free (T1, T2) environment. Expression levels are reported in ΔCt over the mean expression of GAPDH and 18S housekeeping genes; n=5.

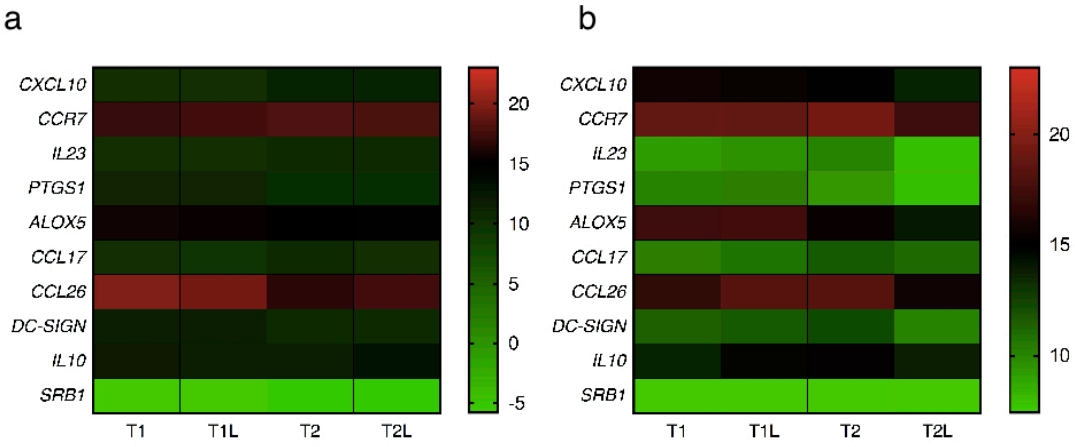

Figure 36. Expression profile of myeloid cells from 2D microenvironmental co-cultures. Heat maps indicating the gene expression level of sorted CD45+ cells during the process of biofabrication (T1 and T2) and treated in different conditions (LDL-enriched and free environment). (**a**) Gene expression data from 2D co-cultures with blood-derived cells (n=3). (**b**) Gene expression data from 2D co-cultures with thp-1 cells (n=3). Expression levels are reported in ΔCt over the mean expression of GAPDH and 18S housekeeping genes.

3.3.6 Low-density lipoprotein enhances cell death in ps-plaques biofabricated with primed blood cells

To further explore the effects of LDL on the ps-plaque model we conducted a bivalent analysis. First, we investigated the cell viability within the ps-plaque. We measured and compared the ATP levels produced by the biofabricated plaques in LDL-enriched and LDL-free medium. We did not find any significant LDL-dependent differences in ATP levels in either b- or t-plaques (Figure 34b). However, we observed a general tendency of lower ATP levels in plaques produced in LDL-rich environments. We then measured the necrotic area at the circular cross-section and we found that b-plaques fabricated in presence of LDL had a significantly larger necrotic area in comparison to their LDL-free counterparts, suggesting an LDL-dependent necrotic effect ($p<0.001$, Figure 34d, e). Second, we investigated differences in plaque dimensions to verify possible effects of LDL on cell proliferation. We found no difference in circular cross-section area – consequently in size – of LDL-enriched vs LDL-free plaques (Figure 34c).

3.4 Discussion

With the biofabrication of the ps-plaque we aimed at replicating cellular architecture and extracellular microenvironment of a human atherosclerotic plaque to close an open modeling gap in the field of atherosclerosis research. It has been described that the fibroatheroma cellular composition is mainly characterized by macrophages and dendritic cells retaining pro-inflammatory and remodeling abilities [75, 196, 197]. To achieve plaque cell populations as similar as possible to human atherosclerotic plaque phenotypes we established a differentiation-priming protocol based on a mild LPS stimulation of cultured adhesive myeloid cells [198, 199]. To visualize and quantify the effects of this procedure on cell population remodeling we used the vi-SNE workflow [168, 169, 200]. With this strategy, we identified a total of 15 cell populations, differently distributed among samples. We were able to classify these populations according to the prevalence of specific surface markers [201, 202]. We were also able to track intra-population density shifts and changes in numbers of events. The sensitivity of the vi-SNE analysis allowed the identification of under-represented myeloid populations, otherwise difficult to identify with commonly used flow cytometry analysis tools. Thanks to the vi-SNE workflow we identified in blood-derived myeloid samples both plasmacytoid dendritic cells (PDC) and pre-classical dendritic cells (pre-cDCs) [202].

The vi-SNE analysis reported a yet unidentified myeloid population in both thp-1 and blood derived samples. We observed a significant decrease of this population upon differentiation-priming treatment in both blood-derived and thp-1 samples. The decrease was concomitant to a significant increase in pre-cDC count in blood-derived samples and to an increase in PDC in thp-1 samples. Based on the current myeloid differentiation map [196, 202] and on our observations, we propose that the yet unidentified population could be classified as a circulating common precursor of pre-cDC and PDC, differentiating from the common dendritic cell precursors located in the bone marrow (Figure 37). Further investigation on this cell population could improve understanding and redesigning of the myeloid differentiation map.

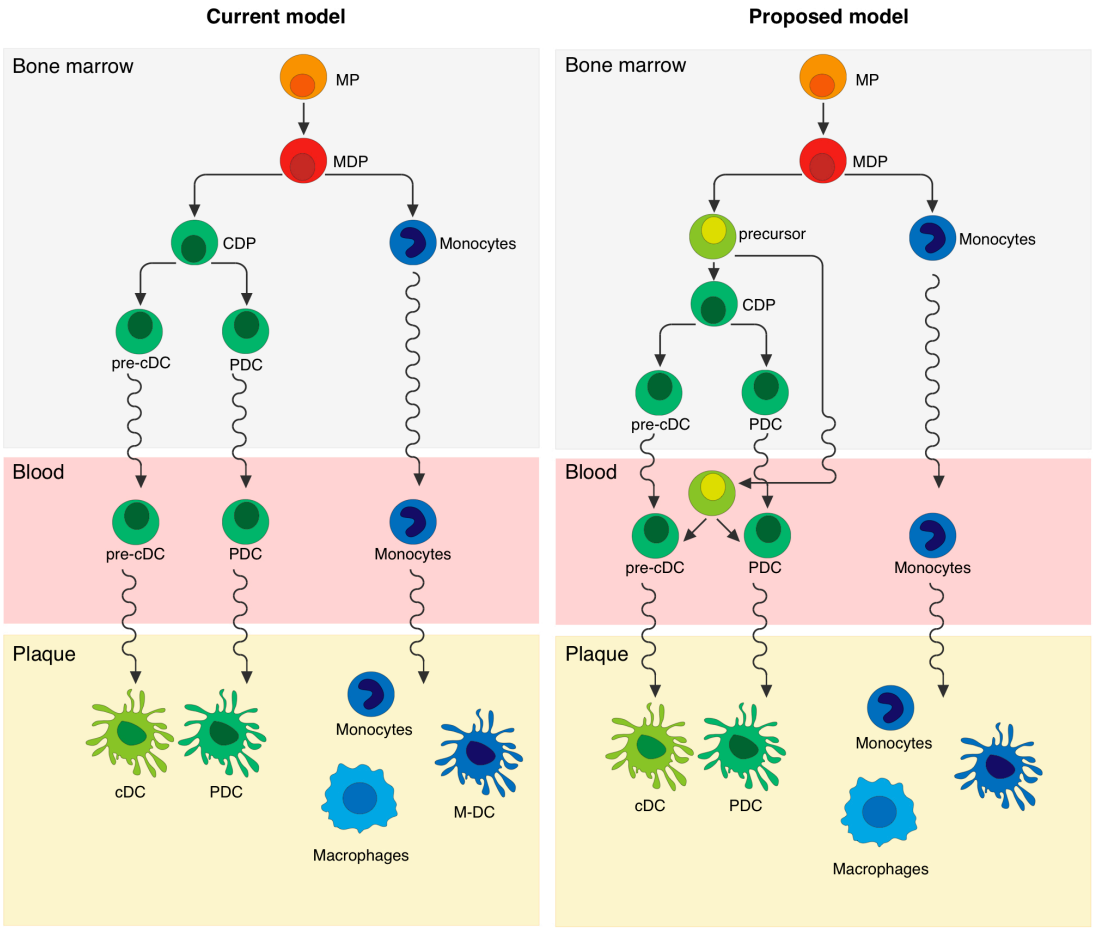

Figure 37. Proposed hematopoietic differentiation model – the myeloid lineage. In the current model of myeloid differentiation, the common macrophage-dendritic cell precursor (MDP) derives from the common myeloid progenitor (MP) and gives rise to monocytes and to the common dendritic cell progenitor (CDP). The latter, differentiates in plasmacytoid dendritic cells (PDC) and pre-classical dendritic cells (pre-cDC). Pre-cDC, PDC and monocytes circulate in the blood and can migrate within the plaque where they differentiate in classical dendritic cells (cDC), tissue resident plasmacytoid dendritic cells (PDC), macrophages or monocyte-derived dendritic cells (M-DC). In the proposed model a dendritic progenitor can circulate in the blood and differentiate in pre-cDC and PDC.

Primed cells and myofibroblasts were used for ps-plaque biofabrication and were combined to generate a stratified cell-spheroid with myofibroblasts located at the periphery and a compact, collagenous and lipid-rich core of CD45+ cells. We sorted and compared the CD45+ populations derived from ps-plaques and native human carotid plaques using qPCR and the vi-SNE workflow. First, we compared the gene expression of CD45+ cells isolated from ps-plaques and native plaques and we reported major differences in transcripts level. Second, we investigated and compared the cell populations between ps-plaques and native plaques and we found that PDC and activated dendritic cells (aDC) are the main myeloid component of thin-cap stage atherosclerotic plaques. This finding is *per se* surprising provided that macrophages

and macrophage-derived foam cells are thought to be the main cellular component of atherosclerotic lesions, at least in early developmental stages, as discussed by Moore and Randolph [203, 204]. Importantly, both PDC and aDC are present in the biofabricated models although in low percentages. It is possible that the differences found in both gene expression and cell composition when comparing ps-plaques and carotid plaques are due to differences in the temporal and developmental stages of both plaque types.

Bonanno et al. previously analyzed the cell component of human carotid plaques using flow cytometry showing that about 17% of the lesion (considering cells of lymphoid and myeloid origin and smooth muscle cells) is constituted by CD68+ cells [205]. They also reported that about 40% of the cells within the plaque expressed MHC class II molecules (HLA-DR+) suggesting that these populations could act as antigen-presenting cells [205]. It was also proven that early-committed immature DCs are positive for CD68 and HLA-DR markers [206], supporting the idea that the cells analyzed by Bonanno et al. might have been in part PDC and activated dendritic cells. Additionally, it is known that PDC aggravate atherosclerotic lesion formation and that their depletion reduces aortic plaque growth by 46% in *Apoe*$^{-/-}$ mice [207, 208]. PDC are also able to uptake oxidized LDL (ox-LDL) *ex vivo*, and promote PDC-driven antigen-specific T-cell proliferation [207]. Finally, it was reported that PDC function and cytokine release is impaired in patients suffering from coronary artery disease [209, 210]. Taken together, these discoveries are in line with our findings and might change the scenario of future atherosclerosis treatments.

Within the PDC population we identified 3 overrepresented sub-populations that we named type-α, type- β and type-γ. We observed that these subpopulations retain some degree of specialization due to differential marker expression levels. This difference could be the basis of a differential contribution to plaque maturation. For instance, PDC type-α display surface marker expression levels (CD36^{high}, CD14^{high} and SRA-1^{high}) of a specialized scavenger population [211]. With the ps-plaque model we were able to investigate LDL effects on intra-plaque population remodeling and cell viability. In detail, we monitored LDL-dependent event density shift within the PDC population towards PDC type-β phenotype. This shift was not concomitant with

the increase in the PDC count implying a PDC polarization towards $CD36^{high}$ and $CD16^{high}$ vi-SNE regions and indicating a possible LDL-triggered acquisition from PDC of scavenger and pro-inflammatory phenotype. Additionally, we found that LDL presence during ps-plaque formation significantly decreased the count of dendritic precursors in both b- and t- plaques and triggered the polarization of aDCs towards $CD11c^{high}$, $CD16^{high}$ and $CD36^{high}$ levels. These findings are supported by the previous observations that LDL and mildly oxidized LDL affect DC maturation and promote pro-inflammatory function [212-214].

We observed an LDL-dependent decrease of plaque cell viability in b-plaques but not in t-plaques. It was shown that LDL and ox-LDL accumulate in the cytoplasm of the phagocyte and ultimately contribute to a deregulation of lipid metabolism by activating the unfolded protein response (UPR), leading to cell death [215]. The non-significant decrease in cell viability observed in t-plaques might be due to intrinsic differences in population counts among ps-plaque types. In fact, t-plaques show higher intermediate monocyte counts when compared to b-plaques. Furthermore, b-plaques display a larger population of activated dendritic cells compared to t-plaques. In summary, t-plaques are constituted by a more immature cellular milieu compared to b-plaques. For this reason, we hypothesize that populations within t-plaques would require more time to develop towards a death-susceptible stage in presence of LDL.

We investigated time-dependent effects of LDL on the expression profile of myeloid cells within the biofabricated plaque. We found no significant difference in transcript levels of selected pro-inflammatory and remodeling target genes [216] comparing LDL-rich and LDL-free plaques. LDL effects on myeloid cell transcriptome were previously investigated by exposing the cells directly in contact with modified forms of LDL and not by directly testing native lipoproteins [217, 218]. However, native LDL might retain slower time of action at the transcriptomic level compared to its modified counterparts, as previously observed [219]. Interestingly, we detected time-dependent gene induction leading to pro-inflammatory cell phenotype independently from LDL treatment. The latter was either prompted by direct up-regulation of pro-inflammatory target genes in b-plaques (*CXCL10*, *CCR7*, *IL23*, *PTGS1*) or indirectly triggered by down-regulation of anti-inflammatory genes in t-

plaques (*CCL17*, *CCL26*, *IL10*). It was recently shown that three-dimensional spheroid cultures of adipose-derived mesenchymal stem cells (MSC) enhance protein levels of the anti-inflammatory tumor necrosis factor alpha stimulated gene/protein 6 (TGS-6) [220]. On the other hand, the study conducted by Bartosh et al. did not include any test to verify the possible concomitant release of pro-inflammatory proteins, leaving an unanswered question open for further investigations.

In conclusion, the ps-plaque is assembled with myeloid cell populations that are shared with human native plaques. These cells are embedded in a collagenous and lipid-rich extracellular matrix surrounded by a fibrotic layer. To our knowledge the ps-plaque can be considered the *in vitro* model closer to human fibroatheroma available up to date. Importantly, the present model has the major limitation to not consider sex, age and genetic predisposition, which, are in fact, key factors influencing plaque initiation and development. In addition, the current model is lacking B and T lymphocytes that might provide and important contribution in exacerbating inflammation at the plaque level. However, the participation of cells from the adaptive immune system to plaque development is still under debate. [221, 222]. In terms of acellular components, the model is missing calcification deposits, often encountered in late-stage plaques. Despite the absence of calcified areas, calcification is per-se not a predictor of unstable plaques (vulnerable plaques) that are prone to rupture and to initiate ischemic events [223]. The intra-plaque calcification mechanisms are tightly regulated by monocyte/macrophages residing within the plaque [224]. In this regard, the 3D plaque model could serve as basis for both (i) further investigations aimed at uncovering the mechanisms driving calcium deposition within the atheroma and (ii) for the biofabrication of more complex and diversified plaque models mimicking different stages of atherosclerosis and peculiar plaque composition.

Despite the ps-plaque model alone cannot address the complexity of the human vascular environment in which wall shear stress, circulating innate and adaptive immune cells and variations in LDL cholesterol, blood pressure and diabetes, play a pivotal role in modulating plaque development, it provides a tool for investigating cellular interplay, viability, metabolism and behavior in a confined environment sharing anatomopathological features with human native plaques. The miniaturized plaque can be integrated in a 96-well or 384-well platform and used for drug design

and screening purposes. Additionally, it can be employed for increasing the basic understanding of late-stage atherosclerosis disease phenomena including possible anti-inflammatory/atheroprotective role of HDL, plaque calcification and rupture or can be integrated in more complex bioengineered dynamic systems, improving existing tissue engineered vascular atherosclerosis models [6]. Finally, the biofabrication process can be applied to blood-derived myeloid cells isolated from patients with different causative mutations of familial hypercholesterolemia (FH, life threatening athero-prone genetic disorder) in order to produce autologous FH-3D models to identify mutation-dependent differences in plaque architecture, cellular composition, cell metabolism and viability, with the aim of predicting mutation-dependent disease prognosis.

Chapter 4

Conclusions

The mechanisms of atherosclerosis are complex, multivariate, and not fully understood. *In vivo* models have been employed to study the disease development. However, the way atherosclerosis manifests within animal models differs from the pathology seen in human, mainly in terms of plaque anatomy and blood lipoprotein profiles. It is thus necessary to create new models that accurately reflect the pathophysiology of atherosclerosis to be either used to understand the underlying mechanisms of plaque formation or to be adopted for pre-clinical studies aiming drug design, testing or screening.

For this dissertation, I successfully biofabricated two new *in vitro* models for the investigation of both early and late-stage atherosclerosis. The models are based on two different tissue engineering approaches. The early-lesion model consists in a vascular construct fabricated using a scaffold-based direct triple co-culture bioengineering strategy where endothelial cells and myofibroblasts are seeded onto a biodegradable PGA-P4HB scaffolds and maintained in dynamic pulsatile flow. Differently, the late-lesion model is based on a two-step scaffold-free static double co-culture approach, where cells from myeloid origin are first cultured in hanging drop and, upon aggregation in spheroid constructs, are coated with a layer of myofibroblasts. Both models are generated employing disease relevant human cell types isolated from different sources, i.e. umbilical vein and freshly drawn blood, and aim at mimicking as close as possible the pathophysiological environment of the disease at the stage of interest. For this purpose, they take advantage from a multidisciplinary approach in which tissue engineering, fluid dynamics and immunology techniques are orchestrated and combined to work in synergy for the design, fabrication and usage of the model.

For the early-lesion model described in chapter 2, I designed and assembled a fluidic chamber for the simultaneous production of 16 vascular constructs. I performed a computational fluid dynamics analysis to understand the flow behavior within the

chamber and to predict velocity, pressure and shear stress encounter by the scaffolds and cells during tissue engineering. With the aim of producing a tool characterized by biologically relevant tunable parameters, as shear stress, pressure and velocity, I investigated the optimal size of vascular constructs that could fit in such a system. I used the model to investigate whether diverse risk environments could influence the differentiation of myeloid populations in the sub-endothelial space of the bioengineered vessel. Furthermore, I employed the model to verify whether such environments could impair the formation of a stable ECM by investigating variations in fibronectin tensional states.

For the late-lesion model I bioengineered a three-dimensional plaque like construct (ps-plaque) using a tailored hanging drop protocol. Using vi-SNE based multidimensional flow cytometry data analysis I compared the myeloid cell-populations in ps-plaques to those in plaques isolated from human carotid arteries. I observed that plasmacytoid and activated dendritic cells are the main myeloid components of human carotid plaques and that both cell types are present in the biofabricated model. Additionally, I found that low-density lipoproteins affect cell viability and contribute to population polarization in ps-plaques. The late-stage atherosclerosis model describes the first human bioengineered *in vitro* model of late atherosclerotic lesion for the investigation of atherosclerosis aetiopathogenesis. Therefore, a patent application has been filed to protect this invention by the technology transfer department of the University of Zurich (EP Patent filed 23.08.2017, EP 17187562.8). Our late-stage atherosclerosis model can potentially facilitate prediction of the main triggers of the disease, estimate disease risk level, determine suitable treatments and ascertain the efficacy of potential treatment options. Additionally, the miniaturized plaque model is suitable for high-throughput analyses: the bioengineered plaques are about 250 μm in diameter and can be easily hosted in a 96 well or 384 well plate setup (Figure 38, Table 6).

In conclusion, both models support the 3R principle (Reduce, Replace and Refine). In fact, such models could potentially reduce and replace many of the experiments performed nowadays on animals, allowing to perform experiments based on human cells, with higher translational power. Concretely, the following animal models could be replaced: WHHL rabbits, NZW rabbits, apoE-knockout mice,

C57BL/6 mice, LDLR-KO (hypercholesteremic) mice, Apob100/100 mice, LDL-DKO mice, senescent non-human primates and others. Moreover, both early and late-stage atherosclerosis models could serve as an empowering tool for current research. The 3D TE models can indeed be used for basic understanding of both early and late-stage atherosclerosis disease phenomena, including initiation of plaque formation, calcification and rupture and can eventually be used in combination to further expand the modeling horizons.

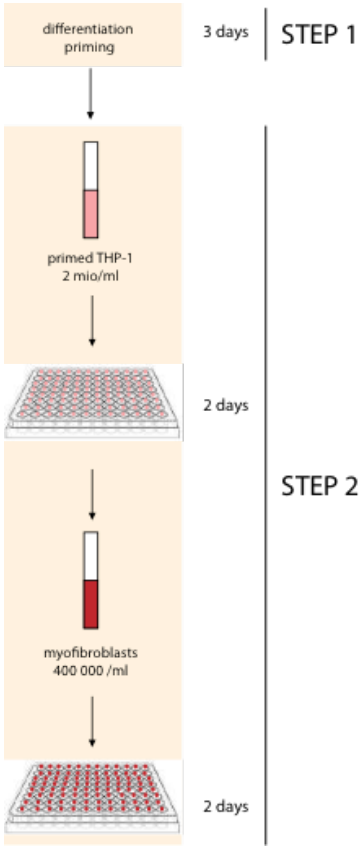

Figure 38. Upscaling pipeline for the 3D ps-plaque model – the creation of a marketable product. Thp1 monocytes will be cultured in vitro up to the desired concentration (about 2 mio cells for one 96 well plate). The STEP1 (differentiation-priming) will last about 3 days (72h + 1h). At this point the cells will be detached and inserted in a robotic system for STEP 2. Hanging drops of 10µl will be generated automatically on the lead of a 96 or 384- well plate. The bottom of the 96/384 well plate be automatically filled with 100µl 1XPBS to create a humid environment necessary to keep the drop volume constant. The plates will be kept at 37°C and 5% CO_2 for 48h. At this point myofibroblasts will be added to the forming bioengineered spheroids and the plates will be kept at 37 °C and 5% CO_2 for additional 48h. After 1 week of processing the product will be ready to be delivered to the costumer.

Drug testing

driving question	how	technique
is the compound reducing plaque volume?	measure the inner necrotic area	calcein/EtBr assay
is the compound preventing plaque formation?	prevents aggregation of myeloid cells	roundess and solidity of 3D plaque model
	reduces intracellular cholesterol accumulation	cholesterol assays and/or Filipin III blue staining
	prevents phagocyte differentiation	immunological staining (e.g. digestion of ps-plaques to single cells followed by flow cytometry)
is the compound targeting a specific population?	prevents a peculiar plaque population to differentiate	immunological staining (e.g. digestion of ps-plaques to single cells followed by flow cytometry)

Table 6. Use of the biofabricated late-lesion model for drug testing.

Chapter 5

List of References

[1] I. Tabas, Macrophage death and defective inflammation resolution in atherosclerosis, Nat Rev Immunol 10(1) (2010) 36-46.

[2] F.J. Schoen, Evolving concepts of cardiac valve dynamics: the continuum of development, functional structure, pathobiology, and tissue engineering, Circulation 118(18) (2008) 1864-80.

[3] D. Schmidt, U.A. Stock, S.P. Hoerstrup, Tissue engineering of heart valves using decellularized xenogeneic or polymeric starter matrices, Philos Trans R Soc Lond B Biol Sci 362(1484) (2007) 1505-12.

[4] D. Schmidt, J. Achermann, B. Odermatt, C. Breymann, A. Mol, M. Genoni, G. Zund, S.P. Hoerstrup, Prenatally fabricated autologous human living heart valves based on amniotic fluid derived progenitor cells as single cell source, Circulation 116(11 Suppl) (2007) I64-70.

[5] R. Sodian, T. Lemke, C. Fritsche, S.P. Hoerstrup, P. Fu, E.V. Potapov, H. Hausmann, R. Hetzer, Tissue-engineering bioreactors: a new combined cell-seeding and perfusion system for vascular tissue engineering, Tissue Eng 8(5) (2002) 863-70.

[6] J. Robert, B. Weber, L. Frese, M.Y. Emmert, D. Schmidt, A. von Eckardstein, L. Rohrer, S.P. Hoerstrup, A three-dimensional engineered artery model for in vitro atherosclerosis research, PLoS One 8(11) (2013) e79821.

[7] B. Weber, P.E. Dijkman, J. Scherman, B. Sanders, M.Y. Emmert, J. Grunenfelder, R. Verbeek, M. Bracher, M. Black, T. Franz, J. Kortsmit, P. Modregger, S. Peter, M. Stampanoni, J. Robert, D. Kehl, M. van Doeselaar, M. Schweiger, C.E. Brokopp, T. Walchli, V. Falk, P. Zilla, A. Driessen-Mol, F.P. Baaijens, S.P. Hoerstrup, Off-the-shelf human decellularized tissue-engineered heart valves in a non-human primate model, Biomaterials 34(30) (2013) 7269-80.

[8] R.C. Elkins, P.E. Dawson, S. Goldstein, S.P. Walsh, K.S. Black, Decellularized human valve allografts, Ann Thorac Surg 71(5 Suppl) (2001) S428-32.

[9] B.P. Chan, K.W. Leong, Scaffolding in tissue engineering: general approaches and tissue-specific considerations, Eur Spine J 17 Suppl 4 (2008) 467-79.

[10] M.P. Rubbens, A. Mol, R.A. Boerboom, R.A. Bank, F.P. Baaijens, C.V. Bouten, Intermittent straining accelerates the development of tissue properties in engineered heart valve tissue, Tissue Eng Part A 15(5) (2009) 999-1008.

[11] R.A. Boerboom, M.P. Rubbens, N.J. Driessen, C.V. Bouten, F.P. Baaijens, Effect of strain magnitude on the tissue properties of engineered cardiovascular constructs, Ann Biomed Eng 36(2) (2008) 244-53.

[12] G.C. Engelmayr, Jr., L. Soletti, S.C. Vigmostad, S.G. Budilarto, W.J. Federspiel, K.B. Chandran, D.A. Vorp, M.S. Sacks, A novel flex-stretch-flow bioreactor for the study of engineered heart valve tissue mechanobiology, Ann Biomed Eng 36(5) (2008) 700-12.

[13] J.P. Vacanti, R. Langer, Tissue engineering: the design and fabrication of living replacement devices for surgical reconstruction and transplantation, Lancet 354 Suppl 1 (1999) Si32-4.

[14] D.T. Simionescu, Q. Lu, Y. Song, J.S. Lee, T.N. Rosenbalm, C. Kelley, N.R. Vyavahare, Biocompatibility and remodeling potential of pure arterial elastin and collagen scaffolds, Biomaterials 27(5) (2006) 702-13.

[15] R. Sodian, S.P. Hoerstrup, J.S. Sperling, D.P. Martin, S. Daebritz, J.E. Mayer, Jr., J.P. Vacanti, Evaluation of biodegradable, three-dimensional matrices for tissue engineering of heart valves, Asaio j 46(1) (2000) 107-10.

[16] M. Chen, P.K. Patra, S.B. Warner, S. Bhowmick, Role of fiber diameter in adhesion and proliferation of NIH 3T3 fibroblast on electrospun polycaprolactone scaffolds, Tissue Eng 13(3) (2007) 579-87.

[17] A. Nathan, T. Kobayashi, D.M. Kolansky, R.L. Wilensky, J. Giri, Bioresorbable Scaffolds for Coronary Artery Disease, Curr Cardiol Rep 19(1) (2017) 5.

[18] R.Y. Kannan, H.J. Salacinski, P.E. Butler, G. Hamilton, A.M. Seifalian, Current status of prosthetic bypass grafts: a review, J Biomed Mater Res B Appl Biomater 74(1) (2005) 570-81.

[19] M. Vert, Aliphatic polyesters: great degradable polymers that cannot do everything, Biomacromolecules 6(2) (2005) 538-46.

[20] C.M. Agrawal, R.B. Ray, Biodegradable polymeric scaffolds for musculoskeletal tissue engineering, J Biomed Mater Res 55(2) (2001) 141-50.

[21] G. Chen, T. Sato, T. Ushida, R. Hirochika, Y. Shirasaki, N. Ochiai, T. Tateishi, The use of a novel PLGA fiber/collagen composite web as a scaffold for engineering of articular cartilage tissue with adjustable thickness, J Biomed Mater Res A 67(4) (2003) 1170-80.

[22] F.T. Moutos, F. Guilak, Composite scaffolds for cartilage tissue engineering, Biorheology 45(3-4) (2008) 501-12.

[23] J.L. Ifkovits, J.A. Burdick, Review: photopolymerizable and degradable biomaterials for tissue engineering applications, Tissue Eng 13(10) (2007) 2369-85.

[24] S. Jockenhoevel, G. Zund, S.P. Hoerstrup, K. Chalabi, J.S. Sachweh, L. Demircan, B.J. Messmer, M. Turina, Fibrin gel -- advantages of a new scaffold in cardiovascular tissue engineering, Eur J Cardiothorac Surg 19(4) (2001) 424-30.

[25] A. Ramamurthi, I. Vesely, Evaluation of the matrix-synthesis potential of crosslinked hyaluronan gels for tissue engineering of aortic heart valves, Biomaterials 26(9) (2005) 999-1010.

[26] T.C. Flanagan, B. Wilkins, A. Black, S. Jockenhoevel, T.J. Smith, A.S. Pandit, A collagen-glycosaminoglycan co-culture model for heart valve tissue engineering applications, Biomaterials 27(10) (2006) 2233-46.

[27] B. Duan, L.A. Hockaday, K.H. Kang, J.T. Butcher, 3D bioprinting of heterogeneous aortic valve conduits with alginate/gelatin hydrogels, J Biomed Mater Res A 101(5) (2013) 1255-64.

[28] G.Q. Chen, Q. Wu, The application of polyhydroxyalkanoates as tissue engineering materials, Biomaterials 26(33) (2005) 6565-78.

[29] R. Sodian, J.S. Sperling, D.P. Martin, A. Egozy, U. Stock, J.E. Mayer, Jr., J.P. Vacanti, Fabrication of a trileaflet heart valve scaffold from a polyhydroxyalkanoate biopolyester for use in tissue engineering, Tissue Eng 6(2) (2000) 183-8.

[30] L. Bacakova, K. Novotna, M. Parizek, Polysaccharides as cell carriers for tissue engineering: the use of cellulose in vascular wall reconstruction, Physiol Res 63 Suppl 1 (2014) S29-47.

[31] M. Yin, F. Xu, H. Ding, F. Tan, F. Song, J. Wang, Incorporation of magnesium ions into photo-crosslinked alginate hydrogel enhanced cell adhesion ability, J Tissue Eng Regen Med 9(9) (2015) 1088-92.

[32] W.Y. Chuang, T.H. Young, C.H. Yao, W.Y. Chiu, Properties of the poly(vinyl alcohol)/chitosan blend and its effect on the culture of fibroblast in vitro, Biomaterials 20(16) (1999) 1479-87.

[33] M.Z. Albanna, T.H. Bou-Akl, H.L. Walters, 3rd, H.W. Matthew, Improving the mechanical properties of chitosan-based heart valve scaffolds using chitosan fibers, J Mech Behav Biomed Mater 5(1) (2012) 171-80.

[34] A. Rajaram, D.J. Schreyer, D.X. Chen, Use of the polycation polyethyleneimine to improve the physical properties of alginate-hyaluronic acid hydrogel during fabrication of tissue repair scaffolds, J Biomater Sci Polym Ed 26(7) (2015) 433-45.

[35] J.G. Hardy, P. Lin, C.E. Schmidt, Biodegradable hydrogels composed of oxime crosslinked poly(ethylene glycol), hyaluronic acid and collagen: a tunable platform for soft tissue engineering, J Biomater Sci Polym Ed 26(3) (2015) 143-61.

[36] F. Bonafe, M. Govoni, E. Giordano, C.M. Caldarera, C. Guarnieri, C. Muscari, Hyaluronan and cardiac regeneration, J Biomed Sci 21 (2014) 100.

[37] P.M. Taylor, S.P. Allen, S.A. Dreger, M.H. Yacoub, Human cardiac valve interstitial cells in collagen sponge: a biological three-dimensional matrix for tissue engineering, J Heart Valve Dis 11(3) (2002) 298-306; discussion 306-7.

[38] M.E. Tedder, J. Liao, B. Weed, C. Stabler, H. Zhang, A. Simionescu, D.T. Simionescu, Stabilized collagen scaffolds for heart valve tissue engineering, Tissue Eng Part A 15(6) (2009) 1257-68.

[39] M.R. Neidert, R.T. Tranquillo, Tissue-engineered valves with commissural alignment, Tissue Eng 12(4) (2006) 891-903.

[40] M. Rothenburger, P. Vischer, W. Volker, B. Glasmacher, E. Berendes, H.H. Scheld, M. Deiwick, In vitro modelling of tissue using isolated vascular cells on a synthetic collagen matrix as a substitute for heart valves, Thorac Cardiovasc Surg 49(4) (2001) 204-9.

[41] M. Dietrich, J. Heselhaus, J. Wozniak, S. Weinandy, P. Mela, B. Tschoeke, T. Schmitz-Rode, S. Jockenhoevel, Fibrin-based tissue engineering: comparison of different methods of autologous fibrinogen isolation, Tissue Eng Part C Methods 19(3) (2013) 216-26.

[42] T.A. Ahmed, E.V. Dare, M. Hincke, Fibrin: a versatile scaffold for tissue engineering applications, Tissue Eng Part B Rev 14(2) (2008) 199-215.

[43] J.K. Kular, S. Basu, R.I. Sharma, The extracellular matrix: Structure, composition, age-related differences, tools for analysis and applications for tissue engineering, J Tissue Eng 5 (2014) 2041731414557112.

[44] T.W. Gilbert, Strategies for tissue and organ decellularization, J Cell Biochem 113(7) (2012) 2217-22.

[45] B. Weber, M.Y. Emmert, R. Schoenauer, C. Brokopp, L. Baumgartner, S.P. Hoerstrup, Tissue engineering on matrix: future of autologous tissue replacement, Semin Immunopathol 33(3) (2011) 307-15.

[46] D.L. Coutu, W. Mahfouz, O. Loutochin, J. Galipeau, J. Corcos, Tissue engineering of rat bladder using marrow-derived mesenchymal stem cells and bladder acellular matrix, PLoS One 9(12) (2014) e111966.

[47] D. Schmidt, S.P. Hoerstrup, Tissue engineered heart valves based on human cells, Swiss Med Wkly 136(39-40) (2006) 618-23.

[48] D.V. Miller, W.D. Edwards, K.J. Zehr, Endothelial and smooth muscle cell populations in a decellularized cryopreserved aortic homograft (SynerGraft) 2 years after implantation, J Thorac Cardiovasc Surg 132(1) (2006) 175-6.

[49] K.A. Daly, S. Liu, V. Agrawal, B.N. Brown, S.A. Johnson, C.J. Medberry, S.F. Badylak, Damage associated molecular patterns within xenogeneic biologic scaffolds and their effects on host remodeling, Biomaterials 33(1) (2012) 91-101.

[50] T. Asahara, T. Murohara, A. Sullivan, M. Silver, R. van der Zee, T. Li, B. Witzenbichler, G. Schatteman, J.M. Isner, Isolation of putative progenitor endothelial cells for angiogenesis, Science 275(5302) (1997) 964-7.

[51] M. Ugurlucan, C. Yerebakan, D. Furlani, N. Ma, G. Steinhoff, Cell sources for cardiovascular tissue regeneration and engineering, Thorac Cardiovasc Surg 57(2) (2009) 63-73.

[52] L. Zhang, Y.H. Zhao, Z. Guan, J.S. Ye, N. de Isla, J.F. Stoltz, Application potential of mesenchymal stem cells derived from Wharton's jelly in liver tissue engineering, Biomed Mater Eng 25(1 Suppl) (2015) 137-43.

[53] D. Schmidt, C. Breymann, A. Weber, C.I. Guenter, S. Neuenschwander, G. Zund, M. Turina, S.P. Hoerstrup, Umbilical cord blood derived endothelial progenitor cells for tissue engineering of vascular grafts, Ann Thorac Surg 78(6) (2004) 2094-8.

[54] D. Schmidt, A. Mol, S. Neuenschwander, C. Breymann, M. Gossi, G. Zund, M. Turina, S.P. Hoerstrup, Living patches engineered from human umbilical cord derived fibroblasts and endothelial progenitor cells, Eur J Cardiothorac Surg 27(5) (2005) 795-800.

[55] B. Weber, M.Y. Emmert, S.P. Hoerstrup, Stem cells for heart valve regeneration, Swiss Med Wkly 142 (2012) w13622.

[56] J.D. Roh, R. Sawh-Martinez, M.P. Brennan, S.M. Jay, L. Devine, D.A. Rao, T. Yi, T.L. Mirensky, A. Nalbandian, B. Udelsman, N. Hibino, T. Shinoka, W.M. Saltzman, E. Snyder, T.R. Kyriakides, J.S. Pober, C.K. Breuer, Tissue-engineered vascular grafts transform into mature blood vessels via an inflammation-mediated process of vascular remodeling, Proc Natl Acad Sci U S A 107(10) (2010) 4669-74.

[57] F. Colazzo, F. Alrashed, P. Saratchandra, I. Carubelli, A.H. Chester, M.H. Yacoub, P.M. Taylor, P. Somers, Shear stress and VEGF enhance endothelial differentiation of human adipose-derived stem cells, Growth Factors 32(5) (2014) 139-49.

[58] M.Y. Emmert, B. Weber, L. Behr, S. Sammut, T. Frauenfelder, P. Wolint, J. Scherman, D. Bettex, J. Grunenfelder, V. Falk, S.P. Hoerstrup, Transcatheter aortic valve implantation using anatomically oriented, marrow stromal cell-based, stented, tissue-engineered heart valves: technical considerations and implications for translational cell-based heart valve concepts, Eur J Cardiothorac Surg 45(1) (2014) 61-8.

[59] S. Levenberg, J.S. Golub, M. Amit, J. Itskovitz-Eldor, R. Langer, Endothelial cells derived from human embryonic stem cells, Proc Natl Acad Sci U S A 99(7) (2002) 4391-6.

[60] J.A. Thomson, J. Itskovitz-Eldor, S.S. Shapiro, M.A. Waknitz, J.J. Swiergiel, V.S. Marshall, J.M. Jones, Embryonic stem cell lines derived from human blastocysts, Science 282(5391) (1998) 1145-7.

[61] K. Takahashi, S. Yamanaka, Induction of pluripotent stem cells from mouse embryonic and adult fibroblast cultures by defined factors, Cell 126(4) (2006) 663-76.

[62] N. Sayed, W.T. Wong, F. Ospino, S. Meng, J. Lee, A. Jha, P. Dexheimer, B.J. Aronow, J.P. Cooke, Transdifferentiation of human fibroblasts to endothelial cells: role of innate immunity, Circulation 131(3) (2015) 300-9.

[63] J.L. Goldstein, M.S. Brown, A century of cholesterol and coronaries: from plaques to genes to statins, Cell 161(1) (2015) 161-72.

[64] A. von Eckardstein, Is there a need for novel cardiovascular risk factors?, Nephrology Dialysis Transplantation 19(4) (2004) 761-765.

[65] J.M. Kelm, M.Y. Emmert, A. Zurcher, D. Schmidt, Y. Begus Nahrmann, K.L. Rudolph, B. Weber, C.E. Brokopp, T. Frauenfelder, S. Leschka, B. Odermatt, R. Jenni, V. Falk, G. Zund, S.P. Hoerstrup, Functionality, growth and accelerated aging of tissue engineered living autologous vascular grafts, Biomaterials 33(33) (2012) 8277-85.

[66] A. Gistera, G.K. Hansson, The immunology of atherosclerosis, Nat Rev Nephrol 13(6) (2017) 368-380.

[67] R. Lozano, M. Naghavi, K. Foreman, S. Lim, K. Shibuya, V. Aboyans, J. Abraham, T. Adair, R. Aggarwal, S.Y. Ahn, M. Alvarado, H.R. Anderson, L.M. Anderson, K.G. Andrews, C. Atkinson, L.M. Baddour, S. Barker-Collo, D.H. Bartels, M.L. Bell, E.J. Benjamin, D. Bennett, K. Bhalla, B. Bikbov, A. Bin Abdulhak, G. Birbeck, F. Blyth, I. Bolliger, S. Boufous, C. Bucello, M. Burch, P. Burney, J. Carapetis, H. Chen, D. Chou, S.S. Chugh, L.E. Coffeng, S.D. Colan, S. Colquhoun, K.E. Colson, J. Condon, M.D. Connor, L.T. Cooper, M. Corriere, M. Cortinovis, K.C. de Vaccaro, W. Couser, B.C. Cowie, M.H. Criqui, M. Cross, K.C. Dabhadkar, N. Dahodwala, D. De Leo, L. Degenhardt, A. Delossantos, J. Denenberg, D.C. Des Jarlais, S.D. Dharmaratne, E.R. Dorsey, T. Driscoll, H. Duber, B. Ebel, P.J. Erwin, P. Espindola, M. Ezzati, V. Feigin, A.D. Flaxman, M.H. Forouzanfar, F.G. Fowkes, R. Franklin, M. Fransen, M.K. Freeman, S.E. Gabriel, E. Gakidou, F. Gaspari, R.F. Gillum, D. Gonzalez-Medina, Y.A. Halasa, D. Haring, J.E. Harrison, R. Havmoeller, R.J. Hay, B. Hoen, P.J. Hotez, D. Hoy, K.H. Jacobsen, S.L. James, R. Jasrasaria, S. Jayaraman, N. Johns, G. Karthikeyan, N. Kassebaum, A. Keren, J.P. Khoo, L.M. Knowlton, O. Kobusingye, A. Koranteng, R. Krishnamurthi, M. Lipnick, S.E. Lipshultz, S.L. Ohno, J. Mabweijano, M.F. MacIntyre, L. Mallinger, L. March, G.B. Marks, R. Marks, A. Matsumori, R. Matzopoulos, B.M. Mayosi, J.H. McAnulty, M.M. McDermott, J. McGrath, G.A. Mensah, T.R. Merriman, C. Michaud, M. Miller, T.R. Miller, C. Mock, A.O. Mocumbi, A.A. Mokdad, A. Moran, K. Mulholland, M.N. Nair, L. Naldi, K.M. Narayan, K. Nasseri, P. Norman, M. O'Donnell, S.B. Omer, K. Ortblad, R. Osborne, D. Ozgediz, B. Pahari, J.D. Pandian, A.P. Rivero, R.P. Padilla, F. Perez-Ruiz, N. Perico, D. Phillips, K. Pierce, C.A. Pope, 3rd, E. Porrini, F. Pourmalek, M. Raju, D. Ranganathan, J.T. Rehm, D.B. Rein, G. Remuzzi, F.P. Rivara, T. Roberts, F.R. De Leon, L.C. Rosenfeld, L. Rushton, R.L. Sacco, J.A. Salomon, U. Sampson, E. Sanman, D.C. Schwebel, M. Segui-Gomez, D.S. Shepard, D. Singh, J. Singleton, K. Sliwa, E. Smith, A. Steer, J.A. Taylor, B. Thomas, I.M. Tleyjeh, J.A. Towbin, T. Truelsen, E.A. Undurraga, N. Venketasubramanian, L. Vijayakumar, T. Vos, G.R. Wagner, M. Wang, W. Wang, K. Watt, M.A. Weinstock, R. Weintraub, J.D. Wilkinson, A.D. Woolf, S. Wulf, P.H. Yeh, P. Yip, A. Zabetian, Z.J. Zheng, A.D. Lopez, C.J. Murray, M.A. AlMazroa, Z.A. Memish, Global and regional mortality from 235 causes of death for 20 age groups in 1990 and 2010: a systematic analysis for the Global Burden of Disease Study 2010, Lancet 380(9859) (2012) 2095-128.

[68] K.S. Cunningham, A.I. Gotlieb, The role of shear stress in the pathogenesis of atherosclerosis, Lab Invest 85(1) (2005) 9-23.

[69] J. Boren, K.J. Williams, The central role of arterial retention of cholesterol-rich apolipoprotein-B-containing lipoproteins in the pathogenesis of atherosclerosis: a triumph of simplicity, Curr Opin Lipidol 27(5) (2016) 473-83.

[70] J.F. Bentzon, F. Otsuka, R. Virmani, E. Falk, Mechanisms of plaque formation and rupture, Circ Res 114(12) (2014) 1852-66.

[71] K. Yahagi, F.D. Kolodgie, F. Otsuka, A.V. Finn, H.R. Davis, M. Joner, R. Virmani, Pathophysiology of native coronary, vein graft, and in-stent atherosclerosis, Nat Rev Cardiol 13(2) (2016) 79-98.

[72] K. Ley, C. Laudanna, M.I. Cybulsky, S. Nourshargh, Getting to the site of inflammation: the leukocyte adhesion cascade updated, Nat Rev Immunol 7(9) (2007) 678-89.

[73] M. Subramanian, I. Tabas, Dendritic cells in atherosclerosis, Semin Immunopathol 36(1) (2014) 93-102.

[74] Y.V. Bobryshev, E.A. Ivanova, D.A. Chistiakov, N.G. Nikiforov, A.N. Orekhov, Macrophages and Their Role in Atherosclerosis: Pathophysiology and Transcriptome Analysis, Biomed Res Int 2016 (2016) 9582430.

[75] K.J. Moore, F.J. Sheedy, E.A. Fisher, Macrophages in atherosclerosis: a dynamic balance, Nat Rev Immunol 13(10) (2013) 709-21.

[76] J. Patel, E. McNeill, G. Douglas, A.B. Hale, J. de Bono, R. Lee, A.J. Iqbal, D. Regan-Komito, E. Stylianou, D.R. Greaves, K.M. Channon, RGS1 regulates myeloid cell accumulation in atherosclerosis and aortic aneurysm rupture through altered chemokine signalling, Nat Commun 6 (2015) 6614.

[77] M.R. Bennett, S. Sinha, G.K. Owens, Vascular Smooth Muscle Cells in Atherosclerosis, Circ Res 118(4) (2016) 692-702.

[78] B. Li, J.H. Wang, Fibroblasts and myofibroblasts in wound healing: force generation and measurement, J Tissue Viability 20(4) (2011) 108-20.

[79] J.L. Johnson, Metalloproteinases in atherosclerosis, Eur J Pharmacol 816 (2017) 93-106.

[80] B. Liu, D. Tang, Computer simulations of atherosclerotic plaque growth in coronary arteries, Mol Cell Biomech 7(4) (2010) 193-202.

[81] A.P. Beltrami, L. Barlucchi, D. Torella, M. Baker, F. Limana, S. Chimenti, H. Kasahara, M. Rota, E. Musso, K. Urbanek, A. Leri, J. Kajstura, B. Nadal-Ginard, P. Anversa, Adult cardiac stem cells are multipotent and support myocardial regeneration, Cell 114(6) (2003) 763-76.

[82] P. Menasche, A.A. Hagege, M. Scorsin, B. Pouzet, M. Desnos, D. Duboc, K. Schwartz, J.T. Vilquin, J.P. Marolleau, Myoblast transplantation for heart failure, Lancet, England, 2001, pp. 279-80.

[83] A.J. Boyle, S.P. Schulman, J.M. Hare, P. Oettgen, Is stem cell therapy ready for patients? Stem Cell Therapy for Cardiac Repair. Ready for the Next Step, Circulation 114(4) (2006) 339-52.

[84] M.Y. Emmert, P. Wolint, N. Wickboldt, G. Gemayel, B. Weber, C.E. Brokopp, A. Boni, V. Falk, A. Bosman, M.E. Jaconi, S.P. Hoerstrup, Human stem cell-based three-dimensional microtissues for advanced cardiac cell therapies, Biomaterials 34(27) (2013) 6339-54.

[85] A. Behfar, R. Crespo-Diaz, A. Terzic, B.J. Gersh, Cell therapy for cardiac repair--lessons from clinical trials, Nat Rev Cardiol 11(4) (2014) 232-46.

[86] E. Forte, I. Chimenti, L. Barile, R. Gaetani, F. Angelini, V. Ionta, E. Messina, A. Giacomello, Cardiac cell therapy: the next (re)generation, Stem Cell Rev 7(4) (2011) 1018-30.

[87] C. Stamm, B. Westphal, H.D. Kleine, M. Petzsch, C. Kittner, H. Klinge, C. Schumichen, C.A. Nienaber, M. Freund, G. Steinhoff, Autologous bone-marrow stem-cell transplantation for myocardial regeneration, Lancet 361(9351) (2003) 45-6.

[88] K. Lunde, S. Solheim, S. Aakhus, H. Arnesen, M. Abdelnoor, T. Egeland, K. Endresen, A. Ilebekk, A. Mangschau, J.G. Fjeld, H.J. Smith, E. Taraldsrud, H.K. Grogaard, R. Bjornerheim, M. Brekke, C. Muller, E. Hopp, A. Ragnarsson, J.E. Brinchmann, K. Forfang, Intracoronary injection of mononuclear bone marrow cells in acute myocardial infarction, N Engl J Med 355(12) (2006) 1199-209.

[89] M. Rota, A. Leri, P. Anversa, Human heart failure: is cell therapy a valid option?, Biochem Pharmacol 88(2) (2014) 129-38.

[90] E. Abdelwahid, A. Kalvelyte, A. Stulpinas, K.A. de Carvalho, L.C. Guarita-Souza, G. Foldes, Stem cell death and survival in heart regeneration and repair, Apoptosis 21(3) (2016) 252-68.

[91] M.Y. Emmert, P. Wolint, S. Winklhofer, P. Stolzmann, N. Cesarovic, T. Fleischmann, T.D. Nguyen, T. Frauenfelder, R. Boni, J. Scherman, D. Bettex, J. Grunenfelder, R. Schwartlander, V. Vogel, M. Gyongyosi, H. Alkadhi, V. Falk, S.P. Hoerstrup, Transcatheter based electromechanical mapping guided intramyocardial transplantation and in vivo tracking of human stem cell based three dimensional microtissues in the porcine heart, Biomaterials 34(10) (2013) 2428-41.

[92] K. Zhu, J. Li, Y. Wang, H. Lai, C. Wang, Nanoparticles-Assisted Stem Cell Therapy for Ischemic Heart Disease, Stem Cells Int 2016 (2016) 1384658.

[93] M. Sepantafar, R. Maheronnaghsh, H. Mohammadi, S. Rajabi-Zeleti, N. Annabi, N. Aghdami, H. Baharvand, Stem cells and injectable hydrogels: Synergistic therapeutics in myocardial repair, Biotechnol Adv (2016).

[94] A. Hasan, R. Waters, B. Roula, R. Dana, S. Yara, T. Alexandre, A. Paul, Engineered Biomaterials to Enhance Stem Cell-Based Cardiac Tissue Engineering and Therapy, Macromol Biosci (2016).

[95] R. Kishore, M. Khan, More Than Tiny Sacks: Stem Cell Exosomes as Cell-Free Modality for Cardiac Repair, Circ Res 118(2) (2016) 330-43.

[96] M.J. Yuan, T. Maghsoudi, T. Wang, Exosomes Mediate the Intercellular Communication after Myocardial Infarction, Int J Med Sci 13(2) (2016) 113-6.

[97] S. Sahoo, D.W. Losordo, Exosomes and cardiac repair after myocardial infarction, Circ Res 114(2) (2014) 333-44.

[98] D.A. Chistiakov, A.N. Orekhov, Y.V. Bobryshev, Cardiac Extracellular Vesicles in Normal and Infarcted Heart, Int J Mol Sci 17(1) (2016).

[99] H. Valadi, K. Ekstrom, A. Bossios, M. Sjostrand, J.J. Lee, J.O. Lotvall, Exosome-mediated transfer of mRNAs and microRNAs is a novel mechanism of genetic exchange between cells, Nat Cell Biol 9(6) (2007) 654-9.

[100] R. Khanabdali, A.A. Rosdah, G.J. Dusting, S.Y. Lim, Harnessing the secretome of cardiac stem cells as therapy for ischemic heart disease, Biochem Pharmacol, 2016. Published by Elsevier Inc.2016.

[101] K.R. Mitchelson, W.Y. Qin, Roles of the canonical myomiRs miR-1, -133 and -206 in cell development and disease, World J Biol Chem 6(3) (2015) 162-208.

[102] F. Pisano, C. Altomare, E. Cervio, L. Barile, M. Rocchetti, M.C. Ciuffreda, G. Malpasso, F. Copes, M. Mura, P. Danieli, G. Viarengo, A. Zaza, M. Gnecchi, Combination of miRNA499 and miRNA133 exerts a synergic effect on cardiac differentiation, Stem Cells 33(4) (2015) 1187-99.

[103] K. Ohshima, K. Inoue, A. Fujiwara, K. Hatakeyama, K. Kanto, Y. Watanabe, K. Muramatsu, Y. Fukuda, S. Ogura, K. Yamaguchi, T. Mochizuki, Let-7 microRNA family is selectively secreted into the extracellular environment via exosomes in a metastatic gastric cancer cell line, PLoS One 5(10) (2010) e13247.

[104] A. Park, J. Barrera-Ramirez, I. Ranasinghe, S. Pilon, R. Sy, D. Fergusson, D.S. Allan, Use of Statins to Augment Progenitor Cell Function in Preclinical and Clinical Studies of Regenerative Therapy: a Systematic Review, Stem Cell Rev (2016).

[105] K.M. Broughton, M.A. Sussman, Empowering Adult Stem Cells for Myocardial Regeneration V2.0: Success in Small Steps, Circ Res 118(5) (2016) 867-80.

[106] J.A. Kamps, G. Krenning, Micromanaging cardiac regeneration: Targeted delivery of microRNAs for cardiac repair and regeneration, World J Cardiol 8(2) (2016) 163-79.

[107] P. Danieli, G. Malpasso, M.C. Ciuffreda, E. Cervio, L. Calvillo, F. Copes, F. Pisano, M. Mura, L. Kleijn, R.A. de Boer, G. Viarengo, V. Rosti, A. Spinillo, M. Roccio, M. Gnecchi,

Conditioned medium from human amniotic mesenchymal stromal cells limits infarct size and enhances angiogenesis, Stem Cells Transl Med 4(5) (2015) 448-58.

[108] F. Arslan, R.C. Lai, M.B. Smeets, L. Akeroyd, A. Choo, E.N. Aguor, L. Timmers, H.V. van Rijen, P.A. Doevendans, G. Pasterkamp, S.K. Lim, D.P. de Kleijn, Mesenchymal stem cell-derived exosomes increase ATP levels, decrease oxidative stress and activate PI3K/Akt pathway to enhance myocardial viability and prevent adverse remodeling after myocardial ischemia/reperfusion injury, Stem Cell Res 10(3) (2013) 301-12.

[109] L. Timmers, S.K. Lim, I.E. Hoefer, F. Arslan, R.C. Lai, A.A. van Oorschot, M.J. Goumans, C. Strijder, S.K. Sze, A. Choo, J.J. Piek, P.A. Doevendans, G. Pasterkamp, D.P. de Kleijn, Human mesenchymal stem cell-conditioned medium improves cardiac function following myocardial infarction, Stem Cell Res 6(3) (2011) 206-14.

[110] S. Yamaguchi, R. Shibata, N. Yamamoto, M. Nishikawa, H. Hibi, T. Tanigawa, M. Ueda, T. Murohara, A. Yamamoto, Dental pulp-derived stem cell conditioned medium reduces cardiac injury following ischemia-reperfusion, Sci Rep 5 (2015) 16295.

[111] C. Akyurekli, Y. Le, R.B. Richardson, D. Fergusson, J. Tay, D.S. Allan, A systematic review of preclinical studies on the therapeutic potential of mesenchymal stromal cell-derived microvesicles, Stem Cell Rev 11(1) (2015) 150-60.

[112] D.M. Reese, Fundamentals--Rudolf Virchow and modern medicine, West J Med 169(2) (1998) 105-8.

[113] J. Fan, S. Kitajima, T. Watanabe, J. Xu, J. Zhang, E. Liu, Y.E. Chen, Rabbit models for the study of human atherosclerosis: from pathophysiological mechanisms to translational medicine, Pharmacol Ther 146 (2015) 104-19.

[114] J.D. Smith, E. Trogan, M. Ginsberg, C. Grigaux, J. Tian, M. Miyata, Decreased atherosclerosis in mice deficient in both macrophage colony-stimulating factor (op) and apolipoprotein E, Proc Natl Acad Sci U S A 92(18) (1995) 8264-8.

[115] Y. Kojima, J.P. Volkmer, K. McKenna, M. Civelek, A.J. Lusis, C.L. Miller, D. Direnzo, V. Nanda, J. Ye, A.J. Connolly, E.E. Schadt, T. Quertermous, P. Betancur, L. Maegdefessel, L.P. Matic, U. Hedin, I.L. Weissman, N.J. Leeper, CD47-blocking antibodies restore phagocytosis and prevent atherosclerosis, Nature 536(7614) (2016) 86-90.

[116] C.A. Reardon, L. Blachowicz, J. Lukens, M. Nissenbaum, G.S. Getz, Genetic background selectively influences innominate artery atherosclerosis: immune system deficiency as a probe, Arterioscler Thromb Vasc Biol 23(8) (2003) 1449-54.

[117] J.K. Williams, M.L. Armstrong, D.D. Heistad, Vasa vasorum in atherosclerotic coronary arteries: responses to vasoactive stimuli and regression of atherosclerosis, Circ Res 62(3) (1988) 515-23.

[118] M.L. Armstrong, M.B. Megan, Lipid depletion in atheromatous coronary arteries in rhesus monkeys after regression diets, Circ Res 30(6) (1972) 675-80.

[119] R.J. Havel, N. Yamada, D.M. Shames, Watanabe heritable hyperlipidemic rabbit. Animal model for familial hypercholesterolemia, Arteriosclerosis 9(1 Suppl) (1989) I33-8.

[120] H. Wang, H. Yang, C.S. Shivalila, M.M. Dawlaty, A.W. Cheng, F. Zhang, R. Jaenisch, One-step generation of mice carrying mutations in multiple genes by CRISPR/Cas-mediated genome engineering, Cell 153(4) (2013) 910-8.

[121] J. Fan, S.P. McCormick, R.M. Krauss, S. Taylor, R. Quan, J.M. Taylor, S.G. Young, Overexpression of human apolipoprotein B-100 in transgenic rabbits results in increased levels of LDL and decreased levels of HDL, Arterioscler Thromb Vasc Biol 15(11) (1995) 1889-99.

[122] J.A. Piedrahita, S.H. Zhang, J.R. Hagaman, P.M. Oliver, N. Maeda, Generation of mice carrying a mutant apolipoprotein E gene inactivated by gene targeting in embryonic stem cells, Proc Natl Acad Sci U S A 89(10) (1992) 4471-5.

[123] S. Ishibashi, M.S. Brown, J.L. Goldstein, R.D. Gerard, R.E. Hammer, J. Herz, Hypercholesterolemia in low density lipoprotein receptor knockout mice and its reversal by adenovirus-mediated gene delivery, J Clin Invest 92(2) (1993) 883-93.

[124] A.H. Lichtman, Adaptive immunity and atherosclerosis: mouse tales in the AJP, Am J Pathol 182(1) (2013) 5-9.

[125] G.S. Getz, C.A. Reardon, Use of Mouse Models in Atherosclerosis Research, Methods Mol Biol 1339 (2015) 1-16.

[126] H.G. Tsang, N.A. Rashdan, C.B. Whitelaw, B.M. Corcoran, K.M. Summers, V.E. MacRae, Large animal models of cardiovascular disease, Cell Biochem Funct 34(3) (2016) 113-32.

[127] J. Shim, R.H. Al-Mashhadi, C.B. Sorensen, J.F. Bentzon, Large animal models of atherosclerosis--new tools for persistent problems in cardiovascular medicine, J Pathol 238(2) (2016) 257-66.

[128] R.H. Al-Mashhadi, C.B. Sorensen, P.M. Kragh, C. Christoffersen, M.B. Mortensen, L.P. Tolbod, T. Thim, Y. Du, J. Li, Y. Liu, B. Moldt, M. Schmidt, G. Vajta, T. Larsen, S. Purup, L. Bolund, L.B. Nielsen, H. Callesen, E. Falk, J.G. Mikkelsen, J.F. Bentzon, Familial hypercholesterolemia and atherosclerosis in cloned minipigs created by DNA transposition of a human PCSK9 gain-of-function mutant, Sci Transl Med 5(166) (2013) 166ra1.

[129] B.T. Davis, X.J. Wang, J.A. Rohret, J.T. Struzynski, E.P. Merricks, D.A. Bellinger, F.A. Rohret, T.C. Nichols, C.S. Rogers, Targeted disruption of LDLR causes hypercholesterolemia and atherosclerosis in Yucatan miniature pigs, PLoS One 9(4) (2014) e93457.

[130] X.F. Leong, C.Y. Ng, K. Jaarin, Animal Models in Cardiovascular Research: Hypertension and Atherosclerosis, Biomed Res Int 2015 (2015) 528757.

[131] R.G. DePalma, L. Klein, E.M. Bellon, S. Koletsky, Regression of atherosclerotic plaques in rhesus monkeys. Angiographic, morphologic, and angiochemical changes, Arch Surg 115(11) (1980) 1268-78.

[132] T.E. Hamm, Jr., J.R. Kaplan, T.B. Clarkson, B.C. Bullock, Effects of gender and social behavior on the development of coronary artery atherosclerosis in cynomolgus macaques, Atherosclerosis 48(3) (1983) 221-33.

[133] C.A. Marzetta, L.L. Rudel, A species comparison of low density lipoprotein heterogeneity in nonhuman primates fed atherogenic diets, J Lipid Res 27(7) (1986) 753-62.

[134] V. Blaton, H. Peeters, The nonhuman primates as models for studying human atherosclerosis: studies on the chimpanzee, the baboon and the rhesus macacus, Adv Exp Med Biol 67(00) (1976) 33-64.

[135] D.J. Graham, J.J. Alexander, R. Miguel, Aortic endothelial and smooth muscle cell co-culture: an in vitro model of the arterial wall, J Invest Surg 4(4) (1991) 487-94.

[136] M. Navab, G.P. Hough, L.W. Stevenson, D.C. Drinkwater, H. Laks, A.M. Fogelman, Monocyte migration into the subendothelial space of a coculture of adult human aortic endothelial and smooth muscle cells, J Clin Invest 82(6) (1988) 1853-63.

[137] B. Dorweiler, M. Torzewski, M. Dahm, V. Ochsenhirt, H.A. Lehr, K.J. Lackner, C.F. Vahl, A novel in vitro model for the study of plaque development in atherosclerosis, Thromb Haemost 95(1) (2006) 182-9.

[138] K. Islam, S.B. Timraz, R. Nasser, D.L. Gater, Y.E. Pearson, N. Christoforou1, J.C. Teo, Co-culture Methods Used to Model Atherosclerosis In Vitro Using Endothelial, Smooth Muscle and Monocyte Cells, in: *K.U. Department of Biomedical Engineering, United Arab Emirates* (Ed.) SM Journal of Biomedical Engineering, 2016.

[139] E. Lee, A.J. Grodzinsky, P. Libby, S.K. Clinton, M.W. Lark, R.T. Lee, Human vascular smooth muscle cell-monocyte interactions and metalloproteinase secretion in culture, Arterioscler Thromb Vasc Biol 15(12) (1995) 2284-9.

[140] Y. Zhu, Y. Hojo, U. Ikeda, M. Takahashi, K. Shimada, Interaction between monocytes and vascular smooth muscle cells enhances matrix metalloproteinase-1 production, J Cardiovasc Pharmacol 36(2) (2000) 152-61.

[141] M. Navab, S.S. Imes, S.Y. Hama, G.P. Hough, L.A. Ross, R.W. Bork, A.J. Valente, J.A. Berliner, D.C. Drinkwater, H. Laks, et al., Monocyte transmigration induced by modification of low density lipoprotein in cocultures of human aortic wall cells is due to induction of monocyte chemotactic protein 1 synthesis and is abolished by high density lipoprotein, J Clin Invest 88(6) (1991) 2039-46.

[142] M. Navab, S.Y. Hama, B.J. Van Lenten, D.C. Drinkwater, H. Laks, A.M. Fogelman, A new antiinflammatory compound, leumedin, inhibits modification of low density lipoprotein and the resulting monocyte transmigration into the subendothelial space of cocultures of human aortic wall cells, J Clin Invest 91(3) (1993) 1225-30.

[143] D. Proudfoot, C. Fitzsimmons, J. Torzewski, D.E. Bowyer, Inhibition of human arterial smooth muscle cell growth by human monocyte/macrophages: a co-culture study, Atherosclerosis 145(1) (1999) 157-65.

[144] J.J. Boyle, P.L. Weissberg, M.R. Bennett, Tumor necrosis factor-alpha promotes macrophage-induced vascular smooth muscle cell apoptosis by direct and autocrine mechanisms, Arterioscler Thromb Vasc Biol 23(9) (2003) 1553-8.

[145] J. Khallou-Laschet, A. Varthaman, G. Fornasa, C. Compain, A.T. Gaston, M. Clement, M. Dussiot, O. Levillain, S. Graff-Dubois, A. Nicoletti, G. Caligiuri, Macrophage plasticity in experimental atherosclerosis, PLoS One 5(1) (2010) e8852.

[146] B. Semmling, S. Nagel, K. Sternberg, W. Weitschies, A. Seidlitz, Development of hydrophobized alginate hydrogels for the vessel-simulating flow-through cell and their usage for biorelevant drug-eluting stent testing, AAPS PharmSciTech 14(3) (2013) 1209-18.

[147] A. Seidlitz, W. Schick, T. Reske, V. Senz, N. Grabow, S. Petersen, S. Nagel, W. Weitschies, In vitro study of sirolimus release from a drug-eluting stent: Comparison of the release profiles obtained using different test setups, Eur J Pharm Biopharm 93 (2015) 328-38.

[148] E.M. Cunnane, M.T. Walsh, Towards the development of an in vitro model of atherosclerotic peripheral vessels for evaluating drug-coated endovascular technologies, Drug Discov Today 21(9) (2016) 1512-1520.

[149] A. Mallone, C. Stenger, A. Von Eckardstein, S.P. Hoerstrup, B. Weber, Biofabricating atherosclerotic plaques: In vitro engineering of a three-dimensional human fibroatheroma model, Biomaterials 150 (2018) 49-59.

[150] S. Kim, W. Kim, S. Lim, J.S. Jeon, Vasculature-On-A-Chip for In Vitro Disease Models, Bioengineering (Basel) 4(1) (2017).

[151] M.F. van Buul-Wortelboer, H.J. Brinkman, K.P. Dingemans, P.G. de Groot, W.G. van Aken, J.A. van Mourik, Reconstitution of the vascular wall in vitro. A novel model to study interactions between endothelial and smooth muscle cells, Exp Cell Res 162(1) (1986) 151-8.

[152] K. Ishikawa, M. Navab, N. Leitinger, A.M. Fogelman, A.J. Lusis, Induction of heme oxygenase-1 inhibits the monocyte transmigration induced by mildly oxidized LDL, J Clin Invest 100(5) (1997) 1209-16.

[153] G.J. Randolph, T. Luther, S. Albrecht, V. Magdolen, W.A. Muller, Role of tissue factor in adhesion of mononuclear phagocytes to and trafficking through endothelium in vitro, Blood 92(11) (1998) 4167-77.

[154] A. Shioi, M. Katagi, Y. Okuno, K. Mori, S. Jono, H. Koyama, Y. Nishizawa, Induction of bone-type alkaline phosphatase in human vascular smooth muscle cells: roles of tumor necrosis factor-alpha and oncostatin M derived from macrophages, Circ Res 91(1) (2002) 9-16.

[155] P.N. Seshiah, D.J. Kereiakes, S.S. Vasudevan, N. Lopes, B.Y. Su, N.A. Flavahan, P.J. Goldschmidt-Clermont, Activated monocytes induce smooth muscle cell death: role of macrophage colony-stimulating factor and cell contact, Circulation 105(2) (2002) 174-80.

[156] S. Kunigal, A. Kusch, N. Tkachuk, S. Tkachuk, U. Jerke, H. Haller, I. Dumler, Monocyte-expressed urokinase inhibits vascular smooth muscle cell growth by activating Stat1, Blood 102(13) (2003) 4377-83.

[157] Q. Cai, L. Lanting, R. Natarajan, Interaction of monocytes with vascular smooth muscle cells regulates monocyte survival and differentiation through distinct pathways, Arterioscler Thromb Vasc Biol 24(12) (2004) 2263-70.

[158] B. Dorweiler, M. Torzewski, M. Dahm, C.J. Kirkpatrick, K.J. Lackner, C.F. Vahl, Subendothelial infiltration of neutrophil granulocytes and liberation of matrix-destabilizing enzymes in an experimental model of human neo-intima, Thromb Haemost 99(2) (2008) 373-81.

[159] S. Chaterji, K. Park, A. Panitch, Scaffold-free in vitro arterial mimetics: the importance of smooth muscle-endothelium contact, Tissue Eng Part A 16(6) (2010) 1901-12.

[160] A.M. Gan, M.M. Pirvulescu, D. Stan, V. Simion, M. Calin, I. Manduteanu, E. Butoi, Monocytes and smooth muscle cells cross-talk activates STAT3 and induces resistin and reactive oxygen species production [corrected], J Cell Biochem 114(10) (2013) 2273-83.

[161] S. Weinert, D.M. Poitz, S. Auffermann-Gretzinger, L. Eger, J. Herold, S. Medunjanin, A. Schmeisser, R.H. Strasser, R.C. Braun-Dullaeus, The lysosomal transfer of LDL/cholesterol from macrophages into vascular smooth muscle cells induces their phenotypic alteration, Cardiovasc Res 97(3) (2013) 544-52.

[162] A. Ghattas, H.R. Griffiths, A. Devitt, G.Y. Lip, E. Shantsila, Monocytes in coronary artery disease and atherosclerosis: where are we now?, J Am Coll Cardiol 62(17) (2013) 1541-51.

[163] S.A. Kocaman, U. Arslan, Y. Tavil, H. Okuyan, A. Abaci, A. Cengel, Increased circulating monocyte count is related to good collateral development in coronary artery disease, Atherosclerosis 197(2) (2008) 753-6.

[164] J.H. Kim, S. Lim, K.S. Park, H.C. Jang, S.H. Choi, Total and differential WBC counts are related with coronary artery atherosclerosis and increase the risk for cardiovascular disease in Koreans, PLoS One 12(7) (2017) e0180332.

[165] J.C. LaRosa, D. Hunninghake, D. Bush, M.H. Criqui, G.S. Getz, A.M. Gotto, Jr., S.M. Grundy, L. Rakita, R.M. Robertson, M.L. Weisfeldt, et al., The cholesterol facts. A summary of the evidence relating dietary fats, serum cholesterol, and coronary heart disease. A joint statement by the American Heart Association and the National Heart, Lung, and Blood Institute. The Task Force on Cholesterol Issues, American Heart Association, Circulation 81(5) (1990) 1721-33.

[166] L.F. Hong, X.L. Li, S.H. Luo, Y.L. Guo, J. Liu, C.G. Zhu, P. Qing, R.X. Xu, N.Q. Wu, L.X. Jiang, J.J. Li, Relation of leukocytes and its subsets counts with the severity of stable coronary artery disease in patients with diabetic mellitus, PLoS One 9(3) (2014) e90663.

[167] S.S. Martin, R.S. Blumenthal, M. Miller, LDL cholesterol: the lower the better, Med Clin North Am 96(1) (2012) 13-26.

[168] A.D. Amir el, K.L. Davis, M.D. Tadmor, E.F. Simonds, J.H. Levine, S.C. Bendall, D.K. Shenfeld, S. Krishnaswamy, G.P. Nolan, D. Pe'er, viSNE enables visualization of high dimensional single-cell data and reveals phenotypic heterogeneity of leukemia, Nat Biotechnol 31(6) (2013) 545-52.

[169] S. Van Gassen, B. Callebaut, M.J. Van Helden, B.N. Lambrecht, P. Demeester, T. Dhaene, Y. Saeys, FlowSOM: Using self-organizing maps for visualization and interpretation of cytometry data, Cytometry A 87(7) (2015) 636-45.

[170] S. Arnoldini, A. Moscaroli, M. Chabria, M. Hilbert, S. Hertig, R. Schibli, M. Behe, V. Vogel, Novel peptide probes to assess the tensional state of fibronectin fibers in cancer, Nat Commun 8(1) (2017) 1793.

[171] A. Mol, M.I. van Lieshout, C.G. Dam-de Veen, S. Neuenschwander, S.P. Hoerstrup, F.P. Baaijens, C.V. Bouten, Fibrin as a cell carrier in cardiovascular tissue engineering applications, Biomaterials 26(16) (2005) 3113-21.

[172] L. Van Der Maaten, G. Hinton, Visualizing high-dimensional data using t-sne. journal of machine learning research, J Mach Learn Res 9 (2008) 26.

[173] H.R. Schelbert, Anatomy and physiology of coronary blood flow, J Nucl Cardiol 17(4) (2010) 545-54.

[174] Y. Wada, A. Sugiyama, T. Kohro, M. Kobayashi, M. Takeya, M. Naito, T. Kodama, In vitro model of atherosclerosis using coculture of arterial wall cells and macrophage, Yonsei Med J 41(6) (2000) 740-55.

[175] J.T. Dodge, Jr., B.G. Brown, E.L. Bolson, H.T. Dodge, Lumen diameter of normal human coronary arteries. Influence of age, sex, anatomic variation, and left ventricular hypertrophy or dilation, Circulation 86(1) (1992) 232-46.

[176] S. Aharinejad, W. Schreiner, F. Neumann, Morphometry of human coronary arterial trees, Anat Rec 251(1) (1998) 50-9.

[177] H. Samady, P. Eshtehardi, M.C. McDaniel, J. Suo, S.S. Dhawan, C. Maynard, L.H. Timmins, A.A. Quyyumi, D.P. Giddens, Coronary artery wall shear stress is associated with progression and transformation of atherosclerotic plaque and arterial remodeling in patients with coronary artery disease, Circulation 124(7) (2011) 779-88.

[178] E.O. Ofili, M.J. Kern, A.J. Labovitz, J.A. St Vrain, J. Segal, F.V. Aguirre, R. Castello, Analysis of coronary blood flow velocity dynamics in angiographically normal and stenosed arteries before and after endolumen enlargement by angioplasty, J Am Coll Cardiol 21(2) (1993) 308-16.

[179] S.S. Dhawan, R.P. Avati Nanjundappa, J.R. Branch, W.R. Taylor, A.A. Quyyumi, H. Jo, M.C. McDaniel, J. Suo, D. Giddens, H. Samady, Shear stress and plaque development, Expert Rev Cardiovasc Ther 8(4) (2010) 545-56.

[180] P.B. Aldo, V. Craveiro, S. Guller, G. Mor, Effect of culture conditions on the phenotype of THP-1 monocyte cell line, Am J Reprod Immunol 70(1) (2013) 80-6.

[181] A. Ohradanova-Repic, C. Machacek, M.B. Fischer, H. Stockinger, Differentiation of human monocytes and derived subsets of macrophages and dendritic cells by the HLDA10 monoclonal antibody panel, Clin Transl Immunology 5(1) (2016) e55.

[182] S. Tsuchiya, M. Yamabe, Y. Yamaguchi, Y. Kobayashi, T. Konno, K. Tada, Establishment and characterization of a human acute monocytic leukemia cell line (THP-1), Int J Cancer 26(2) (1980) 171-6.

[183] A.B. Reiss, D.W. Wan, K. Anwar, J.T. Merrill, P.A. Wirkowski, N. Shah, B.N. Cronstein, E.S. Chan, S.E. Carsons, Enhanced CD36 scavenger receptor expression in THP-1 human monocytes in the presence of lupus plasma: linking autoimmunity and atherosclerosis, Exp Biol Med (Maywood) 234(3) (2009) 354-60.

[184] J.J. Manning-Tobin, K.J. Moore, T.A. Seimon, S.A. Bell, M. Sharuk, J.I. Alvarez-Leite, M.P. de Winther, I. Tabas, M.W. Freeman, Loss of SR-A and CD36 activity reduces atherosclerotic lesion complexity without abrogating foam cell formation in hyperlipidemic mice, Arterioscler Thromb Vasc Biol 29(1) (2009) 19-26.

[185] H.W. Ziegler-Heitbrock, R.J. Ulevitch, CD14: cell surface receptor and differentiation marker, Immunol Today 14(3) (1993) 121-5.

[186] P. Antal-Szalmas, J.A. Strijp, A.J. Weersink, J. Verhoef, K.P. Van Kessel, Quantitation of surface CD14 on human monocytes and neutrophils, J Leukoc Biol 61(6) (1997) 721-8.

[187] A. Devitt, S. Pierce, C. Oldreive, W.H. Shingler, C.D. Gregory, CD14-dependent clearance of apoptotic cells by human macrophages: the role of phosphatidylserine, Cell Death Differ 10(3) (2003) 371-82.

[188] C. Whatling, H. Bjork, S. Gredmark, A. Hamsten, P. Eriksson, Effect of macrophage differentiation and exposure to mildly oxidized LDL on the proteolytic repertoire of THP-1 monocytes, J Lipid Res 45(9) (2004) 1768-76.

[189] R. Escate, T. Padro, L. Badimon, LDL accelerates monocyte to macrophage differentiation: Effects on adhesion and anoikis, Atherosclerosis 246 (2016) 177-86.

[190] R. Pankov, K.M. Yamada, Fibronectin at a glance, J Cell Sci 115(Pt 20) (2002) 3861-3.

[191] J.E. Schwarzbauer, D.W. DeSimone, Fibronectins, their fibrillogenesis, and in vivo functions, Cold Spring Harb Perspect Biol 3(7) (2011).

[192] K.E. Kubow, R. Vukmirovic, L. Zhe, E. Klotzsch, M.L. Smith, D. Gourdon, S. Luna, V. Vogel, Mechanical forces regulate the interactions of fibronectin and collagen I in extracellular matrix, Nat Commun 6 (2015) 8026.

[193] S. Katsuda, Y. Okada, T. Minamoto, Y. Oda, Y. Matsui, I. Nakanishi, Collagens in human atherosclerosis. Immunohistochemical analysis using collagen type-specific antibodies, Arterioscler Thromb 12(4) (1992) 494-502.

[194] R. Virmani, A.P. Burke, F.D. Kolodgie, A. Farb, Pathology of the thin-cap fibroatheroma: a type of vulnerable plaque, J Interv Cardiol 16(3) (2003) 267-72.

[195] K. Menck, D. Behme, M. Pantke, N. Reiling, C. Binder, T. Pukrop, F. Klemm, Isolation of human monocytes by double gradient centrifugation and their differentiation to macrophages in teflon-coated cell culture bags, J Vis Exp (91) (2014) e51554.

[196] M.I. Cybulsky, C. Cheong, C.S. Robbins, Macrophages and Dendritic Cells: Partners in Atherogenesis, Circ Res 118(4) (2016) 637-52.

[197] G. Chinetti-Gbaguidi, S. Colin, B. Staels, Macrophage subsets in atherosclerosis, Nat Rev Cardiol 12(1) (2015) 10-7.

[198] F. Awad, E. Assrawi, C. Jumeau, S. Georgin-Lavialle, L. Cobret, P. Duquesnoy, W. Piterboth, L. Thomas, K. Stankovic-Stojanovic, C. Louvrier, I. Giurgea, G. Grateau, S. Amselem, S.A. Karabina, Impact of human monocyte and macrophage polarization on NLR expression and NLRP3 inflammasome activation, PLoS One 12(4) (2017) e0175336.

[199] M. Peters, K. Dudziak, M. Stiehm, A. Bufe, T-cell polarization depends on concentration of the danger signal used to activate dendritic cells, Immunol Cell Biol 88(5) (2010) 537-44.

[200] H. Chen, M.C. Lau, M.T. Wong, E.W. Newell, M. Poidinger, J. Chen, Cytofkit: A Bioconductor Package for an Integrated Mass Cytometry Data Analysis Pipeline, PLoS Comput Biol 12(9) (2016) e1005112.

[201] J. Yang, L. Zhang, C. Yu, X.F. Yang, H. Wang, Monocyte and macrophage differentiation: circulation inflammatory monocyte as biomarker for inflammatory diseases, Biomark Res 2(1) (2014) 1.

[202] F. Geissmann, M.G. Manz, S. Jung, M.H. Sieweke, M. Merad, K. Ley, Development of monocytes, macrophages, and dendritic cells, Science 327(5966) (2010) 656-61.

[203] K.J. Moore, I. Tabas, Macrophages in the pathogenesis of atherosclerosis, Cell 145(3) (2011) 341-55.

[204] G.J. Randolph, Mechanisms that regulate macrophage burden in atherosclerosis, Circ Res 114(11) (2014) 1757-71.

[205] E. Bonanno, A. Mauriello, A. Partenzi, L. Anemona, L.G. Spagnoli, Flow cytometry analysis of atherosclerotic plaque cells from human carotids: a validation study, Cytometry 39(2) (2000) 158-65.

[206] K. Kishimoto, G. Tate, T. Kitamura, M. Kojima, T. Mitsuya, Cytologic features and frequency of plasmacytoid dendritic cells in the lymph nodes of patients with histiocytic necrotizing lymphadenitis (Kikuchi-Fujimoto disease), Diagn Cytopathol 38(7) (2010) 521-6.

[207] Y. Doring, H.D. Manthey, M. Drechsler, D. Lievens, R.T. Megens, O. Soehnlein, M. Busch, M. Manca, R.R. Koenen, J. Pelisek, M.J. Daemen, E. Lutgens, M. Zenke, C.J. Binder, C. Weber, A. Zernecke, Auto-antigenic protein-DNA complexes stimulate plasmacytoid dendritic cells to promote atherosclerosis, Circulation 125(13) (2012) 1673-83.

[208] N. Macritchie, G. Grassia, S.R. Sabir, M. Maddaluno, P. Welsh, N. Sattar, A. Ialenti, M. Kurowska-Stolarska, I.B. McInnes, J.M. Brewer, P. Garside, P. Maffia, Plasmacytoid dendritic cells play a key role in promoting atherosclerosis in apolipoprotein E-deficient mice, Arterioscler Thromb Vasc Biol 32(11) (2012) 2569-79.

[209] I. Van Brussel, E.A. Van Vre, G.R. De Meyer, C.J. Vrints, J.M. Bosmans, H. Bult, Decreased numbers of peripheral blood dendritic cells in patients with coronary artery disease are associated with diminished plasma Flt3 ligand levels and impaired plasmacytoid dendritic cell function, Clin Sci (Lond) 120(9) (2011) 415-26.

[210] J.J. Corrales, M. Almeida, R.M. Burgo, P. Hernandez, J.M. Miralles, A. Orfao, Decreased production of inflammatory cytokines by circulating monocytes and dendritic cells in type 2 diabetic men with atherosclerotic complications, J Diabetes Complications 21(1) (2007) 41-9.

[211] V.V. Kunjathoor, M. Febbraio, E.A. Podrez, K.J. Moore, L. Andersson, S. Koehn, J.S. Rhee, R. Silverstein, H.F. Hoff, M.W. Freeman, Scavenger receptors class A-I/II and CD36 are the principal receptors responsible for the uptake of modified low density lipoprotein leading to lipid loading in macrophages, J Biol Chem 277(51) (2002) 49982-8.

[212] R. Zaguri, I. Verbovetski, M. Atallah, U. Trahtemberg, A. Krispin, E. Nahari, E. Leitersdorf, D. Mevorach, 'Danger' effect of low-density lipoprotein (LDL) and oxidized LDL on human immature dendritic cells, Clin Exp Immunol 149(3) (2007) 543-52.

[213] C.J. Alderman, P.R. Bunyard, B.M. Chain, J.C. Foreman, D.S. Leake, D.R. Katz, Effects of oxidised low density lipoprotein on dendritic cells: a possible immunoregulatory component of the atherogenic micro-environment?, Cardiovasc Res 55(4) (2002) 806-19.

[214] L. Perrin-Cocon, F. Coutant, S. Agaugue, S. Deforges, P. Andre, V. Lotteau, Oxidized low-density lipoprotein promotes mature dendritic cell transition from differentiating monocyte, J Immunol 167(7) (2001) 3785-91.

[215] B. Feng, P.M. Yao, Y. Li, C.M. Devlin, D. Zhang, H.P. Harding, M. Sweeney, J.X. Rong, G. Kuriakose, E.A. Fisher, A.R. Marks, D. Ron, I. Tabas, The endoplasmic

reticulum is the site of cholesterol-induced cytotoxicity in macrophages, Nat Cell Biol 5(9) (2003) 781-92.

[216] F.O. Martinez, S. Gordon, M. Locati, A. Mantovani, Transcriptional profiling of the human monocyte-to-macrophage differentiation and polarization: new molecules and patterns of gene expression, J Immunol 177(10) (2006) 7303-11.

[217] S. Bekkering, J. Quintin, L.A. Joosten, J.W. van der Meer, M.G. Netea, N.P. Riksen, Oxidized low-density lipoprotein induces long-term proinflammatory cytokine production and foam cell formation via epigenetic reprogramming of monocytes, Arterioscler Thromb Vasc Biol 34(8) (2014) 1731-8.

[218] L.J. van Tits, R. Stienstra, P.L. van Lent, M.G. Netea, L.A. Joosten, A.F. Stalenhoef, Oxidized LDL enhances pro-inflammatory responses of alternatively activated M2 macrophages: a crucial role for Kruppel-like factor 2, Atherosclerosis 214(2) (2011) 345-9.

[219] S. Damian-Zamacona, P. Toledo-Ibelles, M.Z. Ibarra-Abundis, L. Uribe-Figueroa, E. Hernandez-Lemus, K.P. Macedo-Alcibia, B. Delgado-Coello, J. Mas-Oliva, J.P. Reyes-Grajeda, Early Transcriptomic Response to LDL and oxLDL in Human Vascular Smooth Muscle Cells, PLoS One 11(10) (2016) e0163924.

[220] T.J. Bartosh, J.H. Ylostalo, A. Mohammadipoor, N. Bazhanov, K. Coble, K. Claypool, R.H. Lee, H. Choi, D.J. Prockop, Aggregation of human mesenchymal stromal cells (MSCs) into 3D spheroids enhances their antiinflammatory properties, Proc Natl Acad Sci U S A 107(31) (2010) 13724-9.

[221] H.M. Dansky, S.A. Charlton, M.M. Harper, J.D. Smith, T and B lymphocytes play a minor role in atherosclerotic plaque formation in the apolipoprotein E-deficient mouse, Proc Natl Acad Sci U S A 94(9) (1997) 4642-6.

[222] F. Cheng, L. Twardowski, K. Reifenberg, K. Winter, A. Canisius, E. Pross, J. Fan, E. Schmitt, L.D. Shultz, K.J. Lackner, M. Torzewski, Combined B, T and NK Cell Deficiency Accelerates Atherosclerosis in BALB/c Mice, PLoS One 11(8) (2016) e0157311.

[223] F. Otsuka, K. Sakakura, K. Yahagi, M. Joner, R. Virmani, Has our understanding of calcification in human coronary atherosclerosis progressed?, Arterioscler Thromb Vasc Biol 34(4) (2014) 724-36.

[224] Y. Tintut, J. Patel, M. Territo, T. Saini, F. Parhami, L.L. Demer, Monocyte/macrophage regulation of vascular calcification in vitro, Circulation 105(5) (2002) 650-5.